
Editorial Office of *Earth's Cryosphere (Kriosfera Zemli)*
Institute of Geography, Russian Academy of Sciences
37 Vavilov str., office 22, Moscow, 117312, Russia
Editorial staff: *N.V. Arutyunyan*, *N.G. Belova, O.M. Lisitsyna, G.E. Oblogov*
Phone: 8(985) 957-10-01, e-mail: kriozem@gmail.com
Editor of the English translation: *D.E. Konyushkov*

Journal promoted by
Russian Academy of Sciences, Siberian Branch, Novosibirsk
Earth's Cryosphere Institute, Tyumen Scientific Centre SB RAS, Tyumen
Melnikov Permafrost Institute, SB RAS, Yakutsk

Editorial Manager *M.A. Trashkeeva*
Designed by *N.F. Suranova*
Typeset by *N.M. Raizvikh*

RUSSIAN ACADEMY OF SCIENCES
SIBERIAN BRANCH
EARTH'S CRYOSPHERE INSTITUTE, TYUMEN SCIENTIFIC CENTRE
MELNIKOV PERMAFROST INSTITUTE

EARTH'S CRYOSPHERE
SCIENTIFIC JOURNAL

Founded in January 1997	6 issues per year	Vol. XXVI, No. 3	May–June 2022

CONTENTS

EARTH'S CRYOSPHERE
SCIENTIFIC JOURNAL

Earth's Cryosphere, 2022, vol. XXVI, No. 3, pp. 3–9

REGIONAL AND HISTORICAL GEOCRYOLOGY

NEW DATA ON PERMAFROST THICKNESS ON THE LENA–ALDAN INTERFLUVE

A.R. Kirillin[1, *], M.N. Zheleznyak[1], V.I. Zhizhin[1]

[1]*Melnikov Permafrost Institute, Siberian Branch of the Russian Academy of Sciences, ul. Merzlotnaya 36, Yakutsk, 677010 Russia*

**Corresponding author; e-mail: mouks@ya.ru*

For the first time, data on the ground temperature to a depth of 650 m in a borehole with a restored thermal regime have been obtained f for the Lena–Aldan interfluve. The results of geothermal measurements attest to an anomalous permafrost thickness for this territory (750–780 m). Changes in the ground temperature with depth reflect the nonstationary thermal regime of permafrost with a negative geothermal gradient to a depth of 200–300 m. The permafrost thickness is estimated, and possible reasons for its difference in relatively nearby areas are considered.

Keywords: *geothermal research, ground temperature, permafrost, Quaternary deposits, thermophysical properties, permafrost thickness.*

Recommended citation: Kirillin A.R., Zheleznyak M.N., Zhizhin V.I., 2022. New data on permafrost thickness on the Lena–Aldan interfluve. *Earth's Cryosphere*, XXVI (3), 3–9.

INTRODUCTION

The surface of the Central Yakutian Lowland within the Lena–Aldan interfluve was finally shaped in the Quaternary period. This is a flat slightly dissected plain with absolute heights up to 240 m asl, often swampy, with a large number of lakes and with pronounced manifestation of various cryogenic processes. The plain relief of the Lena–Aldan interfluve is complicated by a series of terraces, thermokarst basins, heaving mounds, and polygonal formations. Quaternary deposits have different thicknesses (30–50 m) and composition (mainly quartz–feldspar sands, gray clays, sands with an insignificant content of pebbles) depending on the particular conditions. They compose the upper part of the slightly undulating structural denudation plain. Quaternary deposits are underlain by the Jurassic deposits, whose thickness in the borehole reaches 520 m. They are mainly represented by coarse and medium-grained quartz–feldspar sandstones with rare interlayers of fractured shale. At their base, there is a layer of conglomerates with carbonate cement and interlayers of coarse-grained sandstone of 20–30 m in thickness. The lower part of the sedimentary strata of the platform is represented by the Middle Cambrian deposits consisting of dense gray dolomite with interlayers of limestone of white to black color; their thickness recovered in the borehole is 190 m. These calcareous rocks contain numerous quartz veinlets.

According to the geological-structural zoning, the site is located on the closing flank of the Aldan Anteclise, which is complicated by the eastern flank of the blocky Yakutian Uplift and the Ust-Aldan Depression [*Geodynamic map..., 1992*].

The climate of the region is sharply continental with the mean annual air temperature of –8.5°C and the mean annual precipitation of 200–250 mm; about 80–85% of the annual precipitation falls the warm period (April–October) [*Kotlyakov, Lorius, 2000; Balobaev, Shepelev, 2001*]. According to geocryological zoning, the territory belongs to the zone of continuous permafrost with rock temperatures from –2.0 to –4.5°C [*Geocryological map..., 1997*]. The geocryological conditions of the Lena–Aldan interfluve were considered in a number of works [*Katasonov, Ivanov, 1973; Ivanov, 1984; Shepelev et al., 1984*]; however, data on the permafrost thickness in this region are very limited. The basis for assessing the depth of the base of the permafrost was geophysical research and the discovery of fresh aquifers in the course of drilling of geological and hydrogeological exploration and production boreholes. According to these data, the thickness of the permafrost zone was estimated at 240 m (village of Tuora-Kyuyol), 400 m (village of Telei-Diring), 561 m (village of Churapcha), and 530 m (village of Arylakh). Targeted geothermal studies of the territory were not conducted because of technical difficulties in the preparation and equipment of boreholes.

The purpose of our study was to clarify the depth of the permafrost base and to more fully characterize the natural conditions for the formation and temperature changes of rocks.

METHODS

Geothermal research. During drilling, the thermal field of the rocks is disturbed and then restored to its natural state. The temperature of frozen strata takes a particularly long time to recover. Even 4–5 months after the completion of drilling, the temperature curves for boreholes (thermograms) are characterized by the presence of non-gradient zones (Fig. 1).

When determining the permafrost thickness, the method of temperature measurements in a borehole with restored temperature conditions was used. To do this, the borehole was equipped with a stationary geothermal installation with 10 sensors based on semiconductor thermistors and MASTECH MY65 multimeters recording the resistance of thermistors. A detailed description of the characteristics of thermistors, preparation of geothermal installations, and field research methods is given in [*Balobaev et al., 1985*].

The lower boundary of the permafrost was found from the data of temperature measurements in the borehole by extrapolating the measured temperature to the 0°C isotherm. For this purpose, structural features and geothermal parameters of the particular sections of the stratigraphic column were taken into account [*Zheleznyak, 1999*].

Thermophysical research. To determine the thermophysical properties of rocks, 17 samples were taken from the core of borehole 2. The thermophysical study was carried out at room temperature. Before the experiment, the samples were moistened in a desiccator. This created the conditions of the sub-permafrost stratum, where the rocks are, as a rule, in a state of complete water saturation. Since the samples had a significant density, their moisture content, even with excessive moisture, was negligible. Therefore, the thermophysical information obtained for positive-temperature rocks could also be applied to their negative-temperature counterparts.

Measurements of thermal conductivity and thermal diffusivity of the rocks were carried out using the Thermal Conductivity Scanning (TCS) setup (Fig. 2) with an error in determining the values of thermophysical properties of 3% (at a confidence level of 0.95). This setup implements the method of optical scanning of rock proposed by Yu.A. Popov [*Popov et al., 1983, 1999, 2012*]. During TCS operation, the sample under study is heated by a light spot that moves along the flat or cylindrical surface of the core sample at a constant speed.

The initial temperature and degree of heating of the sample are recorded by infrared (IR) radiation receivers. The field of view of each of them moves along the same sample surface at the same speed as

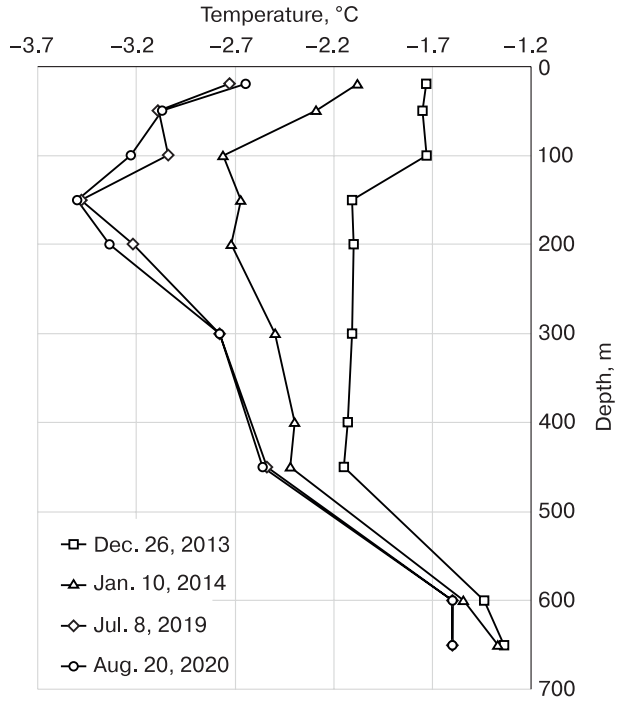

Fig. 1. Ground temperature distribution in borehole 2.

See Fig. 3 for location.

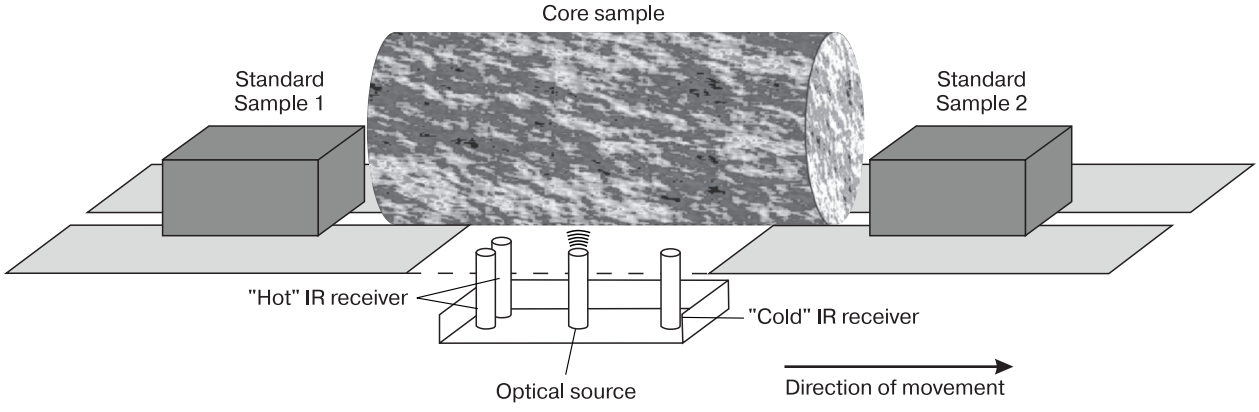

Fig. 2. Schematic design of the method of optical scanning of rock samples to determine their thermophysical properties.

the heating spot. The test sample is placed in the setup together with two reference samples with known values of thermal conductivity and thermal diffusivity. The thermophysical properties of a rock sample are determined based on a comparison of their heating levels with the heating level of reference samples.

Measurements were made on the cylindrical surface of the core (when scanning the samples along the core axis) and on the flat surface of the samples. In some cases, measurements on the cylindrical surface of the core and on its ends were combined.

When scanning samples with an optical radiation source and temperature sensors, a thermal conductivity profile is recorded. This makes it possible to determine both the average values of thermal conductivity for the entire sample and its local values in separate parts of the sample. Thus, it becomes possible to differentiate between the rocks with close thermal conductivity values but with different structural and textural characteristics.

RESULTS

In 2012 and 2013, the Yakutian survey expedition of Yakutskgeologiya JSC drilled hydrogeological boreholes to provide drinking water for the villages of Churapcha and Dyabyla (Ozhulun) (Fig. 3). Borehole 1 was located 100 m from the shore of the pond in the village of Churapcha, and borehole 2 was found 200 m from a thermokarst lake near the village of Dyabyla. The absolute heights of the borehole heads were 181 and 172 m asl, respectively. Thermokarst mounds were found near the lake at the Dyabyla site. The project assumed the drilling of the boreholes to a depth of 600 m. In borehole 1 (Fig. 4), Quaternary deposits to a depth of 12 m were represented by loam; deeper, to a depth of 45 m, by sand with inclusions of small and coarse gravels (up to 5% of the volume). Under the Quaternary deposits, to a depth of 566 m, poorly cemented frozen sandstones with siltstone interbeds of the Jurassic system were found. At the base of the exposed section of Jurassic deposits, gray sandstones and conglomerates were present. Below, limestones of the Cambrian system occurred.

At the depths of 561–569 m, within the layer of light-colored sandstones with lenses of conglomerates, water inflow into the borehole was recorded, as a result of which the groundwater level was established at a depth of 169.2 m. The borehole was drilled to a depth of 625 m; after drilling and logging operations were completed, geothermal measurements were carried out in the borehole. According to the obtained data, subzero temperatures of the rocks were noted down to a depth of 561 m, and their minimum values (–1.3°C) were at the depth interval of 300–325 m. A sharp change in the temperature gradient of rocks in the range of 561–569 m was due to the presence of an aquifer associated with the contact of sandstones of the Jurassic system and limestones of the Cambrian system. Judging by the drilling data, the contact zone of sandstones and limestones was

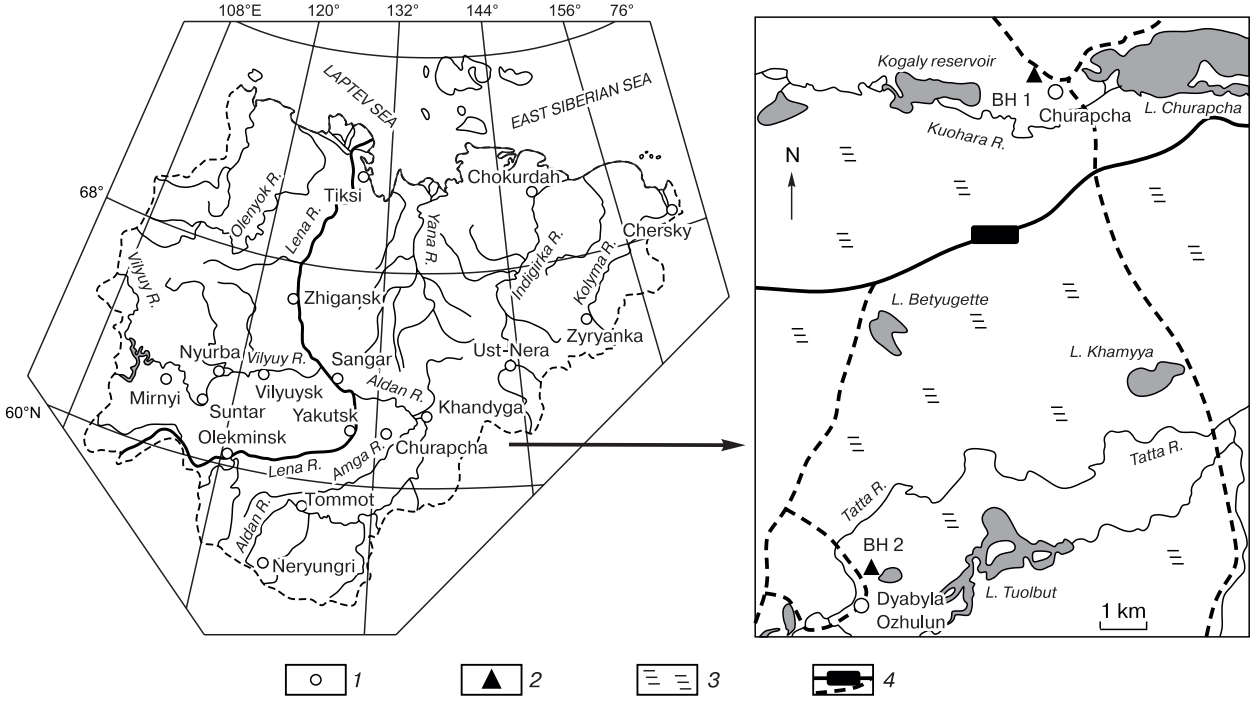

Fig. 3. Scheme of location of boreholes.

1 – settlements, *2* – borehole, *3* – thermokarst, *4* – roads.

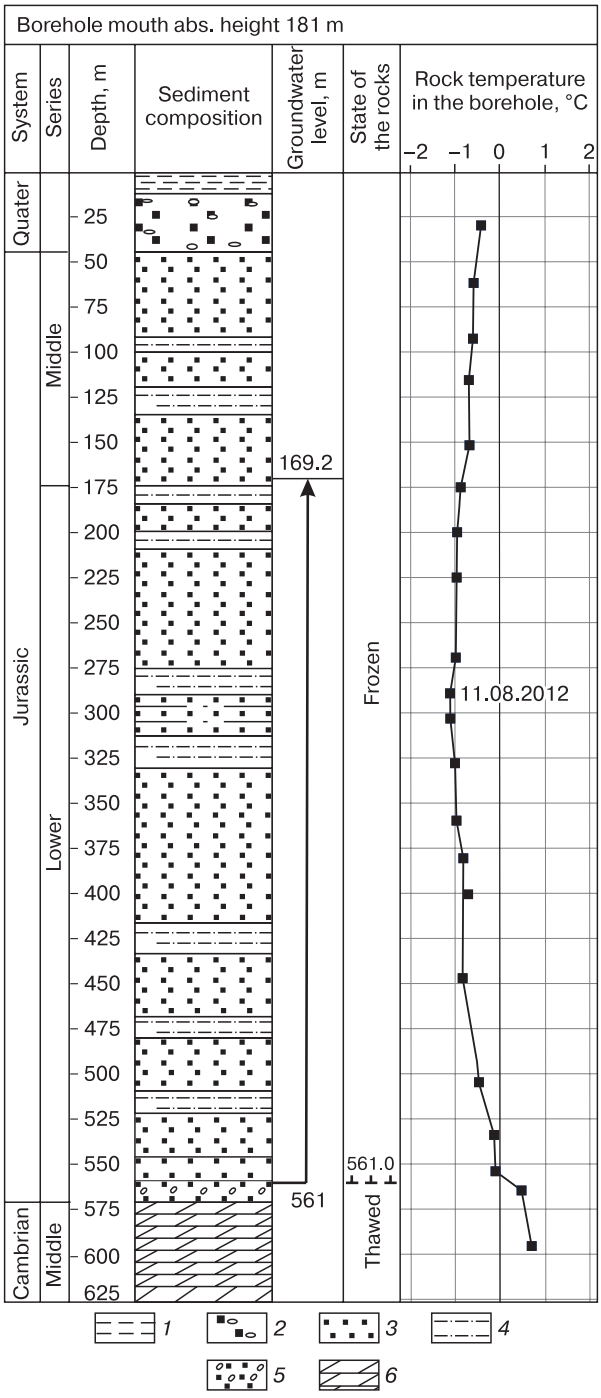

Fig. 4. Geological section and rock temperature distribution in borehole 1 (Churapcha).

1 – loam, *2* – coarse-grained sand with inclusions of fine and coarse gravels, *3* – sandstone, *4* – siltstone, *5* – conglomerate with sandstone interlayers, *6* – limestone.

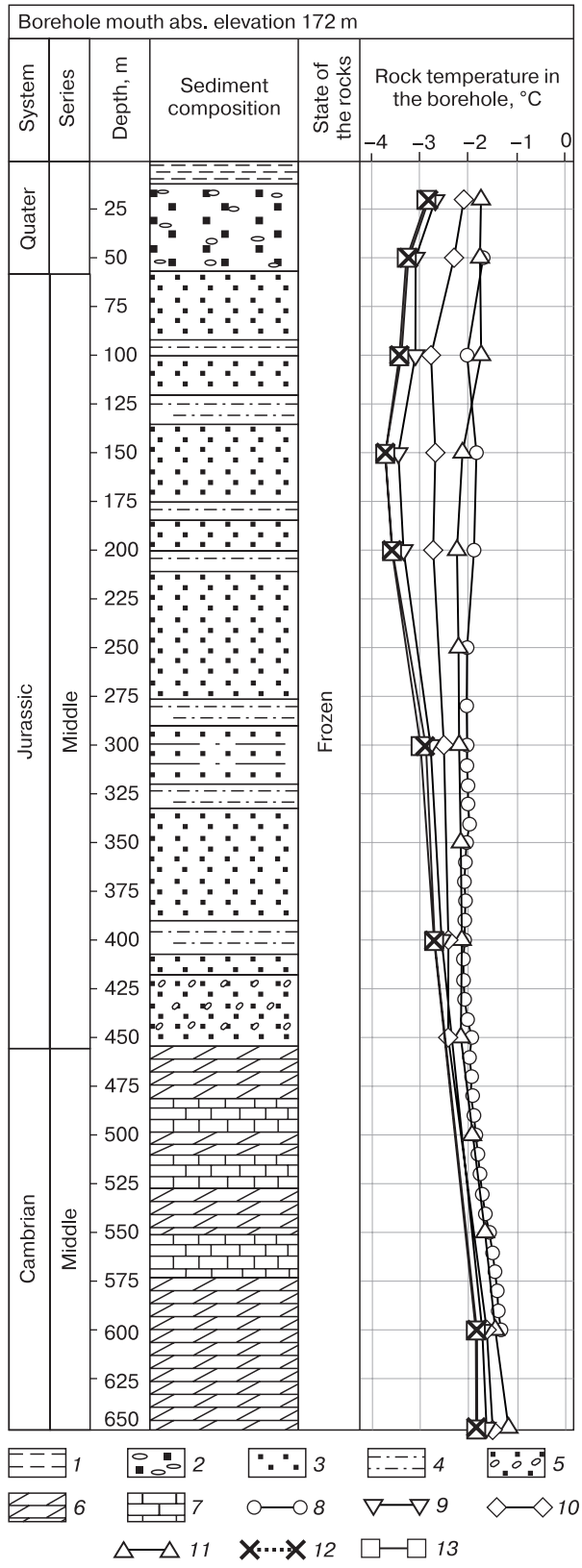

Fig. 5. Geological section and rock temperature distribution in borehole 2 (Dyabyla).

1 – loam, *2* – coarse-grained sand with inclusions of fine and coarse gravels, *3* – sandstone, *4* – siltstone, *5* – conglomerate with sandstone interlayers, *6* – limestone, *7* – dolomite. Dates of temperature measurements: *8* – December 13, 2013; *9* – December 26, 2013; *10* – January 10, 2014; *11* – February 7, 2015; *12* – June 20, 2018; *13* – August 20, 2020.

fractured, aquiferous, and its thickness was 7–8 m. Above this interval, the rocks were in the frozen state; below it, dense limestones that served as a water barrier were present.

In 2013, 9.5 km south of borehole 1, on the outskirts of Dyabyla, hydrogeological borehole 2 was drilled with a design depth of up to 600 m (Fig. 5). Quaternary sediments were represented by loams in the upper 12 m; below, to a depth of 58.8 m, there were gray sands with inclusions of coarse and fine gravels. The underlying Jurassic deposits with a total thickness of 394.2 m were represented by gray fine- and medium-grained quartz-feldspar sandstones with siltstone interlayers. The lower part of Jurassic deposits (from a depth of 412.5 m) was represented by conglomerates with gravels of metamorphic and igneous rocks cemented by calcareous sandstones, with interlayers of medium- and coarse-grained silicified sandstone. Below 453 m, rocks of the Cambrian system – limestones and ferruginous limestones with interlayers of marls and dolomitic limestones – were found. Core samples were taken from typical layers characterizing the strata along the section, and the thermophysical properties of the rocks were determined from them (Table 1).

In the course of drilling borehole 2, water inflows were not recorded. Geothermal measurements carried out immediately after the end of drilling and then after one week showed subzero temperatures along the entire borehole; at the bottom (600 m), the rock temperature was –1.3°C. Further drilling of the borehole continued to a depth of 650 m; however, no water inflow was observed. At the end of drilling, geothermal measurements established a subzero temperature of –1.2°C at the bottom of the borehole.

At the time of the initial geothermal measurements, the temperatures of the rocks along the borehole had not recovered. It was decided to equip the borehole with a stationary geothermal unit to a depth of 650 m. In the period from 2013 to 2020, repeated temperature measurements were taken in the borehole every year. So, after a year and a half, the temperature regime in the borehole changed significantly; in recent years, the temperature of the rocks at the same depth intervals has been constant, which indicates the restoration of the thermal regime.

Temperature curve for borehole 2 has a pronounced non-stationary regime associated with climate warming and the influence of a talik under a nearby lake. The minimum rock temperatures (–3.6°C) are observed at a depth of 150 m; down to this depth, the geothermal gradient has a negative value (–0.6°C/100 m). Below, there is an area with a positive temperature gradient from 0.45 to 0.90°C/100 m, which varies depending on the thermal conductivity of the rocks. Based on six geothermal measurements (2013–2020) and using the method of two and three thermograms [*Kutasov, 1976*], the depth of the zero isotherm (permafrost thickness) was estimated at 750–780 m. An anomalously large permafrost thickness was established for this location in the study area.

Table 1. **Thermophysical properties of rocks in borehole 2**

Depth, m	Rock	λ, W/(m·K)	$a \cdot 10^{-6}$, m^2/s	c_γ, kJ/(m^3·K)
466	Limestone gray	1.88	1.2	1567
486	Limestone light gray	2.05	0.93	2204
500	Dolomite limestone, light gray, massive	2.14	1.4	1529
506	Light gray limestone, drain (micro-granular)	2.28	1.2	1900
522	Limestone with marl, almond-tone texture	2.25	1.01	2228
534	Limestone ferruginate	1.87	1.14	1640
559	Limestone marl, dark gray, microgranular	2.81	1.18	2381
570	Marl dark gray	1.43	0.66	2167
597	Limestone brown with inclusions of gray crushed limestone	2.07	1.19	1739
598	Limestone ferruginous, grayish brown, microgranular	2.21	1.09	2028
605	Limestone ferruginous, brown	2.16	1.15	1878
615	Limestone wavy banded, light gray	2.11	1.6	1319
630	Limestone ferruginous, brown, spotted	2.27	1.33	1707
633	Limestone ferruginous, wavy-banded	2.23	1.23	1813
640	Limestone wavy-banded, brownish gray, microgranular	2.31	1.21	1909
644	Limestone with wavy ferruginous areas, microgranular	2.02	1.3	1554
650	Limestone, interlayering of brown and light gray, microcrystalline	2.34	1.09	2147

Note: λ – thermal conductivity; a – thermal diffusivity; c_γ – volumetric heat capacity.

Thus, in the borehole near the village of Dyabyla, carbonate strata of the Cambrian system are found at a depth of more than 450 m; in the village Churapcha, they occur at a depth of more than 575 m. Thus, a gentle slope of the Cambrian strata from the Yakutian Uplift of the Aldan Anteclise towards the Lower Aldan Depression is traced.

Based on the results of determination of the thermophysical properties of rocks along the section and reference data, it was established that they differ insignificantly in the junction zone of the Cambrian carbonate and Jurassic silicate deposits. Consequent-

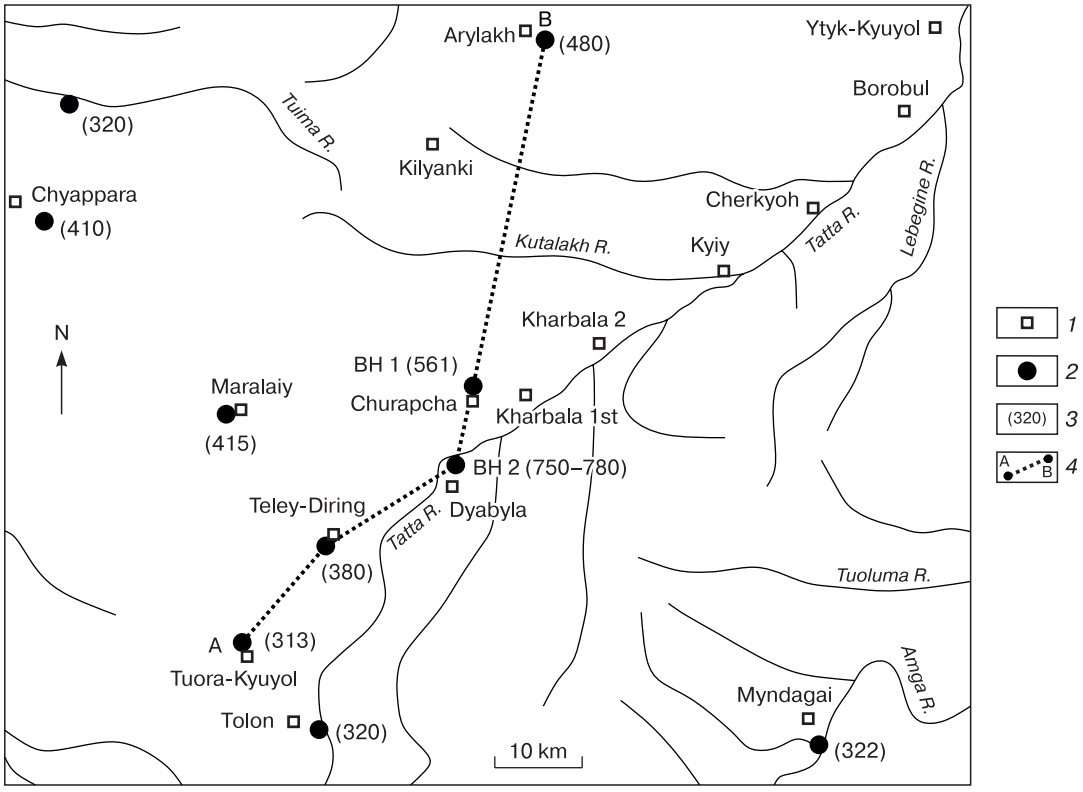

Fig. 6. Scheme of location of boreholes with data on the depth of the base of the frozen strata.

1 – settlements, *2* – hydrogeological boreholes, in which the base of the frozen strata was determined, *3* – depth of the base of frozen strata, *4* – line of geocryological section A–B (see Fig. 7).

ly, a change in the temperature gradient of rocks can only be due to the presence of cracks, as well as the existence of aquifers or ice-saturated horizons [*Geological map..., 2000*].

An analysis of the morphology of the roof of the rocks underlying the Late Pliocene–Quaternary deposits of the Lena–Aldan interfluve [*Kamaletdinov, 1982*] made it possible to establish that modern neo-

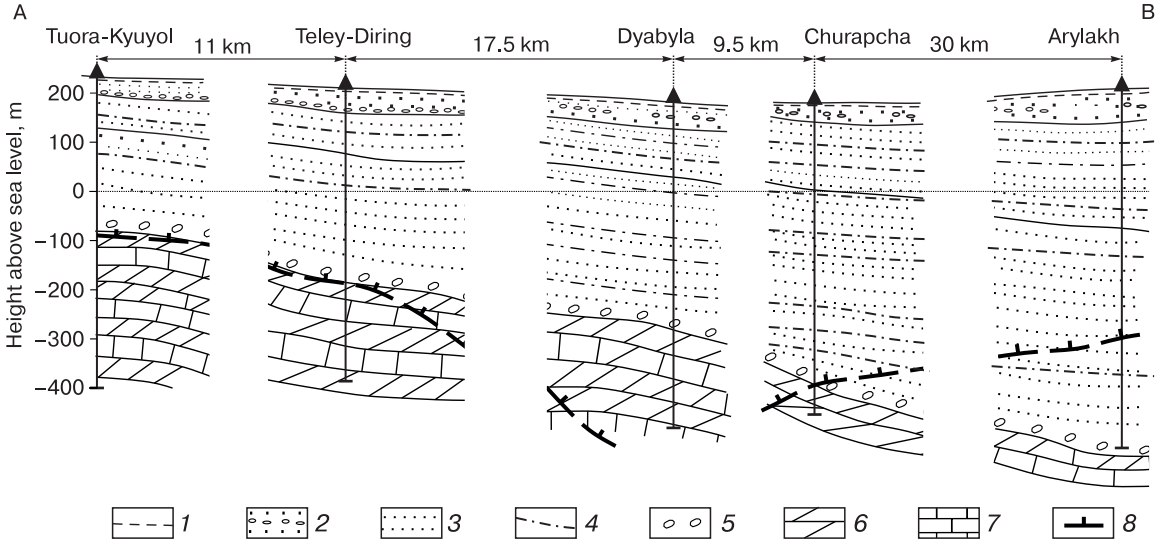

Fig. 7. Schematic geocryological section along profile A–B (see Fig. 6).

1 – loam, *2* – fine- and medium-grained sand with inclusions of fine and coarse gravels, *3* – coarse-grained sandstone, *4* – siltstone, *5* – conglomerate, *6* – limestone, *7* – dolomite, *8* – bottom of the rock mass with subzero temperatures.

tectonic movements and erosional processes had little effect on the vertical amplitudes of geological structures, which is manifested in the structure of the Quaternary strata and in the modern topography of the territory. The influence of changes in the base of erosion during the development of permafrost on the relief was insignificant. Therefore, in the opinion of the authors, the relief of the territory could not strongly affect the freezing depth. Nevertheless, the difference in the depth of the permafrost base in the boreholes is considerable, though the boreholes are found at a relatively small distance from one another. It is difficult to explain such a difference in temperature and thickness of the permafrost by geomorphological or lithological reasons. In this regard, the authors compared and analyzed the position of the permafrost base and the boundaries of sediments of different compositions of different ages (Figs. 6, 7).

According to the authors, the position of the permafrost base is specified by the presence and circulation of groundwater in fractured rocks formed in the course of changes in tectonic and paleogeographic situation rather than by changes in the composition of sediments at the boundary of the Jurassic and Cambrian systems. The formation of the zone of cryogenic disintegration of rocks had a significant influence on the hydrogeothermal conditions, the parameters and depths of which in this area of the Siberian Craton sedimentary section depend on the geological structure of the sedimentary strata and the depth of the crystalline basement during the freezing period.

CONCLUSIONS

1. First geothermal data have been obtained to a depth of 650 m for the Central Yakutia region, within the eastern flank of the Yakutian Uplift at the junction of the Ust-Aldan Depression and the Aldan Anteclise. Temperature distribution in the rocks attest to the nonstationary state of the frozen strata with a negative geothermal gradient to a depth of 150 m.

2. Permafrost thickness in the area of the village of Churapcha, as estimated from geothermal measurements, reaches 750–780 m, which is an anomalously high value for the studied region.

3. From the analysis of geological and geothermal data, it follows that the depth of the permafrost base is controlled by the groundwater circulation in the fractured rocks formed in the course of tectonic and paleogeographic events with a significant influence of cryogenic disintegration rather than by changes in the composition of the rocks at the boundary between the Jurassic and Cambrian deposits.

Funding. *This work was carried out within the framework of state assignment of the Ministry of Science and Higher Education of the Russian Federation no. AAAA-A20-120111690010-2 "Specific features of thermal field and cryogenic strata in the northeast of Russia."*

Rreferences

Balobaev V.T., Shepelev V.V., 2001. Cosmoplanetary climatic cycles and their role in the evolution of the Earth's biosphere. *Dokl. Earth Sciences,* 379 (5), 607–610.

Balobaev V.T., Volod'ko V.N., Devyatkin V.N. et al., 1985. Manual on application of semiconductor thermistors for geocryological measurements. Yakutsk, Melnikov Permafrost Institute, 48 p. (in Russian).

Geocryological map of the USSR on a scale of 1:2 500 000. Ershov E.D., Kondrat'eva K.A. (Eds.), 1997. Vinnitsa, Kart. predpriyatie, 16 sheets (in Russian).

Geodynamic map of Yakutia and adjacent territories on a scale of 1:1 500 000. Parfenov L.M. (Ed.), 1992. Yakutsk, GUBK, 12 sheets (in Russian).

Geological map of Yakutia on a scale of 1:500 000, Central Yakutia block. Kamaletdinov V.A., Grinenko V.S., Slastenov Yu.L. et al. (Eds.), 2000. Yakutsk, YaGPSE, 8 sheets (in Russian).

Ivanov M.S., 1984. Cryogenic structure of the Quaternary deposits in the Lena–Aldan Depression. Novosibirsk, Nauka, 126 p. (in Russian).

Kamaletdinov V.A., 1982. The relief of the basement and the structure of the Quaternary cover of the Lena–Amga interfluve. In: Geology of the Cenozoic of Yakutia. Yakutsk, Izd. Sib. Otd. Akad. Nauk SSSR, 94–103 (in Russian).

Katasonov E.M., Ivanov M.S., 1973. Cryolithology of Central Yakutia: A Guide. Yakutsk, Melnikov Permafrost Institute, 37 p. (in Russian).

Kotlyakov V.M., Lorius K., 2000. Four climatic cycles based on ice core data from a deep borehole at the Vostok station in Antarctica. Izvestiya Ross. Akad. Nauk, Ser. Geogr., no. 1, 7–19 (in Russian).

Kutasov I.M., 1976. Thermal characteristics of boreholes in permafrost areas. Moscow, Nedra, 119 p. (in Russian).

Popov Y., Bayuk I., Parshin A. et al., 2012. New methods and instruments for determination of reservoir thermal properties. In: 37th Workshop on Geothermal Reservoir Engineering (Stanford, California, January 30 – February 1, 2012). Stanford University, 1122–1132.

Popov Yu.A., Pimenov V., Tertychny V., 1983. Achievements in the field of geothermal research of oil and gas fields. Moscow, Moscow State Geological Exploration Academy, 216 p. (in Russian).

Popov Y.A., Pribnow D.F.C., Sass J.H. et al., 1999. Characterization of rock thermal conductivity by high-resolution optical scanning. Geothermics, Elsevier Science Ltd., 253–276.

Shepelev V.V., Tolstikhin O.N., Piguzova V.M. et al., 1984. Permafrost-hydrogeological conditions of Eastern Siberia. Novosibirsk, Nauka, 192 p. (in Russian).

Zheleznyak M.N., 1999. Some aspects of geocryological research in the development of a rational option for the placement of engineering structures and the development of mineral deposits. In: *Far North: Problems of Ecology*. Moscow, Resource-Info, 129–159 (in Russian).

Received July 1, 2021
Revised January 27, 2022
Accepted April 6, 2022

Translated by A.V. Muravyov

EARTH'S CRYOSPHERE
SCIENTIFIC JOURNAL

Earth's Cryosphere, 2022, vol. XXVI, No. 3, pp. 10–17

GEOCRYOLOGICAL MONITORING AND FORECAST

EMERGENCY FORECAST BASED ON PERMAFROST TEMPERATURE MONITORING DATA NEAR AN UNDERGROUND OIL PIPELINE

L.N. Khrustalev[1,*], V.Z. Khilimonyuk[1]

[1] *Lomonosov Moscow State University, Geological Faculty, Leninskie gory 1, Moscow, 119991 Russia*

[*] *Corresponding author; e-mail: lev_kh@rambler.ru*

Permafrost temperature monitoring near underground oil pipelines makes it possible to estimate permafrost thawing depth under structures and predict changes in the soil temperature over time and the time of emergency, in case the latter one will occur in the future. Permafrost temperature monitoring is carried out in close proximity to the oil pipeline and at depths below the bottom of the layer of seasonal temperature fluctuations. The results of monitoring are processed according to the methodology described in the article.

Keywords: *permafrost, oil pipeline, thawing depth, temperature monitoring, forecast, time of emergency.*

***Recommended citation*:** Khrustalev L.N., Khilimonyuk V.Z., 2022. Emergency forecast based on permafrost temperature monitoring data near an underground oil pipeline. *Earth's Cryosphere*, XXVI (3), 10–17.

INTRODUCTION

Any engineering structure on permafrost interacts with the frozen soil base during the entire period of operation. This interaction often leads to negative consequences, so it is necessary to be able to manage, control, and predict it. These actions are known as geotechnical monitoring. The latter is especially important for those structures, where accidents lead to unpredictable environmental consequences; in particular, for oil pipelines. An oil pipeline accident often leads to an oil spill, which is associated with significant damage to the natural environment and even with the withdrawal of vast territories from economic use.

An essential part of geotechnical monitoring is monitoring of permafrost temperature. Temperature monitoring along the main underground oil pipelines is carried out both at potentially dangerous sections equipped before or during the pipeline laying, and selectively on certain sections, where safety concerns appear during pipeline operation. Temperature sensors can be located in the soil directly under the pipeline and in wells in the immediate vicinity of the pipeline. In 2010–2012, JSC "Transneft" together with the Bauman Moscow State Technical University developed and implemented a system for multiple monitoring of geological processes at the experimental sections of the pipeline laying, including technical diagnostics of the pipeline, monitoring of the planned altitudinal position of the pipeline, and parameters characterizing the hydrogeological conditions of the pipeline laying. This system allows one to control the following parameters: the change in the position of the pipeline, the groundwater level, the distribution of soil temperature, the displacement of soil on slopes, and its acceleration under seismic influences [*Lisin, Alexandrov, 2013*]. The control is carried out in an automatic mode with the transmission of information by radio to the information processing center, whose main functions are diagnostics of the monitoring system and display of warning messages about exceeding the threshold values or remaining reserves up to the threshold values of the monitored parameters on the display screen. Thus, the system allows us to constantly monitor the temperature of the oil pipeline and the surrounding soil. This is a sophisticated state-of-the art system, which has not yet become widespread.

In the permafrost area, one of the main tasks of monitoring is to control the development of permafrost thawing around underground oil pipelines. This control is carried out at experimental sites and allows one not only to identify extreme thawing values that endanger the integrity of the pipeline in real time but also to forecast them for the future, which is of especial importance. For this purpose, calibrated mathematical models of thawing zone are used; these models are defined in the Company's regulatory documents.

Calibration is commonly referred to as changing the structure and composition of a mathematical model in such a way that the edited model is adequate "to nature" for each of the parameters set in the mod-

el. Calibration is carried out on the basis of solving the inverse problem of thermal conductivity with phase transition of soil moisture (the so-called Stefan problem). This involves an additional problem related to the fact that the inverse problem of thermal conductivity (restoration of the initial and boundary conditions from the temperatures at certain moments of time) is mathematically incorrect and has no unambiguous solution. Therefore, a direct problem solution is used for calibration, in which the initial and boundary conditions are changed blindly in hope to obtain a result adequate "to nature." This is a long and unpromising way. Today, this process can be significantly simplified by replacing the three-dimensional Stefan problem with a sum of one-dimensional problems, the number of which is determined by the number of calculation points [*Khrustalev, 1971*].

As known, a mathematical model consists of two parts that can be referred to as the core and the shell. By the core, we will understand the numerical solutions of the Stefan problem; by the shell, we will understand the initial data necessary for this. Core can be different (for example, numerical solutions of the Stefan problem by the finite difference method using explicit and implicit schemes and the finite element method) and the calculation result with the same source data will always be the same, because the difference in modeling results is determined only by the difference in shells, i.e. by the source data. Therefore, calibration of a mathematical model is an adjustment of the initial data to obtain the desired result. It does not matter, which core the model contains. Moreover, under certain conditions, the core may be not numerical, but analytical. Based on these considerations, a fast calibration method was developed for a mathematical model of the interaction of an underground pipeline with host frozen soils [*Gunar et al., 2021*], which made it possible to significantly simplify the calibration method and to obtain a reliable tool for predicting permafrost thawing zone around an underground water pipeline or oil pipeline. However, this method is not free from shortcomings. Thus, to use a mathematical model, it is necessary to set the boundary and initial conditions, as well as thermophysical properties of soils, which is not always possible, because some of the information is lost over time. In this regard, the technique described below has clear advantages, in particular, the possibility of using it for unequipped sites.

FORECASTING TECHNIQUE

For unequipped sites that are discussed below, direct control over the development of thawing is impossible, because borehole drilling near the oil pipeline is strictly prohibited. However, by drilling a borehole at a minimum distance from the pipeline, which is determined by safety requirements (at a distance of 0.5–1.5 m from the element of the pipe) and measuring the temperature of frozen soil in this borehole, it is possible to estimate the depth of permafrost under the center of the pipeline at the moment. The soil temperature o should be measured no higher than the bottom of the layer of annual temperature fluctuations. This will allow us to take the current temperature values as the mean annual values and to determine the soil thawing depth from them. This is the first problem, the solution of which is considered in this article.

If such temperature measurements are carried out regularly, a temporary sample of temperatures will be obtained, which can then be extrapolated over time to obtain a forecast temperature for a given period (forecast period). Only one difficulty is faced here: the choice of extrapolation function. This is the second problem considered in this article.

Having predicted temperatures and using solution of the first problem, it is possible to calculate the depth of permafrost thawing under the pipeline for the forecast period.

It remains only to clarify whether the soil subsidence, at this depth of thawing, will cause an oil pipeline accident and, if so, when this accident will occur. This is the third problem to be discussed in this paper.

Calculation of the depth of permafrost thawing under an underground oil pipeline based on the results of temperature measurements in a closely located borehole

The calculations are based on the idea of a quasistationary ground temperature field (mean annual temperatures) in the area adjacent to the pipeline, which is formed during the development of permafrost thawing around the pipeline. Its analytical description can be found, for example, in the monograph [*Porkhaev, 1970*]. Knowing the mean annual ground temperature at certain points of this field, it is possible to judge the thawing depth under the pipeline. To do this, it is necessary to solve a system of transcendental equations with two unknowns: the depth of permafrost thawing under the central part of the pipeline as measured from the ground surface (h) and the soil temperature at the depth of zero annual heat turnover, which existed in natural conditions before the beginning of the pipeline operation (T_0).

Let us write down this system for two observation points (x, y_i) and (x, y_{i+k}), which are located in a test borehole near an oil pipeline (from 0.5 to 2.0 m):

$$\begin{cases} T(x,y_i)-T_{bf}=(T_0-T_{bf})\dfrac{f(0,h)-f(x,y_i)}{f(0,h)}, \\ T(x,y_{i+k})-T_{bf}=(T_0-T_{bf})\dfrac{f(0,h)-f(x,y_{i+k})}{f(0,h)}, \end{cases} \quad (1)$$

where x is the distance from the observation borehole to the axis of the oil pipeline, m; y_i, y_{i+k} are the depths

of the temperature sensors in the observation borehole, m; $T(x, y_i)$, $T(x, y_{i+k})$ are subzero mean annual ground temperatures at two observation points, °C; T_0 is the ground temperature at the depth of zero annual heat turnover under natural conditions before the start of the pipeline operation, °C; T_{bf} is the temperature of the beginning of soil freezing, °C; and h is the depth of permafrost thawing under the middle of the pipeline measured from the soil surface, m.

The coordinate function is determined by the formula

$$f(x,y)=\frac{1}{2A_p}\ln\frac{x^2+\left(y+\sqrt{h_p^2-r_{ins}^2}\right)^2}{x^2+\left(y-\sqrt{h_p^2-r_{ins}^2}\right)^2},$$

$$A_p=\ln\left(\frac{h_p}{r_{ins}}+\sqrt{\frac{h_p^2}{r_{ins}^2}-1}\right),$$

where x, y are the coordinates of the point, m; h_p is the distance from the soil surface to the center of the underground oil pipeline, m; and r_{ins} is the radius of the oil pipeline with circular thermal insulation along its external generating line, m.

The solution of Eq. (1) is carried out by the iteration method. As a result, an array of data is formed equal to the number of combinations (by two) of temperature measurements at depth points (according to the number of unknowns in Eq. (1)). Naturally, the average value of this array should be taken for the calculation. To facilitate calculations, the authors have developed a computer program (macro 1, see Appendix).

Permafrost temperature forecast based on initial observations in the monitoring borehole

Predictive calculations of temperature fields based on actual soil temperatures constitute the problem of extrapolating the actual temperatures specified on a discrete set of measurement moments in time. In this case, the so-called inverse problem of thermal conductivity arises. As noted above, this problem is mathematically incorrect and does not have a precise analytical solution.

A compromise approach, in which the physical essence of the problem serves as the basis for finding a class of support functions that allow finding the best extrapolation function by relatively simple calculations, seems to be reasonable.

To implement this, the authors used an approximate method for calculating temperature fields in the construction basements, which was developed in 1971 and called the equivalent temperature method [*Khrustalev, 1971*]. Its idea is to reduce the three-dimensional problem of thermal conductivity to a set of one-dimensional problems (according to the number of calculated points). Omitting the details that can be found in [*Khrustalev, 1971*], we can express the dependence of temperature (T) on time (τ) in the form:

$$T(\tau)=aE(\tau)+b,$$

$$E(\tau)=1-\mathrm{erf}\left(\frac{y}{2\sqrt{(\lambda_f/C_f)\tau}}\right), \qquad (2)$$

where a and b are unknown parameters associated with equivalent and initial temperatures; y is the depth of the calculated point; C_f is the volumetric heat capacity of frozen soil, W·h/(m^3·°C); λ_f is the thermal conductivity coefficient of frozen soil, W/(m·°C); erf is the probability integral, tabulated function.

To determine unknown parameters, we have the values of soil temperature T_i, measured at certain moments of time τ_i and constituting a system of equations:

$$a_iE_{ij}+b_i=T_{ij},\ i=1, 2, ..., n,\ j=1, 2, ..., m,$$

where n is the number of temperature measurement points in the borehole; m is the number of temperature measurements in time, separated by a period of a number of years; E_{ij} is the value of the function (2) at point (x, y_i) in time τ_j.

Thus, for each i-th point we have a set of m equations. Grouping them into pairs, we get $m/2$ systems of equations equal to the number of combinations of elements of this set by two ($m/2$), of the following form:

$$\begin{cases}a_iE_{i,j}+b_i=T_{i,j},\\ a_iE_{i,j+k}+b_i=T_{i,j+k}.\end{cases} \qquad (3)$$

Having solved the system of Eqs. (3), we will obtain the values a_i and b_i. There will be $m/2$ of such values according to the number of equations. It is natural to take their average value as a_i^{av}, b_i^{av} for calculation. After that, we will get an extrapolation formula in time for each depth at which the temperature was measured:

$$T(x,y_i,\tau)=a_i^{av}\left(1-\mathrm{erf}\frac{y_i}{2\sqrt{(\lambda_f/C_f)\tau}}\right)+b_i^{av}, \qquad (4)$$

where $T(x, y_i, \tau)$ is the predicted temperature at point (x, y_i) at the moment τ, °C; τ is the forecast period counted from the start of operation of the pipeline, years.

The duration of observations is determined by the forecast period. Usually, when extrapolating, the ratio of the forecast period to the observation period is 1:3, if linear polynomials are used as an extrapolation function. In our case, the extrapolation function is found from an approximate analytical solution of a physical problem, to which this restriction does not apply. The calculations below show that it can be equal to 2:1.

To facilitate calculations according to Eq. (4), the authors have developed a computer program (macro 2, Appendix).

Calculation of the emergency subsidence of underground oil pipeline and the critical depth of permafrost thawing under its central part

The calculation of the maximum subsidence is carried out according to the methodology described in the monograph [*Tartakovsky, 1976*]. This calculation consists in checking four limiting conditions for a given subsidence. A subsidence is considered an emergency if one or several conditions are violated. The limiting conditions are given below.

1. Pipe strength condition:

$$\lim 1 = \frac{1}{\gamma_n} \cdot \frac{\sigma_{tem}}{|\sigma_{\lim N}|} \geq 1,$$

where $\sigma_{\lim N}$ is the total longitudinal strain in the pipe, Pa; γ_n is a dimensionless reliability coefficient taken from 1.0 to 1.1 according to [*SNiP 2.05.06-85*, 2005*]; σ_{tem} is the temporal steel strength, Pa according to [*GOST TU 14-3-1344-85, 1985*]. The total longitudinal strain is equal to

$$\sigma_{\lim N} = 0.3\sigma_{cir} + \sigma_T + \sigma_s,$$

where σ_{cir} is the circular strain caused by the internal pressure in the pipe, Pa; σ_T, σ_s are the longitudinal strains in the pipe from temperature changes and elastic bending of the pipeline during its subsidence, respectively, Pa. Their values are determined by the following formulas:

$$\sigma_{cir} = 1.15\frac{p_p d_{p,in}}{2\delta_p},$$

$$\sigma_T = E_{st}\alpha_T \Delta T,$$

$$\sigma_s = 3\cdot 10^5 \psi_p \sqrt{\frac{q_{ent} s}{\beta_1 d_p \delta_p}},$$

where p_p is the internal pressure in the pipe, Pa; $d_{p,in}$ is the inner diameter of the pipe, m; δ_p is the wall thickness of the pipe, m; E_{st} is the modulus of elasticity of steel, $2\cdot 10^{11}$ Pa; α_T is the coefficient of linear expansion of steel, $1.2\cdot 10^{-5}$ 1/°C; ΔT is the difference between maximum and minimum pipe wall temperatures during the entire time of operation of the pipeline; it is assumed to be 40°C for underground pipelines; d_p is the outer diameter of the pipe, m; s is the subsidence of the pipeline during permafrost thawing, m; ψ_p, β_1 are dimensionless coefficients determining the operation of the pipe on an elastic base during bending and depending on the length of the section (L_{sp}, m) of the pipeline subjected to bending; and q_{ent} is the total weight loading on 1 m of the pipe, N/m.

The length of the pipeline section subjected to bending during its subsidence is determined by the fitting according to the formulas:

$$L_{sp} = \sqrt[4]{\frac{384 E_{st} I_p s}{\beta_1 q_{ent}}},$$

$$\beta_1 = 1 + 6w + 16w^2,$$

$$w = \frac{14\,389 d_p}{L_{sp}\sqrt[3]{\left(k_b L_{sp} d_p\right)/\delta_p}},$$

$$\psi_p = \frac{10 + 15w + 6w^2}{10(1+2w)},$$

where I_p is the equatorial moment of inertia of the pipe section: $I_p = \pi\left(d_p^4 - d_{p,in}^4\right)/64$; k_b is the coefficient of the bed, N/m^3; w is the auxiliary design parameter; q_{ent} is the total weight load per 1 m of pipe, N/m. The total weight load is equal to

$$q_{ent} = 1.1\left(q_p + q_{ins} + q_{pr} + q_{ba} + q_{soil}\right),$$

where q_p, q_{ins}, q_{pr}, q_{ba}, q_{soil} are the weights of 1 m of the pipe, insulation, product, ballast, and soil lying on the pipe, N/m. The values are determined by the following formulas:

$$q_p = \frac{\pi}{4}\rho_{st} g\left(d_p^2 - d_{p,in}^2\right),$$

$$q_{ins} = \frac{\pi}{4}\rho_{ins} g\left(d_{ins}^2 - d_p^2\right),$$

$$q_{pr} = \frac{\pi}{4}\rho_{pr} g d_{p,in}^2,$$

$$q_{soil} = 0.88 g \rho_{th} d_{ins} h_p,$$

$$q_{ba} = \frac{\rho_{ba}}{\rho_{ba} - \rho_w} q_{ba,w},$$

$$q_{ba,w} = 1.05 g \rho_w \frac{\pi d_{ins}^2}{4} - 0.95\left(q_p + q_{ins}\right) - q_{soil,w},$$

$$q_{soil,w} = \frac{\rho_s - \rho_w}{\rho_s (1 + w_{tot})} q_{soil},$$

where ρ_{st}, ρ_{ins}, ρ_{pr}, ρ_{th}, ρ_{ba}, ρ_w, ρ_s are the densities of steel, thermal insulation, transported liquid, thawed soil, ballast, water, soil particles, kg/m^3; w_{tot} is the total moisture content of frozen soil, decimal fraction; d_{ins} is the outer diameter of the pipeline with circular thermal insulation, m; h_p is the distance from the soil surface to the center of the underground pipeline, m; and g is the acceleration of gravity, 9.81 m/s^2.

The bed coefficient is determined by the formula

$$k_b = 0.523E/d_p,$$

where E is the modulus of deformation of thawed soil, Pa.

2. The condition of stability of the pipe in the longitudinal direction:

$$\lim 2 = \frac{N_{\lim}}{(0.2\sigma_{cir} + \sigma_T) F_p} \geq 1,$$

where $F_p = (\pi/4)\left(d_p^2 - d_{p,in}^2\right)$; $N_{\lim}$ are the maximum compressive forces that can be perceived by the pipe without losing its stability in the longitudinal direction, N. The formulas by which these values are determined:

$$N_{\lim} = \min \begin{cases} 4.09\sqrt[11]{p_0^2 q_H^4 F_p^2 E_{st}^5 I_p^3}, \\ 2\sqrt{k_b d_p E_{st} I_p}, \end{cases}$$

$$p_0 = \pi d_p (p_1 \operatorname{tg} \varphi + c),$$

$$p_1 = \frac{1.6 g \rho_{th} h_p d_p \left[1 + \operatorname{tg}^2\left((\pi/4) - 0.5\varphi\right)\right] + q_1}{\pi d_p},$$

$$q_1 = 0.95\left(q_p + q_{ins} + q_{ba}\right),$$

$$q_H = q_1 + 0.8 g \rho_{th} d_p \left(h_p - \frac{\pi d_p}{8}\right),$$

where φ is the angle of internal friction of thawed soil, rad; c is the traction of thawed soil, Pa. The remaining values are given above.

3–4. Conditions for the absence of elastic deformations in the pipe:

$$\lim 3 = \frac{1}{\gamma_n} \frac{\sigma_{fl}}{|\sigma_{\lim N}|} \geq 1,$$

$$\lim 4 = \frac{1}{\gamma_n} \frac{\sigma_{fl}}{|\sigma_{cir}|} \geq 1,$$

where σ_{fl} is the flow stress of steel, Pa.

The algorithm to determine emergency subsidence (s_u) implies multiple checking of limit conditions by setting the subsidence of the pipeline and increasing it every time until a violation of at least one of the limiting conditions. The pipeline subsidence corresponding to this event is considered an emergency. Knowing s_u, it is easy to calculate the critical depth of thawing, H_{cr}, under the pipeline . The calculation is carried out according to the formula

$$H_{cr} = \frac{s_u}{\delta} + h_p + \frac{d_{ins}}{2},$$

where s_u is the value of the emergency subsidence, m; δ it the relative subsidence during permafrost thawing, fraction of a unity.

The value of δ depends on the ice content of the soil, g_i, and is determined in laboratory from samples taken from the control borehole, or according to the table, as a function of g_i [*STO Gazprom..., 2008*]. In turn, g_i is calculated by the formula $g_i = \rho_{d,f}(w_{tot} - w_w)$, where w_{tot} is the total soil moisture; is the moisture due to unfrozen water; $\rho_{d,f}$ is the density of dry frozen soil, kg/m^3.To facilitate the calculations of s_u and H_{cr}, the authors have developed a computer program (macro 3, see Appendix).

In conclusion, we have to note two important circumstances:

(1) The technique is developed only for permafrost without residual thaw layer (permafrost table merging with the active layer).

(2) The technique, as well as the vast majority of methods for the analytical calculation of bowls and halos of thawing at the basements of constructions, is based on the fact that the soils are homogeneous. In the case of layered soil, the averaged soil characteristics are taken into account. The calculations are carried out within the depth of the averaging to average the coefficients of the thermal conductivity of the soil and other characteristics according to the following formulas:

$$\lambda = \sum_{i=1}^{n} h_i \Big/ \sum_{i=1}^{n} \frac{1}{\lambda_i} h_i,$$

$$A = \sum_{i=1}^{n} A_i h_i \Big/ \sum_{i=1}^{n} h_i,$$

where λ_i, A_i are the numerical values of the ground characteristics of the i-th layer; h_i is the thickness of the i-th layer; n is the number of i-th layers within the depth of averaging. The depth of the location of the deepest temperature sensor in the control borehole is taken as the averaging depth.

VERIFICATION OF THE METHODOLOGY

Comparison of the calculated data with experimental observations in our case will be conventional, because everything concerning the state of existing oil pipelines is a closed information. To complete the task, we will replace the actual data of the results of mathematical modeling using the QFrost software [*Pesotsky, 2016*]. We accept a two-dimensional model, with the computational domain size of 48 × 48 m (Fig. 1).

The designed dimensions of the pipeline are as follows: the radius along the outer circular insulation r_{ins} = 0.75 m, the distance from the earth surface to the center of the pipeline h_p = 1.75 m. The climatic characteristics are taken from data of the Amga weather station (30-yr-long period) in the Republic of Sakha (Yakutia). Let us formulate the boundary conditions of the third kind at the upper boundary of the computational domain (Table 1). On the surface of the circular insulation of the oil pipeline, we assume a boundary condition of the first kind: T_p = 20°C (T_p is the temperature on the surface of the circular insulation of the pipeline); for other boundaries, a boundary condition of the second kind with zero heat

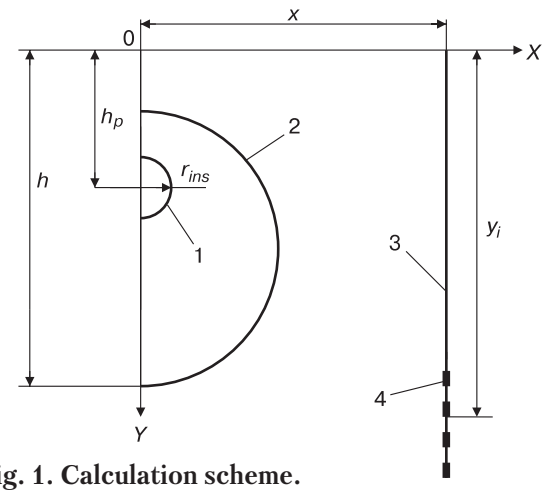

Fig. 1. Calculation scheme.

1 – oil pipeline; 2 – permafrost thawing boundary around the pipeline; 3 – control borehole; 4 – temperature sensor; r_{ins} – radius for the outer boundary of circular insulation; h_p – distance from the ground surface to the center of the pipeline; h – thawing depth under the pipeline; y_i – distance from the earth surface to the temperature sensor (measuring point).

flow is taken. The soil containing the oil pipeline is represented by loam with the following characteristics: thermal conductivity in thawed and frozen state (W/(m·°C)): λ_{th} = 1.33, λ_f = 1.51; volumetric heat capacity in thawed and frozen state (W·h/(m^3·°C)): C_{th} = 777, C_f = 592; density of frozen soil in the dry state $\rho_{d,f}$ = 1600 kg/m^3; the total moisture content of the frozen soil w_{tot} = 0.2; and the amount of unfrozen water w_w = 0.05.

October 1 was taken as the starting date of the simulation. To establish the temperature distribution curve by the depth, a preliminary solution of the linear problem was carried out using the QFrost software.

The depth of the computational domain is assumed to be 48 m. At the upper boundary of the computational domain, a boundary condition of the 3rd kind is set according to Table 1. At the lower and lateral boundaries, the 2nd kind condition is set: the value of the heat flow is taken equal to zero. Modeling was carried out until the establishment of a quasistationary state of the temperature regime of soils. The results of simulation are shown in Table 2.

Table 1. **Boundary conditions of the 3rd kind on the ground surface**

Month	T, °C	α, W/(m^2·°C)	Month	T, °C	α, W/(m^2·°C)
I	–42.0	0.75	VII	18.8	4.2
II	–35.6	0.68	VIII	14.9	4.2
III	–22.0	0.69	IX	6.1	4.2
IV	–6.8	1.31	X	–7.9	2.84
V	6.2	4.2	XI	–28.2	1.09
VI	15.6	4.2	XII	–39.5	0.95

Note: T is the mean monthly air temperature; α is the heat exchange coefficient at the soil surface.

Using macro 1 (see Appendix), we recalculate the modeling data on soil temperature into the depths of thawing and compare them with the depths obtained as a result of modeling using the QFrost software (Fig. 2).

As one can see, the coincidence is not perfect, but it is quite acceptable. Thus, according to this test, our first "temperature–depth" technique is valid.

Using macro 2 (see Appendix), we make a forecast of changes in soil temperature to a depth of 20, 25 m and evaluate it based on the results of modeling. Doing this, we formulate two problems:

(1) For the observation period, we take the period from the 1st to the 5th year (Table 2), for the decadal forecast period.

(2) For the observation period, we take the period from the 1st to the 10th year (Table 2) for the forecast period of three decades.

The results of corresponding calculations are given in Tables 3 and 4.

Table 2. **Changes in the depth of permafrost thawing and soil temperatures under the central part of the pipeline and the temperature of the soil**

Time, years	Depth of thawing, m	Temperature* according to modeling data at a depth (m)					
		15.25	16.25	17.25	18.25	19.25	20.25
0	0	4.82	4.80	4.78	4.77	4.76	4.75
1	5.66	4.60	4.65	4.68	4.70	4.72	4.73
2	6.74	4.15	4.27	4.37	4.45	4.51	4.57
3	7.50	3.75	3.91	4.04	4.16	4.26	4.34
4	8.02	3.45	3.60	3.76	3.90	4.02	4.12
5	8.51	3.15	3.35	3.52	3.67	3.80	3.92
10	10.1	2.32	2.54	2.74	2.92	3.08	3.23
30	13.0	1.15	1.38	1.58	1.77	1.94	2.10

*Temperature of the soil at a distance of 4.25 m from the pipeline axis.

It is difficult to judge the reliability of the proposed method (observed temperature – predicted temperature) only from data in Tables 3 and 4. Therefore, using macro 1 (Appendix), we recalculate the predicted ground temperatures indicated in Tables 3 and 4 into the predicted thawing depths and compare them with the depths obtained as a result of modeling (Table 5).

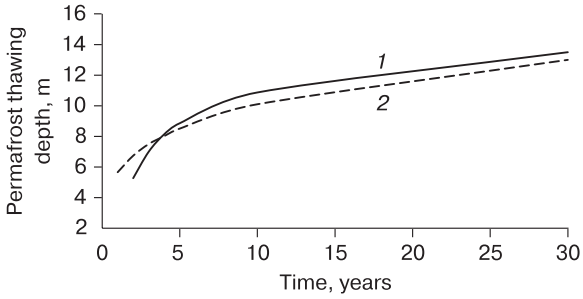

Fig. 2. Dependence of permafrost thawing depth under the oil pipeline on time.

1 – the results of mathematical modeling; *2* – the results of calculation of permafrost temperature at a distance of 4.25 m from the pipeline axis.

Table 3. **Forecast of permafrost temperature as based on the results of modeling for 10 years**

Depth, m	Temperature, °C	
	forecast	modeling data
15.25	–2.84	–2.32
16.25	–2.92	–2.54
17.25	–3.08	–2.74
18.25	–3.17	–2.92
19.25	–3.26	–3.08
20.25	–3.67	–3.23

Table 4. **Forecast of permafrost temperature as based on the results of modeling for 30 years**

Depth, m	Temperature, °C	
	forecast	modeling data
15.25	–1.73	–1.15
16.25	–1.88	–1.38
17.25	–2.10	–1.58
18.25	–2.22	–1.77
19.25	–2.33	–1.94
20.25	–2.95	–2.10

Table 5. **Forecast of permafrost thawing depth under the central part of the pipeline as based on the forecast temperature**

Time, years		Depth of permafrost thawing, m		Forecast error, %
observations	forecast	forecast	modeling data	
5	10	9.13	10.1	9.6
10	30	12.39	13.0	4.7

Table 5 presents generalized data. They indicate that the proposed methodology "Prediction of the depth of permafrost thawing under an underground oil pipeline based on the results of observations of soil temperature in a closely located borehole" gives satisfactory results.

Example of calculating the possibility of an oil pipeline emergency

Let us summarize the above statements. For this, we will consider a problem covering all aspects of the proposed methodology: we will estimate the time of occurrence (non-occurrence) of an oil pipeline emergency from the results of initial observations of soil temperature in a borehole located close to the oil pipeline. The sequence of actions is as follows.

Conditionally, the results of mathematical modeling for the first 10 years (Table 2) are taken as initial observations in a borehole located at a distance of 4.25 m from the axis of the pipeline. Using this spatio-temporal sampling of temperatures, we determine the forecast temperature fields for the periods of 15, 20, 25 and 30 years. Further, using the obtained temperature fields, we find the depth of permafrost thawing under the central part of the pipeline, which we then compare with the critical depth of thawing and determine the time when the predicted thawing depth will reach the critical level. The soil characteristics are assumed to be equal to the soil characteristics used in in mathematical modeling.

Sequentially using macros 2, 1, and 3 (see Appendix), we obtain data that allow us to draw graphs (Fig. 3).

As can be seen, before the end of the pipeline operation period, the critical depth is greater than the predicted depth, which indicates the absence of an emergency situation because of permafrost thawing.

Thus, only on the basis of initial observations of the soil temperature, the authors came to the conclusion about the oil pipeline basement safety.

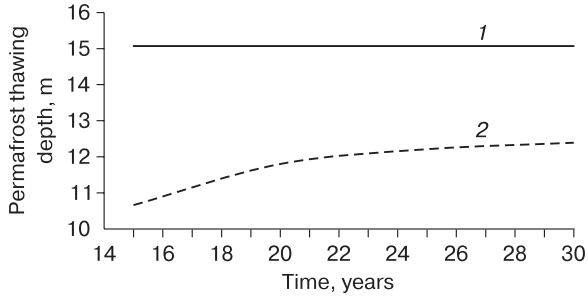

Fig. 3. Permafrost thawing depth under the central part of the pipeline (from the soil surface).

1 – the result of the forecast; *2* – the critical thawing depth.

CONCLUSIONS

1. The proposed methodology for predicting the emergency situation of an underground oil pipeline based on the results of observations of the ground temperature in a nearby borehole is simple to use; it can be applied to sections of an oil pipeline within permafrost areas without a comprehensive system of permafrost temperature monitoring.

2. The technique is applicable only in permafrost areas without a residual thaw layer.

3. The application of this technique allows one to judge the reliability or unreliability of the oil pipeline basement from temperature observations in a borehole drilled at a safe distance (0.5–1.5 m) from an underground oil pipeline.

The data presented in this article indicate that this technique ensures quite satisfactory results and can be recommended for practical use.

References

GOST (State Standard) TU 14-3-1344-85, 1985. Seamless Thin-Walled Pipes Made of Steel (Grades EP288 and EP288SH). Technical Specifications. Moscow, Izd-vo Standartov, 15 p. (in Russian).

Gunar A.Yu., Khilimonyuk V.Z., Khrustalev L.N., Pelich E.A., Korotkov A.A., 2021. An express method for calibration of a mathematical model of the interaction of underground pipeline with permafrost soils. *Nauka Tekhnol. Truboprovodn. Transp. Nefti Nefteproduktov*, **11** (2), 126–135 (in Russian).

Khrustalev L.N., 1971. Temperature Regime of Permafrost in the Built-Up Area. Moscow, Nauka, 168 p. (in Russian).

Lisin Yu.V., Alexandrov A.A., 2013. Monitoring of oil pipelines in difficult geological conditions. *Nauka Tekhnol. Truboprovodn. Transp. Nefti Nefteproduktov*, **2** (10), 22–27 (in Russian).

Pesotsky D.G., 2016. State Register of Computer Programs. Qfrost program for calculating the thermal interaction of structures with permafrost. Certificate No. 2016614404 (April 22, 2016).

Porkhaev G.V., 1970. Thermal Interaction of Buildings and Structures with Permafrost. Moscow, Nauka, 208 p. (in Russian).

SNiP 2.05.06-85*, 2005. Trunk Pipelines. Moscow, FGUP TsPP, 60 p. (in Russian).

STO Gazprom 2-3. 1-233-2008, 2008. Regulatory Documents for the Design, Construction and Operation of JSC Gazprom's Facilities. Methodology for Conducting Geocryological Surveys in the Exploration and Development of Deposits. Gazprom Standard, 120 p. (in Russian).

Tartakovsky G.A., 1976. Construction Mechanics of Pipelines. Moscow, Nedra, 224 p. (in Russian).

Appendix. – https://yadi.sk/d/xva4hnsryVklgA

Received June 1, 2021
Revised October 10, 2021
Accepted April 17, 2022

Translated by S.B. Sokolov

APPENDIX

The computer programs (macros) offered to the reader are written in the Visual Basic language using the Excel 2007 platform (VBA Excel). To view them, you should press the "Developer" key on the Excel sheet corresponding to the selected macro in the command line and then the "Visual Basic" key. The programs are ready for practical use, for which the user must perform only two simple operations: fill in the yellow field on the Excel sheet with their source data and make one mouse click on the "Start" button placed at the top of the sheet. The result of the calculation can be read on the gray field of this sheet.

Access to the programs is provided through URL: https://yadi.sk/d/xva4hnsryVklgA

EARTH'S CRYOSPHERE
SCIENTIFIC JOURNAL

Earth's Cryosphere, 2022, vol. XXVI, No. 3, pp. 18–25

PROPERTIES OF FROZEN GROUND AND ICE

TANGENTIAL FROST HEAVING FORCES OF CLAY AND SANDY SOILS ACTING ALONG THE METAL SURFACE

A.G. Alekseev[1,2,*]

[1] *Gersevanov Research Institute of Bases and Underground Structures, Vtoraya Institutskaya ul. 6, Moscow, 109428 Russia*
[2] *Moscow State University of Civil Engineering, Yaroslavskoye sh. 26, Moscow, 129337 Russia*

**Corresponding author; e-mail: adr-alekseev@yandex.ru*

The results of experimental studies of the tangential frost heaving forces of clay and sandy soils in laboratory conditions on three installations with different single-plane shear rates at constant normal load are presented. The installations made it possible to perform conditionally instantaneous shift, long-term tests with the application of a stepwise shifting load and a shift at a constant speed. As a result of complex studies, the dependences of shear resistance or equivalent tangential forces of frost heaving of sand and loam on water content (from 10 to 28%) and temperature (from 0 to –10°C) on the metal surface have been established. An increase in soil water content and a decrease in soil temperature leads to an increase in the resistance to soil shear. The shear resistance of sand is up to two times higher than similar values for loam under identical shear conditions, temperature and water content. An increase in soil moisture leads to an increase in the contact area of soil particles through ice layers with a metal foundation and to an increase in the bonds between the particles as a result of an increase in the volume of ice. It is established that the resistance to conditionally instantaneous shear is up to three times higher than the values of extremely long-term shear resistance and shear at a constant speed under similar thermal humidity conditions.

Keywords: *tangential forces, frost heaving forces, frozen soil, resistance to the shift, foundation surface, laboratory studies.*

Recommended citation: Alekseev A.G., 2022. Tangential frost heaving forces of clay and sandy soils acting along the metal surface. *Earth's Cryosphere*, XXVI (3), 18–25.

INTRODUCTION

When building foundations in heaving soils below the depth of seasonal freezing, frost heaving forces act on the foundation along its lateral surface. Under the action of frost heaving, the foundations are deformed: they move upwards and, according to some observations, the displacement reaches 15 cm or more, and the magnitude of the tangential heaving forces exceeds 200 kN [*Safronov, 1985; Ivanin et al., 2020; Shulyatiev, 2020*]. Deformation of structures under the action of tangential forces of frost heaving leads to significant costs for the restoration of damaged structures. Therefore, the assessment of the magnitude of the tangential forces of frost heaving is an important scientific and practical task.

The tangential forces of frost heaving were quite actively studied in the Soviet Union [*Dalmatov, 1957; Dubnov, 1967; Peretrukhin, 1967; Orlov et al., 1977*]. Laboratory studies by B.I. Dalmatov [*1957*] and then Yu.D. Dubnov [*1967*] made it possible to establish the following regularity: the value of stable freezing forces is close to the value of tangential forces of frost heaving of soils. As a design characteristic, the steady value of freezing resistance under certain permafrost-soil conditions should be taken [*Dubnov, 1967*]. The experiments of Yu.D. Dubnov showed that a consistent increase or decrease in the speed of soil movement according to the foundation model does not change the value of stable freezing resistance, provided that the speed of soil movement differs by no more than ten times. A change in the speed of soil movement by 50–100 times has a significant effect, which changes the stable freezing resistance by 40–50%. Under natural conditions, there are no sharp changes in the speed of soil movement along the foundation, so the effect of speed when measuring stable freezing resistance under laboratory conditions can be ignored. To reduce the experiment time, the recommended rate of soil movement along the foundation material is 10–20 mm/day.

Similar time dependences of the tangential frost heaving forces and heaving deformation are found in foreign works (for example, [*Penner, 1974*]).

Due to the complexity of the field method of studying frost heaving of soils, it has not found wide application in construction practice and is used exclusively for scientific purposes [*Safronov, 1985;*

Ivanin et al., 2020; Shulyatyev, 2020], although the only Russian regulatory document [*GOST 27217-2012, 2013*] was developed specifically for field studies of the tangential forces of soil heaving. Foreign regulatory documents [*ASTM D 5918-063, 2006; BS 812-124:2009, 2009; Eurocode 7, 2013*] also do not contain requirements for determining the shear forces of soil heaving and methods for their determination.

In 2016, with the participation of the author, a standard was developed for the laboratory determination of the specific shear forces of frost heaving [*GOST R 56726-2015, 2016*]. The document took into account the only method for determining the tangential forces of frost heaving of soils under laboratory conditions [*Guidelines..., 1973*], which was not widely used due to the complexity of the design of the experimental setup.

The purpose of this study is to optimize the determination of the integral tangential heaving force, taking into account the thermal and moisture regimes of freezing heaving soils. The experiments were carried out by three methods using different soil shear rates on a metal foundation (conditionally instantaneous tests, long-term tests, and tests at a constant rate) for sandy and clayey soils. The results obtained can be used in engineering-geological surveys and calculation of foundations on heaving soils.

METHOD FOR DETERMINING THE TANGENTIAL FORCES OF FROST HEAVING OF SOILS UNDER LABORATORY CONDITIONS

The experiments were carried out by three laboratory methods: (1) conditionally instantaneous tests, (2) long-term tests with the application of a stepped load, and (3) shear at a constant speed. The experimental setup made it possible to set loads both in the normal and tangential directions with respect to the sample under study, so that a single-plane shear was ensured.

The normal stress of 0.1 MPa was applied for all installations. The studies were carried out for two types of soil: loam and sand, the characteristics of which are presented in the table. The moisture content was set equal to 10, 20, and 28% for loam soil and to 10, 15, and 20% for sandy soil. The studies were carried out for a metal plate made of steel grade 09G2S. The experiment was performed in triplicate.

Method for studying the conditionally instantaneous shear resistance along the freezing surface. Tests to determine the value of the conditionally instantaneous shear resistance along the freezing surface were carried out on a VSV-25 device, the scheme of which and the methodology of work followed [*Guidelines..., 1973*]. A soil sample in a metal ring was installed in the upper part of the shear carriage, and a foundation sample in the form of a metal plate was located in the lower cage.

The soil sample was installed in the device and loaded with a given normal load using a dynamometer. A continuously and uniformly increasing shear load was applied to the foundation sample quickly (more than 100 mm/day), but without impact. The duration of the test was 20–30 s. The experiment ended when the metal plate was torn off the ground or when the soil sample moved without further increase in load. The value of conditionally instantaneous resistance soil shear along the freezing surface was determined as the quotient of the breaking force divided by the area of the sample. The test temperature was set at 0, –1, –2, –4, –6 and –10°C.

Method for studying the ultimate long-term shear resistance. Tests to determine the value of the maximum long-term shear resistance along the contact of the freezing soil surface and the metal surface were carried out according to the method described in [*GOST 12248-2010, 2012*], in shear devices. A foundation sample was installed in the lower part of the shear carriage of the device; a metal ring was built into the upper part of the device body, into which the soil under study was placed.

A carriage with a foundation sample and a frozen soil sample was placed in the device, after which a dynamometer was installed, with which the normal load was maintained during the test, as well as a displacement sensor, then a shear load was applied stepwise.

Table 1. **Physical characteristics of soils in the study of shear forces of frost heaving**

Soil type*	Particle content (%) of different size (mm)							C_u	W_g	ρ_s	W_L/W_{sat}	W_p	I_p	I_{om}
	1–0.5	0.5–0.25	0.25–0.1	0.1–0.05	0.05–0.01	0.01–0.002	<0.002							
	$A_{0.5}$	$A_{0.25}$	$A_{0.1}$	$A_{0.05}$	$A_{0.01}$	$A_{0.002}$	A_0							
Silty sand (heterogeneous)	1.3	7.4	53.4	28.2	2.6	4.8	2.3	3.21	0.6	2.60	–/17.0	–	–	0.7
Clayey silt loam	0.8	2.7	15.2	17.7	28.7	20.4	14.5	–	2.4	2.61	30.8/–	18.7	12.1	2.4

Note: C_u is the degree of grain composition inhomogeneity; W_g is hygroscopic moisture, %; ρ_s is the density of soil particles, g/cm^3; W_L/W_{sat} is the ratio of moisture at the yield point to the total moisture capacity, %; W_p is the moisture content at plastic (rolling) limit, %; I_p is the plasticity number; and I_{om} is the relative content of organic matter, %.

* According to [*GOST 25100-2011, 2013*].

The load at the first stage of the test was set taking into account temperature conditions and type of soil according to Table 6.2 [*GOST 12248-2010, 2012*]; the increment of the tangential load was set taking into account Table 6.3 [*GOST 12248-2010, 2012*]. Each load step was maintained until conditional stabilization of the deformation. The strain increment not exceeding 0.01 mm per 12 h was taken as conditional strain stabilization. The next load stage was applied to the specimen after strain stabilization was achieved at the previous stage. If no stabilization of the deformation was observed at the next stage of loading, the load was maintained until the development of deformation at a constant rate during two successive 12-hour intervals.

The test was terminated if a constant strain rate was set for at least two steps of the shear load, or if strains developed at an increasing rate. The limiting long-term value of shear resistance along the freezing surface with the foundation material was determined as the highest shear stress at which the sample deformation was stabilized at a given normal stress. The test temperature was 0, –1, –2, –6, –10°C.

The processing of experimental data was carried out according to the creep ε–t curves (ε, mm; t, h) and the relationship between shear stress and total strain at the moment of stabilization ln t–ln ε in logarithmic coordinates according to [*GOST 12248-2010, 2012*].

Method for studying shear resistance at constant speed. Studies of shear at a constant rate or specific shear forces of frost heaving were carried out in an experimental setup that provided shear along a fixed plane with a constant speed of movement of a foundation sample over a soil sample in the range of 5–20 mm/day [*Cheverev, Alekseev, 2016*].

The installation had a carriage with a holder for a soil sample in the upper part and a foundation sample in the lower part. A normal load was applied to the soil sample, and a shear load at a constant speed was applied to the foundation sample. The soil shear resistance was measured with a force sensor with an accuracy of 0.01 MPa, the movement of the sample in time was measured with a displacement sensor with an accuracy of 0.01 mm.

Stable shear resistance in the experiment was recorded at the moment when the maximum displacement of the foundation material sample relative to the soil sample reached at least 10 mm. The experiments were carried out at five temperatures: 0, –1, –2, –4, and –6°C. At temperatures of –1, –2, –4°C, a constant carriage movement speed of 0.42 mm/h (10 mm/day) was set; at a temperature of –6°C, the carriage movement speed was set to 0.21 mm/h (5 mm/day), as the speed of 10 mm/day at this temperature could not be ensured because of the failure of the samples.

Procedure for preparing soil samples for shear testing. The soil and foundation samples for all test facilities were identical, so sample preparation was carried out in the same way. The soil was placed in a metal ring of 71.5 mm in diameter and 35 mm in height.

The studied soil at room temperature was laid into the ring by layer-by-layer compaction and then combined with the foundation sample. After preparing and testing of the soil sample, the bulk density and moisture content of the soil were monitored. The samples of the soil and foundation were placed in a freezer with a low subzero temperature (–26°C) for freezing and formation of a massive cryostructure. After freezing, the soil and foundation samples were transferred to a freezer, where the test temperature was maintained for the experiment. Before testing, soil and foundation samples were kept in a freezer at a given temperature for at least 12 h.

PATTERNS OF DEVELOPMENT OF TANGENTIAL FORCES OF FROST HEAVING OF SOILS

Studies carried out by three laboratory methods with different shear load application rates made it possible to identify patterns in the development of tangential heaving forces or stable shear resistance in dependence on temperature and moisture content for sandy and clayey soils along the freezing interphase with a metal surface.

Dependence of the conditionally instantaneous shear resistance along the freezing surface on the temperature and moisture regimes of soils. A decrease in the temperature of sandy soil from 0 to –10°C leads to an increase in conditionally instantaneous shear resistance from 0.04 to 1.21 MPa at the moisture content of 10%, from 0.07 to 2.01 MPa at the moisture content of 15%, and from 0.09 to 2.58 MPa at the moisture content of 20% (Fig. 1).

For loam, lowering the test temperature from 0 to –10°C led to an increase in shear resistance from 0.07 to 1.14 MPa at the moisture content of 10%, from 0.10 to 1.39 MPa at the moisture content of 20%, and from 0.18 to 1.65 MPa at the moisture content of 28% (Fig. 2). The dependence of the shear resistance on the moisture content was clearly manifested: with an increase in the moisture content, the shear resistance also increased within the considered temperature range.

The resistance to conditionally instantaneous shear of sand at the studied temperatures was significantly higher than that of loam.

The temperature of the soil is decisive in the formation of the freezing interphase between the wet soil and the foundation structure. At high soil temperatures (to –1°C), the shear resistance is low (<0.5 MPa) for both loam and sand; a further decrease in temperature leads to an almost linear increase in shear resistance.

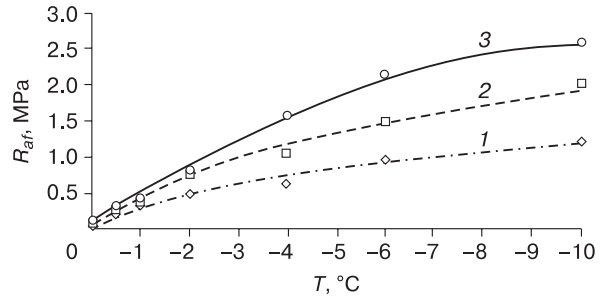

Fig. 1. Dependence of conditionally instantaneous shear strength (R_{af}) of frozen sand on test temperature and initial moisture content:

(*1*) W = 10%; (*2*) W = 15%; (*3*) W = 20%.

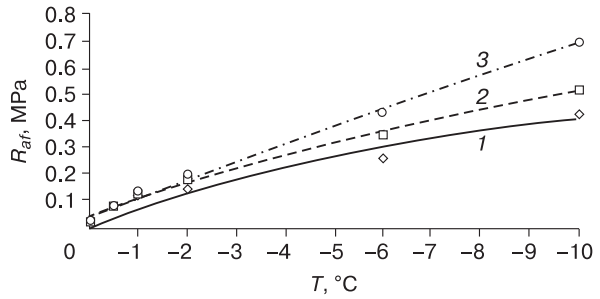

Fig. 3. Dependence of the ultimate long-term shear resistance (R_{af}) of frozen sand on a metal surface on the test temperature and initial moisture content:

(*1*) W = 10%; (*2*) W = 15%; (*3*) W = 20%.

Dependence of the maximum long-term shear resistance on the temperature and moisture regime of soils. The ultimate long-term shear resistance increases with an increase in the moisture content of the soil sample and a decrease in the test temperature from 0 to −10°C increased both for sand and loam. For sandy soil, it increased from 0.02 to 0.42 MPa at the moisture content of 10%, from 0.02 to 0.52 MPa at the moisture content of 15% and from 0.03 to 0.70 MPa at the moisture content of 20% (Fig. 3). For loam, it increased from 0.01 to 0.33 MPa at 10% moisture, from 0.02 to 0.37 MPa at 20% moisture, and from 0.03 to 0.49 MPa at 28% moisture (Fig. 4). The values of the ultimate long-term shear resistance for sand were significantly higher than for loam: at the moisture content of 10%, the difference was 0.05–0.09 MPa; at the moisture content of 20%, the difference was 0.05–0.33 MPa.

In the zone of high temperatures (0 to −1°C), a more intensive increase in the value of the maximum long-term shear resistance was noted than at low temperatures (−1 to −10°C), which is explained by the transition of soil from a thawed state to a frozen state and an increase in shear resistance not only due to the adhesion of the soil to the foundation but also due to the freezing of these materials. The ultimate long-term shear resistance of both clay and sandy soils depends on the temperature and moisture regime and increases with decreasing temperature and increasing soil moisture content.

A stepwise increase in the shear load during testing can be used when assessing the magnitude of the tangential frost heaving forces for conditions of uniform freezing of the soil and an increase in the external load on the shear area. However, the obtained value does not fully reflect the desired value of the specific tangential force of frost heaving, which is characterized by the sliding friction resistance of frozen soil over the freezing surface. In tests to determine the maximum long-term shear resistance, the value is estimated at which the displacement deformations of the foundation are stabilized, i.e., sliding friction does not occur. Long-term tests precede the stage of frozen soil sliding on the foundation surface. The objective value of the specific tangential forces of frost heaving should be determined under the condition that frozen soil moves along the foundation at a speed that characterizes the resistance of sliding friction. To estimate the desired value, the next series of tests was carried out at a given constant speed of soil movement along the contact with the foundation.

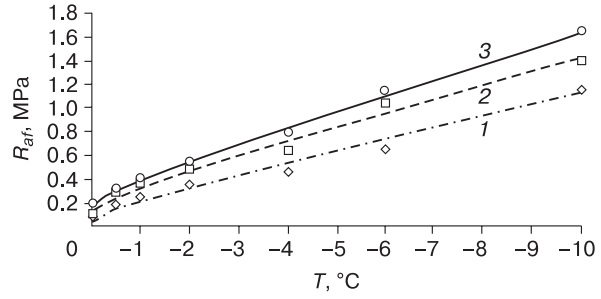

Fig. 2. Dependence of conditionally instantaneous shear strength (R_{af}) of frozen loam on test temperature and initial moisture content:

(*1*) W = 10%; (*2*) W = 20%; (*3*) W = 28%.

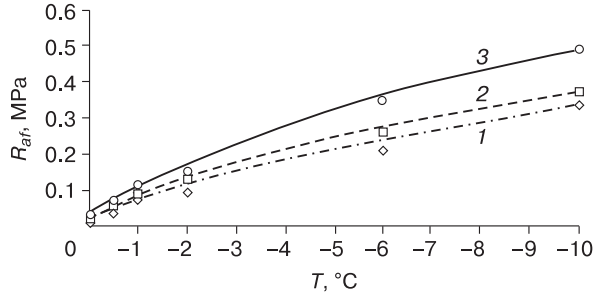

Fig. 4. Dependence of the ultimate long-term shear resistance (R_{af}) of frozen loam on a metal surface on the test temperature and initial moisture content:

(*1*) W = 10%; (*2*) W = 20%; (*3*) W = 28%.

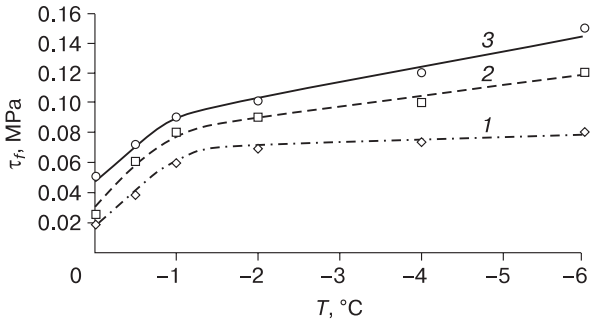

Fig. 5. Dependence of the specific tangential heaving forces (τ_f) of frozen sand on a metal surface on the test temperature and initial moisture content:

(*1*) W = 10%; (*2*) W = 15%; (*3*) W = 20%.

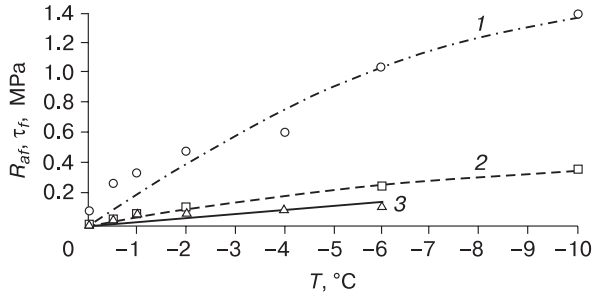

Fig. 7. Dependence of shear resistance (R_{af}) and specific tangential heaving forces (τ_f) on temperature for loam with the moisture content of 20%:

(*1*) method 1, conditionally instantaneous shear resistance; (*2*) method 2, extremely long shear resistance; (*3*) method 3, shear at a constant speed τ_f.

Dependence of the specific tangential forces of frost heaving on the temperature and moisture regimes of soils. The specific shear forces of frost heaving of the soil were estimated from the value of the stable shear resistance of the frozen soil sample relative to the model of a metal foundation moving at a constant speed.

With a decrease in the temperature of the experiment from 0 to −6°C, the values of the specific tangential heaving forces for the studied soils increased. For sandy soil, the tangential forces increased from 0.02 to 0.08 MPa at the moisture content of 10%, from 0.03 to 0.12 MPa at the moisture content of 15%, and from 0.05 to 0.15 MPa at the moisture content of 20% (Fig. 5). For loam, the specific tangential frost heaving forces increased from 0.01 to 0.12 MPa at the moisture content of 10%, from 0.02 to 0.13 MPa at the moisture content of 20%, and from 0.04 to 0.14 MPa at the moisture content of 28% (Fig. 6).

Freezing of the soil with the foundation is due to the appearance of ice-cement bonds formed as a result of freezing of water at the contact of the soil and the foundation. At high temperatures during experiments, when not all the pore water is frozen, the resistance to the shear consisted of freezing forces and adhesion forces of soil particles with the foundation material through water films; at zero temperatures, of the adhesion forces of soil particles with the foundation.

The freezing forces of sandy soil and foundations are higher than those for loamy soils because sandy soils do not have a double electrical layer around sand particles, unlike loamy soils. In addition, the size of sand particles is much larger than that of clay particles, which leads to an increase in cohesive forces.

With a decrease in soil temperature, the amount of unfrozen water decreases, and the area of freezing of soil particles with the foundation increases.

An increase in the moisture content and, accordingly, the degree of filling of soil pores with water in the sample leads to an increase in the contact area of soil particles through ice layers with the foundation and an increase in the number of bonds between particles due to an increase in the volume of ice. This circumstance leads to a general increase in the shear resistance forces of wetter soils.

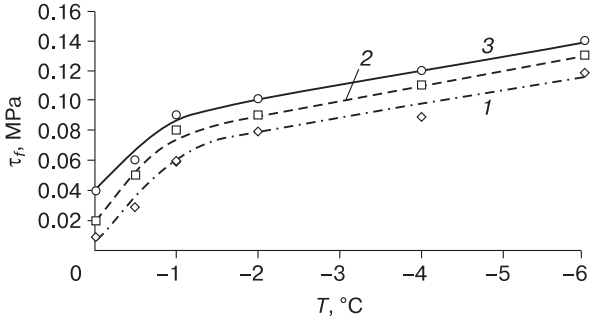

Fig. 6. Dependence of the specific tangential heaving forces (τ_f) of frozen loam on a metal surface on the test temperature and initial moisture content:

(*1*) W = 10%; (*2*) W = 20%; (*3*) W = 28%.

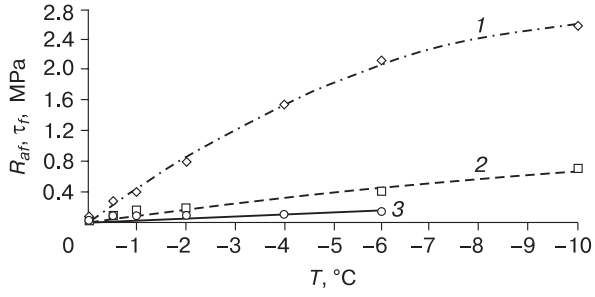

Fig. 8. Dependence of shear resistance (R_{af}) and specific tangential heaving forces (τ_f) on temperature for sand with the moisture content of 20%:

(*1*) method 1; (*2*) method 2; (*3*) method 3.

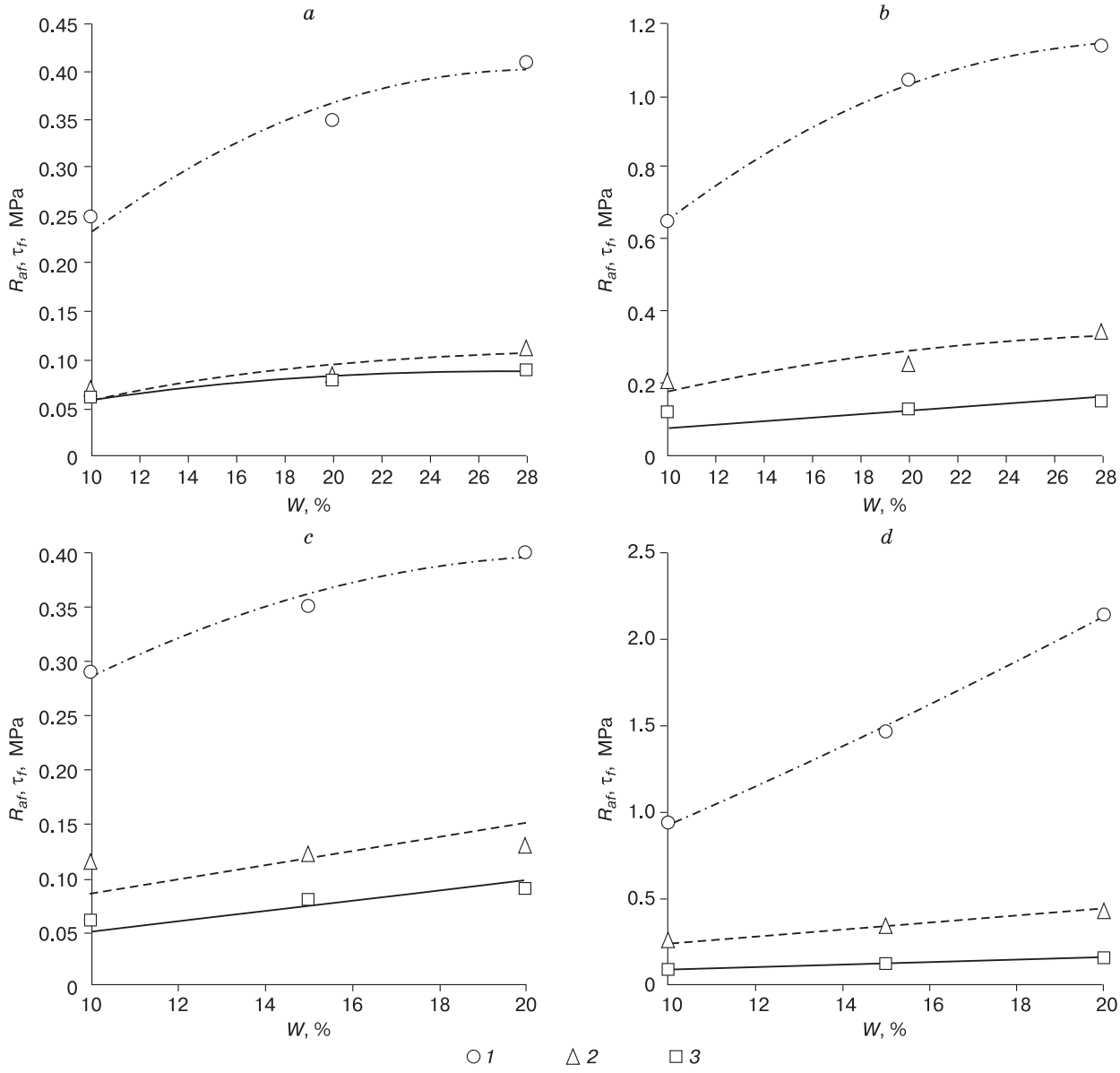

Fig. 9. Dependence of shear resistance (R_{af}) and specific tangential heaving forces (τ_f) on the moisture content (W):

a – loam, $T = -1$°C; *b* – loam, $T = -6$°C; *c* – sand, $T = -1$°C; *d* – sand, $T = -6$°C; (*1*) method 1; (*2*) method 2; (*3*) method 3.

When the soil is moistened, first of all, strongly bound water is formed, then loosely bound and finally free. At the moisture content of 10%, the main part of the water is in a bound state, which ensures a high content of unfrozen water in clay soil at a negative temperature. Thus, with a decrease in soil moisture, the amount of ice in the soil is significantly reduced, and, consequently, the freezing area and shear resistance decrease.

Studies have shown a similar dependence of shear resistance on temperature for all three test methods: with a decrease in soil temperature from 0 to –10°C, an increase in shear resistance takes place (Figs. 7, 8). An increase in shear resistance is also observed with an increase in the soil moisture content. Sandy soils are characterized by higher values of shear resistance than loam (Fig. 9). An increase in the moisture content of sand leads to an increase in the adhesion of sand particles (which are much larger than clay particles) and the foundation sample.

With a conditionally instantaneous shear, the shear resistance value significantly (by more than three times) exceeds the shear resistance values obtained during tests in other installations. The value of

long-term shear resistance is slightly higher than the value obtained when shearing at a constant speed.

The magnitude of shear resistance or tangential heaving forces determined by methods 2 and 3 are identical in direction, but differ in magnitude by 10–40%. The shear resistance values obtained by method 2 (ultimate long shear) exceed the values obtained by method 3. The shear resistance values obtained by conventionally instantaneous shear (method 1) are significantly higher (up to five times) than the values obtained by methods 2 and 3.

The conducted studies have shown that the most reliable value of the specific tangential frost heaving forces, corresponding to the sliding friction resistance of frozen soil over the foundation material, can be determined in the installation ensuring soil shear along the foundation with a constant speed.

Determination of the specific shear forces of frost heaving by the shear method at a constant speed is typical for most cases of soil heaving during freezing near the foundation, when there is an integral increase in the depth of freezing and, as a result, in the pressure of frost heaving.

However, there are special cases, when a sharp freezing of the soil and a rapid deformation of the soil and foundation as a result of heaving are possible, especially when the freezing soil layer is in cramped conditions. These circumstances can arise with a sharp decrease in air temperature and with artificial freezing of the soil. In such cases, when the heaving pressure, which is largely characterized by the forces of crystallization of pore water during freezing, increases at a significant rate (>100 mm/day), it is recommended to determine the magnitude of the tangential frost heaving forces by conditionally instantaneous tests.

CONCLUSIONS

1. Three laboratory methods for estimating the magnitude of shear resistance equivalent to the tangential frost heaving force were selected: conditionally instantaneous tests, long-term tests with a stepped load, and shear at a constant speed.

2. Based on the results of comprehensive studies, the dependences of the shear resistance of sandy and loamy soils on the moisture content (from 10 to 28%) and temperature (from 0 to –10°C) were established: with an increase in soil moisture and a decrease in temperature, an increase in soil shear resistance occurs. The shear resistance of sandy soils is twice as high as that of loamy soils. The forces of sandy soil freezing with the foundation are higher than those of loamy soil because sandy soil does not have a double electrical layer, and the size of sand particles is much larger than the size of clay particles. With a decrease in temperature, the amount of unfrozen water decreases and the area of freezing of soil particles with the foundation increases.

3. An increase in the moisture content and the degree of filling of soil pores with water in the sample leads to an increase in the contact area of soil particles through ice layers with the foundation; in addition, with an increase in the moisture content and in the volume of ice, the number of bonds between particles increases.

4. It was determined that the resistance to conditionally instantaneous shear (speed more than 100 mm/day) is up to three times higher than the values of specific long-term shear resistance and specific shear forces of frost heaving.

References

ASTM D 5918-06, 2006. Standard Test Methods for Frost Heave and Thaw Weakening Susceptibility of Soils. ASTM International, 12 p.

BS 812-124:2009. Testing Aggregates. Method for Determination of Frost Heave. British Standards Institution, 2009, 38 p.

Cheverev V.G., Alekseev A.G., 2016. Method of laboratory determination of the specific tangential force of frost heaving (to the GOST project). In: Proceeding of the Fifth Conference of Geocryologists (Moscow, June 14–17, 2016). Moscow, Univ. Kniga, vol. 3, p. 72–79 (in Russian).

Dalmatov B.I., 1957. Effect of Frost heaving on Foundations of Structures. Leningrad; Moscow, Gosstroiizdat, 60 p. (in Russian).

Dubnov Yu.D., 1967. Laboratory tests of tangential forces of frost heave. In: Frost Heave of Soil and Ways to Protect Structures from Its Impact. Moscow, Transport, p. 55–60 (in Russian).

Eurocode 7, 2013. Geotechnical Design Worked Examples. Publications Office of the European Union, 159 p.

GOST (State Standard) 12248-2010, 2012. Soils. Methods of Laboratory Determination of Strength and Deformability Characteristics. Moscow, Standartinform, 77 p. (in Russian).

GOST (State Standard) 25100-2011, 2013. Soils. Classification. Moscow, Standartinform, 44 p. (in Russian).

GOST (State Standard) 27217-2012, 2013. Soils. Method of Field Determination of Specific Tangential Forces of Frost Heaving. Moscow, Standartinform, 10 p. (in Russian).

GOST (State Standard) R 56726-2015, 2016. Soils. Laboratory Method for Determining Specific Tangential Forces of Frost Heaving. Moscow, Standartinform, 6 p. (in Russian).

Guidelines for Determining the Physical, Thermal and Mechanical Characteristics of Frozen Soils. Moscow, Stroiizdat, 1973, 191 p. (in Russian).

Ivanin A.S., Kumallagov V.A., Smirnov N.V., 2020. Field and laboratory studies of the action of tangential forces of frost heaving of soils on pile foundations. Nauka Tekhnol. Truboprovodn. Transp. Nefti in Nefteproduktov (Science and Technology of Pipeline Transport of Oil and Petroleum Products), **10** (45), 460–469 (in Russian).

Orlov V.O., Dubnov Yu.D., Merenkov N.D., 1977. Heaving of Frozen Soils and Its Impact on the Foundations of Structures. Leningrad, Stroiizdat, 183 p. (in Russian).

Penner E., 1974. Uplift forces on foundations in frost heaving soils. *Can. Geotechn. J.*, No. 11, p. 323–338.

Peretrukhin N.A., 1967. The strength of frosty buckling of foundations. In: Frost Heave of Soil and Ways to Protect Buildings from its Impact. Moscow, Transport, p. 25–54 (in Russian).

Safronov Yu.V., 1985. Frost Heaving of Soils and the Method of Field Determination of Tangential Forces of Heaving: PhD (Cand. Technical Sciences) Thesis. Moscow, 185 p. (in Russian).

Shulyatyev O.A., 2020. Studies of the interaction of the heaving soil with the pile foundation. *Vestnik NITS Stroitelstvo* (Bulletin of the SIC Construction), No. 3 (26), 105–120 (in Russian).

Received August 5, 2021
Revised March 17, 2022
Accepted March 25, 2022

Translated by A.V. Muravyov

EARTH'S CRYOSPHERE
SCIENTIFIC JOURNAL

Earth's Cryosphere, 2022, vol. XXVI, No. 3, pp. 26–36

PHYSICAL AND CHEMICAL PROCESSES IN FROZEN GROUND AND ICE

ANALYTICAL REVIEW OF APPROACHES AND METHODS OF MATHEMATICAL MODELING OF THE PROCESSES OF SOIL FREEZING AND HEAVING

E.V. Safronov[1], V.G. Cheverev[1,*], A.V. Brouchkov[1], S.N. Buldovich[1], V.Z. Khilimonyuk[1], L.V. Grigoriev[2], E.M. Makarycheva[2], E.V. Gnilomedov[2]

[1] *Lomonosov Moscow State University, Faculty of Geology, Department of Geocryology, Leninskie gory 1, Moscow, 119991 Russia*
[2] *Scientific Research Institute of Pipeline Transport (LLC NII Transneft), Department of External Impact Modeling and Stability Calculations of Monitoring Objects, Sevastopolskii prosp. 47a, Moscow, 117186 Russia*

[*] *Corresponding author; e-mail: cheverev44@mail.ru*

The article provides analytical review of existing approaches and specific models for solving problems of freezing, thawing, and frost heaving of soils. The authors analyzed about 100 published works of Russian and 100 works of foreign authors, including articles, monographs, dissertations, patents, conference proceedings, scientific reports. Special attention in the analysis of the physical formulation of mathematical models is paid to taking into account the mechanism of heat and mass transfer, ice segregation, phase transitions of pore water, and the development of deformations and forces of frost heaving of freezing soils.

Keywords: *mathematical modeling, soil freezing, freezing front, frost heaving, cryogenic migration, heat and mass transfer, water phase transitions, shrinkage*.

Recommended citation: Safronov E.V., Cheverev V.G., Brouchkov A.V., Buldovich S.N., Khilimonyuk V.Z., Grigoriev L.V., Makarycheva E.M., Gnilomedov E.V., 2022. Analytical review of approaches and methods of mathematical modeling of the processes of soil freezing and heaving. *Earth's Cryosphere*, XXVI (3), 26–36.

INTRODUCTION

The process of soil freezing is primarily a process of heat and moisture transfer and pore water phase transition into ice. For the physical formulation of mathematical modeling of the process, it is necessary to solve the thermal problem with phase transitions and the problem of moisture transfer in the soil. To solve the thermal problem, the Fourier heat equation is the basic approach. In the three-dimensional version, it can be written as [*Tikhonov, Samarsky, 1999*]:

$$C\rho\frac{\partial T}{\partial t}=\frac{\partial}{\partial x}\left(\lambda\frac{\partial T}{\partial x}\right)+\frac{\partial}{\partial y}\left(\lambda\frac{\partial T}{\partial y}\right)+ +\frac{\partial}{\partial z}\left(\lambda\frac{\partial T}{\partial z}\right)+f(x,y,z,t), \quad (1)$$

where λ is thermal conductivity, W/(m·K); T is temperature, °C; t is time, s; $f(x,y,z,t)$ is the so-called function of heat sources; C is the specific heat capacity, J/kg; x, y, z are coordinates, m; and ρ is density of the material, kg/m^3.

The application of the Fourier equation is valid for a continuous medium. When the soil freezes, there is a boundary between the thawed and frozen states, at which the phase composition of water can change abruptly. In this case, we can talk about the interface between the thawed and frozen soil with different thermophysical characteristics, which imposes an additional boundary condition on Eq. (1).

To solve the thermal problem with a clear boundary between the liquid and solid phases in the presence of the "jump" of moisture at the boundary, the classical formulation of the Stefan problem is used. One of the variants of writing the heat balance equation directly at the freezing front is given, for example, in [*Brovka, 1991*]*:

$$(w_{tot}-w_w)L\rho_d\frac{d\xi}{dt}=\lambda_U\frac{dT}{dx}\Big|_U-\lambda_F\frac{dT}{dx}\Big|_F, \quad (2)$$

where L is the specific heat of ice melting, J/kg; ρ_d is the density of the frozen soil skeleton, kg/m^3; w_{tot} is

* In this paper, as well as in the works of Russian and foreign authors, conventional signs for the same physical values do not always coincide. We present them in the original form with necessary explanation.

the total weight moisture content, f.u. (fraction of a unit); w_w is the specific content of unfrozen water in frozen soil at the freezing front, f.u.; $\frac{d\xi}{dt}$ is the change in the thickness of the frozen part of the soil over time, m/s; $\left.\frac{dT}{dx}\right|_U$, $\left.\frac{dT}{dx}\right|_F$ are temperature gradients in thawed and frozen zones, K/m; λ_U, λ_F is the thermal conductivity of the soil in the thawed and frozen zones, W/(m·K).

The solution of the Stefan problem with various boundary conditions is considered in [*Kudryavtsev, 1978*]. Generalized analytical solution of this problem is suggested in [*Getz, Meirmanov, 2000*].

The application of the Fourier equation for the selected soil zones and the equations of thermal and material balance at the boundaries of these zones allows us to describe the processes of heat transfer in the problem of soil freezing in detail. However, when implementing a numerical solution to this problem, it is very difficult to model both a continuous medium and the boundaries between zones at the same time, primarily due to the deficiency of numerical methods used in modeling.

Two different approaches have been formed to ensure the sustainable solution of this kind of problems. *The first approach* takes into account the equations of thermal and material balance at the freezing front, as well as at the other boundaries inside the soil, at which an abrupt change in properties is assumed while maintaining the continuity of the temperature field.

In the second approach, the abrupt change in the phase composition and thermophysical properties of the soil at the boundaries of the zones is smoothed out. For example, one of the recognized methods of achieving uniformity is the so-called enthalpy formulation of the Stefan problem [*Ershov, 1999*]. In this formulation, all variables in Eqs. (1) and (2), including temperature, are considered as functions of enthalpy. Enthalpy, in turn, becomes a function of not only the temperature, as in the thawed and frozen parts but also of the coordinates of the freezing front boundary. In this case, the boundaries seem to "get fuzzy", and the heat balance equation at the front degenerates into a solution of the modified Fourier equation.

Conventionally, models based on the first approach can be called models with a pronounced front, or front models, whereas models based on the second approach are models with a "fuzzy front", or frontless models.

The main objective of creating models of soil freezing is to solve various geotechnical problems in permafrost areas, in which the stress field created by various construction objects is modeled, and the behavior of the temperature field and possible deformation changes are predicted. Hydrological conditions are taken into account, and a forecast of the influence of various water sources on the deformation of constructions or natural phenomena is given.

Therefore, in addition to direct solution of the thermal problem, soil freezing and heaving necessitate the development of mass transfer equations for water and salt transfer together with thermal energy. In the case of engineering problems solution, it is also necessary to apply the equations of the stress-deformation state of the soil, or modify the equations of heat and mass transfer in such a way that they can take into account the impact of the external load.

When modeling moisture transfer in the frozen part of freezing soils, the researchers relied on the concepts of moisture transfer in thawed soils. This led to two different approaches for solving the problem of moisture transfer. In the first approach, researchers rely on *the dependence of the water flow in soils on the moisture gradient*, applying this approach to frozen soils (wet form). In the alternative approach, *the dependence of the moisture transfer intensity on the pore pressure gradient* is considered.

It should be emphasized that moisture transfer in frozen soil is primarily caused by its inherent temperature gradient. Thus, it is necessary to express the temperature gradient through the pressure gradient inside the pores of the frozen soil to create a single pressure field that determines the flow of water in both thawed and frozen parts. At the same time, different equations of the relationship between pore pressure and temperature are used in the models. This leads to an additional difference between the models in the approach, which considers the dependence of the water transfer intensity on the pore pressure gradient.

OVERVIEW OF FRONT MODELS

The Melamed–Feldman model

V.G. Melamed [*1969*] and later G.M. Feldman [*1988*] presented models that take into account the moisture flow when solving the Stefan problem. To solve the problem, V.G. Melamed accepted the presence of moisture transfer in the thawed zone and its absence in the frozen zone, as well as the fact that segregation ice appears only at the freezing boundary. From a mathematical point of view, the formulation of the problem of heat exchange in the freezing soil was faultless, however, the physical statement of the problem of moisture transfer and segregation ice release had a fundamental disadvantage, due to which the mathematical model did not give reliable results.

The fact is that in order to start cryogenic migration and the formation of water flow to the freezing front in the soil, the moisture gradient was used as the driving force of the calculation models, and not the moisture potential gradient (or its equivalent –

the hydraulic pore pressure gradient). Such a physical formulation of the problem for mathematical modeling, as numerous further experimental studies showed, did not correspond to the physical essence of the process of cryogenic migration and frost heaving of soils [*Kudryavtsev et al., 1973; Cheverev et al., 2021*].

Models based on the concept of the freezing layer

When describing the works of Konrad, Miller, and other foreign authors on the problem of soil freezing based on the consideration of the pore pressure gradient as a driving force and the concept of the existence of a special freezing layer, it should be clarified what they were modeling. In these works, the authors tried to describe the formation of a cryogenic schlieren structure during soil freezing, as well as to take into account the influence of external load on the processes. During freezing, they observed the formation of periodic massive ice lenses located transversely to the thermal current and blocking moisture transfer in the soil. In this case, the rate of change in the thickness of such a lens could be easily measured, and consequently, the amount of water flow entering such a lens could be calculated.

R. Miller proposed the concept of an intermediate (hereinafter, freezing) layer directly behind the freezing front up to the first ice lens. He proved that in the region of temperatures below the freezing point, in some narrow region, there will be such conditions under which part of the pores will be filled with ice, and another part will be supercooled (unfrozen – *Approx. authors*) water, unable to turn into ice due to the small size of the pore itself [*Miller, 1978*]. The temperature gradient in this layer will be proportional to the pressure gradient of the supercooled water in the pores and will determine the amount of water flow coming to the ice lens immediately behind this layer.

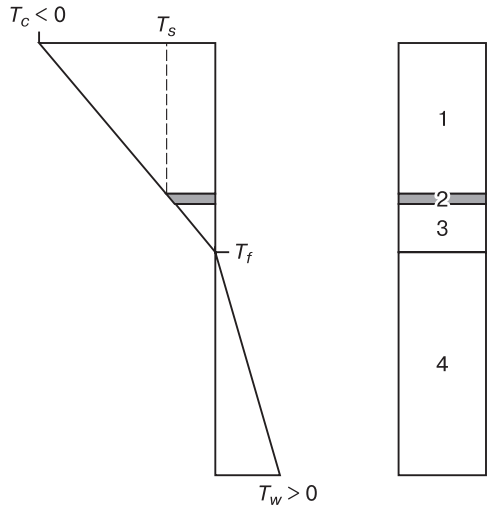

Fig. 1. Simulation model of frost heaving [*Konrad, Morgenstern, 1980*].

1 – frozen layer, 2 – ice lens, 3 – freezing layer, 4 – thawed layer. T_c is the temperature at the boundary of the frozen layer, T_s is the temperature at the boundary of the ice lens, T_f is the temperature at the freezing front, and T_w is the temperature at the boundary of the thawed layer.

The Konrad–Morgenstern model

The authors in [*Konrad, Morgenstern, 1980*] theoretically substantiated and empirically confirmed that the moisture flow in freezing soils is directly proportional to the temperature gradient in the frozen zone. In subsequent papers, the proportionality coefficient between them was named the segregation potential (analogous to the moisture conductivity coefficient). The mass transfer equation proposed by Konrad, can be written as

$$v_u = SP \operatorname{grad}(T_f), \qquad (3)$$

where SP is the segregation potential, $m^4/(K \cdot s)$; v_u is the water flow rate (change in the volume of water entering the ice lens per unit of time), m^3/s; grad (T_f) is the temperature gradient in the frozen zone of the sample, K/m.

As a basis, Konrad used a comparatively simple model, in which two zones were considered: thawed and frozen, separated by a freezing front (Fig. 1).

He took the temperature gradient in the freezing layer to be equal to the temperature gradient in the frozen layer. As a theoretical justification, the author used the Clapeyron–Clausius equation for the connection between the pressure of unfrozen water in the pores of the intermediate layer and the temperature gradient in it. The approach of J.M. Konrad and his co-authors has gained great popularity abroad. On the basis of this empirical concept, for example, the model [*Loranger, 2020*] is constructed, in which heat is added to Eqs. (2) and (3) due to freezing of water, which is supplied by cryogenic migration:

$$\lambda_f \nabla T_- = \lambda_u \nabla T_+ + L_s \frac{\Delta z}{\Delta t} + L_w v,$$

where λ_f, λ_μ are the thermal conductivity of the frozen and thawed zones, respectively; ∇T_-, ∇T_+ are the temperature gradients of the frozen and thawed zones; L_s is the volumetric latent heat of water freezing at the freezing front; L_w is the volumetric latent heat of water freezing at the contact with ice lens; $\Delta z/\Delta t$ is the speed of movement of the freezing front. The application of such a concept made it possible to describe the freezing process with a slow front movement at small temperature gradients.

The Gilpin model

In their works, J.M. Konrad and coauthors showed that the water flow calculated through the pressure gradient at the freezing front, is at least an

order of magnitude higher than that observed in the physical experiment. To resolve this contradiction, R. Gilpin [*1980*] supposed that the temperature gradient in the freezing layer is different from the gradient in the rest of the frozen soil and considered the heat balance equation directly at the boundary of the freezing layer and the ice lens (Fig. 2):

$$k_f \frac{T_{top} - T_l}{H} - k_p \frac{T_f - T_l}{a} = \frac{L}{v_s} V_H,$$

$$k_p \frac{T_f - T_l}{a} - k_{uf} \frac{T_{bot} - T_f}{x} = \rho_d L \frac{dz}{dt},$$

where k_f, k_p, k_{uf} are the thermal conductivity coefficients of the frozen and freezing layers and the thawed zone, respectively, W/(m·K); V_H is the growth rate of the ice lens, m/s; T_{top} is the temperature on the cold face, K; T_l is the temperature at the frozen/freezing layers interface (or, in other words, at the boundary of the formation of a continuous layer of ice), K; T_f is the temperature at the freezing front, K; T_{bot} is the temperature at the boundary with the heat source, K; and v_s is the specific volume of ice, m^3/kg.

R. Gilpin [*1980*] introduced a significant simplification, taking the temperature profile in the freezing layer to be linear, and did not consider the process of soil freezing in this layer and the interaction of the ice formed in it with the ice lens (meantime, the temperature profile bends smoothly [*Ershov, 1999*]).

The paper [*Bronfenbrener, Bronfenbrener, 2010*] provides an analytical solution to this thermal problem. The authors use the transformation of spatial and temporal coordinates and provide an analytical solution for short and long-term forecasts of freezing.

Within the framework of the Gilpin model, the boundary conditions between the thawed and freezing layers, and the freezing layer and the forming ice lens were only considered. Heat and moisture transfer directly in the freezing layer were not considered. In addition, the problem of the impact of the ice accumulating in the freezing layer on the ice lens behind this layer was not disclosed, though the migration of this ice to the ice lens determines the rate of its growth. The concept of water transfer in this layer was considered in detail in [*O'Neill, Miller, 1985*]. The main ideas of the work are as follows. The freezing layer was considered exclusively between the thawed zone and the first ice lens. If an ice lens appears in the freezing layer, the length of the latter is automatically reduced to the new ice lens. Thus, the condition is fulfilled that there is no ice lens in the freezing zone, and this zone consists exclusively of unfrozen water and ice-cement moving to the new ice lens. This ice-cement is tightly related to the ice lens, i.e., the velocity of movement of ice-cement coincides with the growth rate of ice lens.

The water pressure can be calculated from the generalized Clapeyron–Clausius equation:

$$(P_w - P_0)V_w - (P_i - P_0)V_i = L\frac{\Delta T}{T_0}, \qquad (4)$$

where V_w, V_i is the specific volume of water and ice, respectively, m^3/kg; P_i, P_w is the pressure of ice inclusions and unfrozen water, Pa.

As the growth of ice lens is determined by the velocity of migration of ice-cement, the expression of the density of the migration flow through the pressure gradient of the liquid phase in accordance with Darcy's law is not valid. Therefore, as a driving force, the authors consider the gradient of the total pore pressure P_n, which determines the rate of ice lens growth, which can be calculated by the formula

$$P_n = \chi P_w + (1-\chi) P_i, \qquad (5)$$

where χ is a parameter depending on the unfrozen water content.

The equations of heat balance on the basis of the Fourier equation are solved with due account for the release of heat upon water freezing and the mass balance, where the water flow is determined by the pressure gradient.

R. Miller's ideas were implemented in a simplified model, which considers a water-saturated system consisting of a continuous porous non-deformable medi-

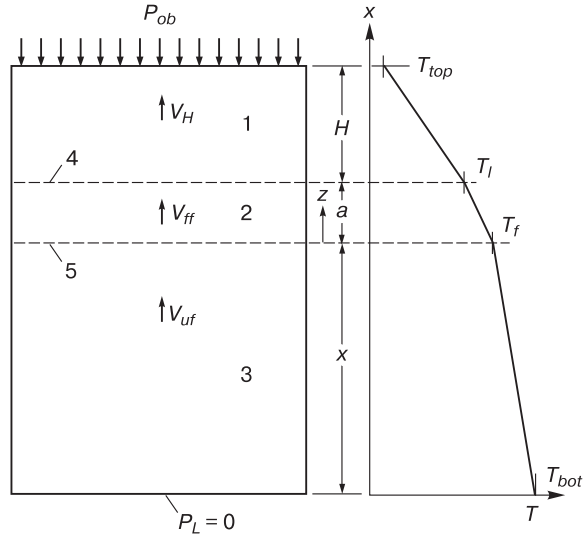

Fig. 2. Simulation model of frost heaving with determination of values [*Gilpin, 1980*].

1 – frozen layer, 2 – freezing layer, 3 – unfrozen (thawed) zone, 4 – ice segregation front, 5 – freezing front. T is the temperature, z is the distance, H is the thickness of the frozen layer, a is the thickness of the freezing layer, T_{bot} is the temperature of the warm border, T_f is the temperature at the freezing front, T_l is the temperature at the ice segregation front, T_{top} is the temperature of the cold boundary, P_{ob} is the mechanical pressure at the cold boundary, P_L is the pore pressure at the warm boundary, V_H is the growth rate of the ice lens, V_{ff} is the water flow rate in the freezing layer, and V_{uf} is the water flow rate in the unfrozen zone.

um (capillary porous ceramics) and an ice lens forming on the cold surface of a ceramic cylinder [*Gorelik, Kolunin, 2002*]. The authors conducted an experiment in which they used a sample of porous ceramics, which is suitable for the role of a permanent non-expandable medium. Water was supplied from one side of the ceramic cylinder; on the opposite side, there was a source of cold under the load and a growing ice lens.

In his solution, Ya.B. Gorelik uses the Stefan condition at the freezing front, as well as at the interface of the porous body and the ice lens. Similar to R. Miller, the author uses the intra-pore pressure gradient determined from the generalized Clapeyron–Clausius equation to determine the moisture transfer. The rate of growth of the ice lens was determined based on the velocity of the freezing front movement at the interface of the porous body and ice.

The question of using the Clapeyron–Clausius equation in the freezing zone remains open and disputed. In [*Akagawa et al., 2006*], the authors point out that the formation of an ice lens in the soil actually takes place in a closed system, until the pressure of the ice lens on the soil exceeds the load on the sample and the tensile strength of the soil. After this rupture occurs, the amount of pressure exerted by the ice lens on the pore water drops sharply and the condition of the closed system is disturbed. This leads to a sharp growth of ice lenses.

In [*Ma et al., 2015*] it is proposed that the function of load distribution during the growth of an ice lens in dependence on the degree of pore filling with ice in the freezing zone. In general, the assessment of the influence of the ice lens pressure during its growth is an ambiguous problem.

The Cheverev–Buldovich model

Equations (4) and (5) are applicable first of all either for a closed, or at least non-expanding medium, which is practically not observed in soils. In [*Cheverev, 1999, 2003a,b, 2004; Ershov, 1999; Cheverev, Safronov, 2012; Cheverev et al., 2013, 2021*], the Edlefsen–Andersen equation is used to describe the dependence of the pore pressure on temperature [*Edlefsen, Anderson, 1943*]:

$$P_w = L\Delta T/(T_0 V_w),$$

where P_w is the equilibrium pressure of the liquid phase of the soil water at the boundary with the solid phase, Pa; L is the specific heat of ice melting, J/kg; ΔT is a decrease in the freezing temperature of the soil (pore solution) relative to the freezing of unbound water; T_0 is the absolute value of the freezing temperature of free water, K; V_w is the specific water volume, m^3/kg.

In this case, the density of the water flow in the frozen soil is determined by the temperature gradient [*Cheverev, 1999; Ershov, 1999*]:

$$i_w = \lambda_w(T) K \frac{dT}{dz}, \qquad (6)$$

where i_w is the density of the water flow (a vector directed towards the temperature gradient with a value equal to the change in the volume of water per unit of time passing through a unit area), m/day; $\lambda_w(T)$ is the moisture conductivity coefficient of the frozen soil zone, m/day; $K = L/(T_0 V_w)$ is the coefficient of proportionality expressed in meters of water column per degree Kelvin and equal to 120 m/K; and dT/dz is the temperature gradient in the measuring zone.

The density of the water flow in the thawed zone is

$$i_w = \lambda_w KL \frac{T_{nz} - T_\xi}{l - \xi},$$

where T_{nz}, T_ξ is the temperature of the beginning of freezing of the soil and the temperature at the freezing front; ξ is the depth of freezing; l is the size of the area of calculations.

In terms of the development of the Cheverev–Buldovich model, a numerical solution of the problem was carried out on the basis of the finite element method and the finite difference method [*Cheverev, Safronov, 2012*]. The solution is based on the calculation of the flow density using Eq. (6). At the same time, for the calculation of T_ξ, not an analytical solution of the heat and mass transfer equations is used, as in the Cheverev–Buldovich model, but a numerical solution by tracking moisture at the freezing front when solving the mass balance equations:

$$dT_\xi = \frac{dW_\xi}{dW/dT},$$

where W_ξ is the content of unfrozen water at the freezing front; $\frac{dW}{dT}$ is the derivative of the function of the unfrozen water content from the temperature at point T_ξ.

OVERVIEW OF FRONTLESS MODELS

The system of moisture transfer equations solved with respect to moisture is one of the widespread approaches for modeling freezing processes in soils. The general system of heat and moisture transfer equations in this form was formulated for building capillary-porous materials in the work [*Lykov, Mikhailov, 1963*]:

$$C_p \frac{dT}{dt} = -\operatorname{div}(I_q) - \sum_{i=0}^{4} (H_i T_i - C_i I_{mi} \Delta T),$$

$$\frac{d(\rho_0 W_i)}{dt} = -\operatorname{div}(I_{mi}) + \sum_{i=0}^{4} I_i,$$

$$\frac{d(\rho_0 W_w)}{dt} = -\operatorname{div} \sum_{i=0}^{4} I_{mi},$$

where C_p is the volumetric heat capacity of the soil, consisting of the volume fractions of the heat capaci-

ties of the components, J/m^3; ρ_0 is the density of the soil, kg/m^3; the index, for example, i denotes the components of the soil: mineral skeleton, air, water, and ice; the following values of these components are considered: I_q – specific heat flux, J/(kg·m^2); I_{mi} – specific heat flux, kg/(m^2·s); I_i – discharge capacity, J/(kg·m^2); C_i – heat capacity, J/(kg·K); H_i – enthalpy, J/kg; W_i, W_w – ice and moisture content, f.u.; the density of the water flow (I_w, kg/(m^2·s)) in the one-dimensional case is determined by the moisture gradient. Examples of models using this approach are discussed below.

The Lavrov model

The main difficulty in constructing numerical models without the allocation of thawed and frozen zones is the choice of a variable common to both zones in the system of heat and moisture transfer equations. In [*Lavrov, 2000*] the total soil moisture was taken as such a value. To solve the heat balance equations Fourier equation was considered taking into account phase transitions due to non-frozen water (1). As the driving force for the equation of mass balance in the frozen area, the author expresses the gradient of the unfrozen water content through the ice content and the total moisture content:

$$\frac{dW}{dT}=\frac{d}{dx}\left(D_W\frac{dW}{dx}\right)+\frac{d}{dx}\left(D_P\frac{dP}{dx}\right)+\frac{d}{dx}\left(D_I\frac{dI}{dx}\right), \quad (7)$$

where W is the total moisture content, f.u.; D_W, D_P, D_I are the corresponding diffusion coefficients due to the gradients of unfrozen water, pressure, and ice; I is the ice content; and dP/dx is the pressure gradient in the system, set by the external pressure.

The heat problem is solved separately from the mass transfer problem. Individual equations defining the behavior of the system as a whole are written for each problem.

The Danielyan–Yanitsky model

In the work [*Danielyan, Yanitsky, 1983*], the authors used two variables: moisture due to non-freezing water and iciness. They considered the freezing process taking into account the effects of the dynamics of the phase transition of water in the freezing ground. The heat balance equation is based on the Fourier equation, taking into account the freezing of water and, accordingly, ice accumulation; mass transfer is based on equation (7) without taking into account the influence of external pressure. The rate of ice accumulation was determined from the equation

$$\frac{dI}{dt}=a\left(W-W_{nz}\right),$$

where dI/dt, the rate of ice accumulation, is the function of moisture content and the direction of the ice melting process or water crystallization; W_{nz} is the content of unfrozen water; and a is the proportionality coefficient obtained by the authors empirically and depending on the rheological properties of frozen soils.

The approach of Danielyan–Yanitsky, apparently, is one of the most interesting from the point of view of ensuring the continuity of the solution of the problem, since the criteria for the formation of ice and the time functions of its appearance are set. It is assumed that ice is "delayed" during crystallization, and this delay sets the ice crystallization process and moisture freezing in a wide area, not just at the interface.

The Li model

A two-dimensional version of the mass transfer problem, preferably in frozen soil, is presented in [*Li et al., 2013*]. To determine the migration of moisture, the authors express the moisture gradient through the temperature gradient:

$$I_w=\rho_0 D\frac{dW}{dx}=\rho_0 D\frac{dW}{dT}\frac{dT}{dx},$$

where D is the diffusion coefficient of water in the soil.

The authors use the Fourier equation taking into account water migration and phase transitions due to unfrozen water:

$$\left(c\rho+L\rho_w\frac{dW}{dT}\right)\frac{dT}{dt}=\left(k_x+L\rho_w\frac{dW}{dT}D_x\right)\frac{dT}{dx}+$$

$$+\left(k_y+L\rho_w\frac{dW}{dT}D_y\right)\frac{dT}{dy},$$

where k_x, k_y are the coefficients of thermal conductivity; D_x, D_y are diffusion coefficients; ρ is the soil density; c is the soil heat capacity; and ρ_w is water density.

POROSITY-BASED MODELS

The Mikhailovsky–Zhu model

The paper [*Michalowski, Zhu, 2006*] presents a model in which a solution of the thermal problem based on the modified Fourier equation for frozen soil is proposed:

$$C\frac{dT}{dt}-L\frac{d\theta_i}{dt}\rho_i-\nabla\left(\lambda\nabla T\right)=0,$$

where ∇ is the symbol of the gradient; θ_i is the volume fraction of ice.

The main idea of the model is an attempt to express the main coefficients included in the equation of heat balance and mass balance through the porosity of the soil, since the accumulation of ice changes primarily the spatial geometry of the distribution of mineral particles. So, the volume fraction of ice, θ_i, is calculated by the formula

$$\theta_i=\frac{V_i}{V}=n\left(1-\nu\right),$$

where V is the total volume of the soil; V_i is the volume of ice; n is the porosity of the soil; and ν is the volume

fraction of unfrozen water relative to the total volume of unfrozen water and ice in the soil:

$$\nu = \frac{V_w}{V_w + V_i},$$

where V_w is the volume of unfrozen water; V_i is the volume of ice.

The dependence of porosity on temperature is characterized by a certain maximum and is given by the equation

$$n = n_m \left(\frac{T - T_0}{T_m} \right)^2 \exp\left[1 - \left(\frac{T - T_0}{T_m} \right)^2 \right],$$

where n is the porosity of the soil; n_m is the maximum porosity; T_0 is the freezing point; T_m is the temperature at maximum porosity; and T is the current temperature.

The equation of material balance is solved with respect to the porosity of the soil:

$$(\rho_i - \rho_s)\frac{dn}{dt} + (\rho_w - \rho_i)\frac{d(n\nu)}{dt} - \rho_w \nabla(\nabla h) = 0,$$

where ρ_i, ρ_w, ρ_s are the densities of ice, water, and mineral (solid) particles, respectively; h is the water pressure, m.

Among recent works, the work [*Ming et al., 2016*] should be noted, as it suggests a solution based on this approach; it takes into account the stress-strain state of the soil and porosity. The authors consider the general deformation of the soil as the sum of thermal expansion, elastic deformation, and deformation due to changes in the porosity of the soil. The stress state equation is proposed:

$$d\sigma = -dE_s \varepsilon^e = -dE_s \left[\varepsilon - \varepsilon^T - \varepsilon^c \right],$$

where σ is tension; E_s is elastic modulus; ε^e is elastic deformation; ε^T is deformation due to thermal expansion; ε^c is creep deformation; and ε is the total deformation, which can be described by changing the porosity by the formula

$$\varepsilon = \frac{n_0 - n}{1 - n},$$

where n_0 is the initial value of porosity, and n is its current value.

In [*Abdalla et al., 2014*], it is also proposed to improve the dependence of the porosity function on temperature for the thawed part and, in addition, to take into account the dependence of thermal conductivity as a function of temperature and porosity with due account for the direction of freezing or thawing.

In [*Li et al., 2018*], a solution to the problem of mass transfer with incomplete water supply is proposed (i.e., the influence of air on the moisture transfer process is taken into account). In addition, in this work, the solution of a mechanical problem is proposed. In contrast to the previous work, the total deformation is considered as the sum of elastic deformation, viscoplastic deformation, and deformation due to frost heaving, which, in turn, depends on porosity. The stress-strain state in the work is solved by representing the total deformation as a sum of deformations due to elastic interaction, heaving deformation, and viscoplastic deformation. Since the stress in the ground, according to [*Li et al., 2018*], arises due to elastic interaction, the elastic component is expressed in terms of the difference between the total deformation, deformation due to heaving, and viscoplastic deformation:

$$\{\Delta\sigma\} = [D_T]\left(\{\Delta\varepsilon\} - \{\Delta\varepsilon_{vp}\} + \{\Delta\varepsilon_{fh}\}\right),$$

where σ is the stress; D_T is the modulus of elasticity; ε is the total deformation; ε_{vp} is the viscoplastic deformation; ε_{fh} is the heaving deformation determined by the formula:

$$\Delta\varepsilon_{fh}^V = \theta_i^{t+\Delta t} + \theta_w^{t+\Delta t} - n_s^t,$$

where θ_i, θ_w are the volume fractions of ice and unfrozen water; and n_s is porosity.

The Pavlov–Permyakov–Romanov model

The transfer of salt dissolved in the soil water is determined by Fick 's law:

$$I_c = D_c \frac{dC}{dx},$$

where I_c is the ion flux density; C is the ion concentration; and D_c is the ion diffusion coefficient.

In the works [*Pavlov, Permyakov, 1983; Permyakov, Romanov, 2000*], a two-dimensional model of salt transfer is considered, which allows modeling the two-dimensional distribution of salt in soils. The model assumes the squeezing of salts from the frozen zone during freezing. For this purpose, a problem is considered that takes into account only conductive heat sources, and salt transfer is determined only by the concentration of salt according to Fick's law:

$$\frac{dC}{dt} = \frac{d}{dx}\left(D\frac{dC}{dx} \right) + \frac{d}{dy}\left(D\frac{dC}{dy} \right).$$

The Popov model

The coupling of the moisture transfer process with salt transfer is most fully considered in the work [*Popov, 2006*]. The author takes into account the thermogradient effect, ion adsorption in the diffusion layer, the cross movement of moisture and salt, and salt capture during ice crystallization in the pores. They propose a system of equations of thermal and material balance, including

– the Fourier equation taking into account convective moisture transport

$$C_p \frac{dT}{dt} = -\frac{d}{dx}\left[\lambda\frac{dT}{dx} + c\rho_0 T J_w \right],$$

– the moisture balance equation

$$\frac{dW}{dt} = -\frac{d}{dx}J_w - I_f,$$

– the general equation of moisture and salt balance

$$\frac{d(WC)}{dt} = -\frac{d}{dx}\left[WD_c\frac{dC}{dx} + CJ_w\right] - k_z CI_f - I_a,$$

– the equation for calculating the total water flow

$$J_w = -K\frac{dW}{dx} + K\delta_{CW}\frac{dC}{dx} - K\delta_{TW}\frac{dT}{dx} + V_f,$$

where I_f is the water outflow due to water crystallization; I_a is the outflow of salt due to ion adsorption by the diffusion layer; J_w is the water flow; K is the diffusion coefficient; $K\delta_{CW}\frac{dC}{dx}$ is the component of the water flow due to the cross flow of salt; $K\delta_{TW}\frac{dT}{dx}$ is the component due to the thermogradient effect; the value of $k_z CI_f$ determines the salt capture during ice crystallization; and V_f is the water filtration rate caused by the pressure gradient.

THERMOMECHANICAL MODELS

A common feature of thermomechanical models is an attempt to describe the joint equations of heat and mass transfer using the equation of the stress-strain state of the soil.

The Grechishchev model

In [*Grechishchev, 1983*], the soil is considered as a filtration-consolidation medium. To describe the heat balance for the frozen and thawed zones, S.E. Grechishchev used the Fourier equations. The model describes the filtration consolidation equations relating the pressure in the soil to the stress-strain state and the water flow velocity in it.

The model considers the phase equilibrium of the linked small and large pores using the Clapeyron–Clausius equation; for large pores, the stress on the pore ice matrix is taken into account. Temperature fields are determined from this equilibrium. In the model, the equations of phase equilibrium take into account the kinetics of mass transfer and the movement of the freezing front.

The Razbegin model

V.N. Razbegin solves a heat problem with a freezing boundary, where three zones are distinguished: thawed, frozen, and freezing [*Razbegin, 1983*]. At the same time, the Fourier equation was used to set the heat balance equations for thawed and frozen zones, and for the material balance in the thawed zone, an equation based on the moisture gradient as a driving force, taking into account the thermogradient coefficient (δ) was applied:

$$\frac{dW}{dT} = \frac{d}{dx}\left(a\frac{dW}{dx} + a\delta\frac{dT}{dx}\right),$$

in the zone of phase transitions, taking into account only the thermogradient coefficient

$$\frac{dW}{dT} = \frac{d}{dx}\left(a\delta\frac{dT}{dx}\right).$$

A feature of the author's approach is the generalization of the equations of material and heat balance regarding the case of the occurrence of deformation and stress fields.

Using the thermodynamic approach and the dependence of generalized thermodynamic functions on the strain-stress state, the author presents a system of equations for the combined solution of the strain-stress state, the heat problem, and the mass transfer problem.

CONCLUSIONS

The models, in which the problems of combined moisture, salt, and heat transfer and the mechanical stresses accompanying this process are solved, are the most perfect models from the point of view of their physical formulation. These models describe the solution of the problems in the most comprehensive way. However, the complexity of these models, primarily in determining the main coefficients included in the equations, sharply limits their practical applicability.

The table shows the typification of the physical formulation of the problem of mathematical models of freezing and heaving of soils, which was compiled by the authors of the article on the basis of the above analysis.

The tasks ***of front models*** can be divided into three groups. In the models of group I used in the works of V.G. Melamed and G.M. Feldman, the moisture gradient is considered as the driving force of moisture transfer. The Stefan problem is solved at the freezing front, and it is assumed that the moisture gradient is determined by the difference in moisture from the initial total soil moisture to the values of the unfrozen water content at the freezing front. Such a solution is not perfect and unambiguous, since it has been experimentally proved that cryogenic migration in the thawed zone can occur in a gradient-free moisture field, but at the same time in a gradient field of pore pressure, which is set by temperature at the phase boundary [*Cheverev, 2004*].

The models based on R. Miller's approach can be combined into Group II. In these models, the freezing soil is divided into three zones: thawed, transitional (freezing), and frozen. In this case, the formation of ice lens is considered at the border of the transitional and frozen zones. The temperature of the freezing

front is always fixed and is equal to the freezing temperature of the pore solution, and the temperature at the boundary of the transition and frozen zones is variable and is a function of pore pressure, moisture, and the thermal regime of freezing. A significant disadvantage of this approach is simplification, in which the process of moisture transfer is considered only in the area of the so-called freezing layer located between the freezing front and the first ice lens, and then, behind the ice lens, the process of mass transfer is ignored. At the same time, the work [*Ershov, 1999*] showed the presence of unfrozen water flow behind the ice lens, i.e., it is quite possible to assume the existence of an intermediate layer with ice lenses.

In this case, the value of the pore pressure in the freezing zone is determined from Eq. (4), and at the contact of the freezing zone with the growing ice lens, the pressure on the ice (in Eq. (4)) is equated to the external load. As a significant advantage of this approach, it is necessary to indicate the possibility of solving a number of engineering problems that take into account the influence of external load [*Gorelik, 2010*].

In Group III models, for example in the Cheverev–Buldovich and Cheverev–Safronov models, the

Table 1. **Typification of the physical formulation of the problem in mathematical models of freezing and heaving of soils**

Group	Model special features	Author
	Front models	
I	The solution of the Stefan problem at the freezing front, taking into account convective moisture transfer. The water flow is set by the moisture gradient before the freezing front. The moisture at the freezing front is assumed to be equal to the moisture of the lower limit of plasticity	[*Melamed, 1969; Feldman, 1988*]
II	The driving force of cryogenic migration is the gradient of pore equilibrium pressure determined from the generalized Clapeyron–Clausius equation. Models with three zones in the freezing soil: thawed, transitional, frozen. Two boundary conditions with a mobile zone: at the interface of thawed and transitional zone and at the interface of transitional and frozen zones	[*Miller, 1978*]
II	Solving the problem of mass transfer to the frozen zone due to the temperature gradient in it. Application of the concept of segregation potential	[*Konrad, Morgenstern, 1980*]
II	Ice release at the boundary of the thawed and frozen zones in the form of a continuous ice lens; the Stefan equation at the boundary is replaced by the ice lens growth equation. Freezing is considered only at the boundaries of the intermediate layer. The segregation criterion is formulated from the condition of the pore pressure to the external load equilibrium	[*Gilpin, 1980*]
II	Following Gilpin, the segregation criterion is formulated from the condition of equality of pore pressure to external load. An algorithm for calculating layered structures has been developed taking into account the external load, but accounting for the properties of real soils	[*O'Neill, Miller, 1985*]
III	Consideration of thawed, transitional (freezing), and frozen zones. Setting the flow of water into the frozen zone through the gradient of the pore pressure of water in the frozen zone based on the Edlefsen–Andersen equations (in potential form). Analytical solution of the problem	[*Ershov, 1999*]
II	Further development of the Miller and Gilpin approach in the freezing zone is considered as in Gilpin, but the pore ice is associated with the body of the growing ice lens	[*Gorelik, Kolunin, 2002*]
III	Development of the Cheverev–Buldovich model. A numerical solution of the problem with an automatic change in the pressure gradient in the thawed zone depending on the state of freezing, gradients of thawed and frozen zones, and boundary conditions is proposed. The Fourier equation is solved in thawed and frozen zones	[*Cheverev, Sarfonov, 2012*]
	Frontless models	
I	The equations of material balance are solved through the total moisture content and iciness. Accounting for phase transitions due to unfrozen water in Fourier equations	[*Lavrov, 2000*]
I	Introduction of relaxation time of ice crystallization and melting. With ice formation in a frozen state	[*Danielyan, Yanitsky, 1983*]
II	Modified Fourier equation for thermal balance and material balance equation based on porosity	[*Michailovsky, Zhu, 2006*]
I	Two-dimensional solution of the problem only for the frozen state of the soil. Transformation of the water flow rate equation from a moisture gradient to a temperature gradient	[*Li et al., 2013*]
I	Solving the problem of joint heat, water, and salt transfer taking into account the cross effects of water transfer, thermogradient effect, the effect of salt adsorption by diffusion layer and salt capture during crystallization	[*Popov, 2006*]
III	Thermorheological model. Finding the water flow velocity taking into account changes in the pore pressure gradient. The pore pressure is derived from the equation of the stress-strain state of the soil. The solution of Stefan's problem is found taking into account the changing pore pressure	[*Grechishchev, 1983*]
III	The solution of the problem taking into account the deformation-stress state of the soil during freezing. The driving force of migration is the gradient of the equilibrium pore pressure determined by the stress-strain state	[*Razbegin, 1983*]

transition zone actually corresponds to the zone of limit of the soil shrinkage, and the freezing process is considered primarily in the zone of intense ice release in the temperature range from T_{bf} to T_{bf} –0.6 (where T_{bf} is the freezing point, °C). In these models, the Edlefsen–Andersen equation is used as the equation of the dependence of pore pressure in the soil on temperature; in fact, this is a modified Clapeyron–Clausius equation, where it is assumed that ice formed during freezing does not apply pressure on water.

This statement is true if the freezing zone, namely, the pore pressure in it, is not affected by the external load factor or hydraulic pressure of a different genesis. The consideration of this factor is implemented in the work [*Cheverev, 2004, p. 16*]. One of the advantages of this approach is the possibility of taking into account hydrogeological conditions and external load, under which it is necessary to simulate the process of deformation of the heaving of freezing soil in the presence of additional pressure from its thawed zone.

A characteristic advantage of ***the frontless models*** currently available is the possibility of two- and three-dimensional modeling of freezing processes with an uneven distribution of both heat and water sources in space and time. Recently, there has been a tendency to expand the scope of application of models of this type by taking into account the influence of mechanical load, for example, in the works [*Ming et al., 2016; Li et al., 2018*].

Frontless models can be conditionally subdivided into three groups. The models constructed on the basis of A.V. Lykov's equations belong to group I. The principle of moisture transfer in these models is based on the moisture gradient. The disadvantage of this approach is the requirement for the presence of moisture gradient in the thawed zone. This is often associated with the difficulty of modeling the freezing of dense soils with the moisture at the shrinkage limit. This is especially characteristic of silty sands and loamy sands. It is also important to take into account the relaxation nature of rheological deformation and, consequently, changes in soil density, even if the zone has internal sources of moisture and the moisture gradient is well defined. In addition, difficulties arise with the use of the moisture content for frozen soils due to the non-monotonous (with an extremum) dependence of the diffusion coefficient of unfrozen water on temperature. There is also the difficulty of physical verification of the model due to the consideration of ice fields when solving the equations of the material balance. The situation becomes even more complicated with salt removal in soils due to the known overlapping effects of mutually intersecting thermal and material flows. It should be emphasized that this method requires complex methods of monitoring the dynamics of moisture and ice content fields in frozen and thawed soils.

Group II should include models in which the equations of material and heat balance are solved by introducing porosity as a variable. An additional advantage of this approach is the possibility of solving a mechanical problem. The main disadvantage of the approach is the difficulty of obtaining the appropriate coefficients in the equations for the practical application of these models, because, in addition to ice and water in frozen soils, air also has a significant effect on porosity. Despite the number of works, in which an attempt was made to theoretically account for this influence, significant refinement of practical methods for determining the appropriate amendments to such an influence is required.

Group III should include models in which, in addition to heat and material balance, problems related to the deformation-stress state of soils are solved. This approach is, in our opinion, the most correct and solves a number of problems for Group I tasks. However, it aggravates the already complex physical verification of the model and the determination of the main parameters specified in the equations of the stress-deformation state, phase equilibrium, and heat and material balance.

This greatly narrows the scope of the actual applicability of these models in pactice at the present time.

Funding. *This study was carried out with financial support of the Research Institute of Transneft JSC (contract no. 4220 P/20-511/2015 dated November 19, 2015).*

References

Abdalla B., Fan C., Mckinnon C. et al., 2014. Extended porosity rate function for frost heave. In: 33rd Int. Conf. Ocean, Offshore and Arctic Engineering. Vol. 10: Polar and Arctic Science and Technology (San Francisco, California, USA, June 8–13, 2014). New York, Publ. ASME, V010T07A046. DOI: 10.1115/OMAE2014-24221

Akagawa S., Satoh M., Kanie S. et al., 2006. Effect of tensile strength on ice lens initiation temperature. In: 13th Int. Conf. Cold Regions Engineering (Orono, Maine, United States, July 23–26, 2006). Reston, VA, United States, Publ. ASCE, p. 1–12. DOI: 10.1061/40836(210)43

Bronfenbrener L., Bronfenbrener R., 2010. Modeling frost heave in freezing soils. *Cold Reg. Sci. Technol.*, **61**, 43–64.

Brovka G.P., 1991. Heat and Mass Transfer in Natural Dispersed Systems during Freezing. Minsk, Nauka i Tekhnika, 126 p. (in Russian).

Cheverev V.G., 1999. Physicochemical theory of the formation of mass-exchange and thermal properties of cryogenic soils. Author's abstract of Doctoral (Geol-Mineral.) Theses. Moscow, 41 p. (in Russian).

Cheverev V.G., 2003a. Classification of water bond forms in the frozen fine-grained soils. *Kriosfera Zemli*, **VII** (3), 31–40 (in Russian).

Cheverev V.G., 2003b. Properties of bound water in cryogenic grounds (analytic review). *Kriosfera Zemli,* **VII** (2), 30–41 (in Russian).

Cheverev V.G., 2004. Nature of Cryogenic Properties of Soils. Moscow, Nauchn. mir, 234 p. (in Russian).

Cheverev V.G., Brushkov A.V., Polovkov S.A., Pokrovskaya E.A., Safronov E.V., 2021. Analysis of concepts on the mechanism of cryogenic water migration in freezing soils. *Earth's Cryosphere,* **XXV** (5), 3–12.

Cheverev V.G., Burnaev R.S., Gagarin V.E., Safronov E.V., 2013. Influence of the external pressure on the degree of frosty heaving of clay soils. *Earth's Cryosphere,* **XVII** (4), 57–62.

Cheverev V.G., Safronov E.V., 2012. Mathematical modeling of soil freezing with visualization of the forming cryogenic structure. In: 10th Int. Conf. Permafrost (TICOP) Resources and Risks of Permafrost Regions in a Changing World (Salekhard, 2012). Tyumen, Pechatnik, vol. 3, p. 561–564 (in Russian).

Danielyan Yu.S., Yanitsky P.A., 1983. Features of nonequilibrium redistribution of moisture during freezing and thawing of dispersed soils. *Inzhen-Fizich. Zh.*, **44** (1), 91–98 (in Russian).

Edlefsen N.E., Anderson A.B.C., 1943. Thermodynamics of Soil Moisture. Hilgardia, p. 31–298.

Ershov E.D. (Ed.), 1999. Fundamentals of Geocryology. Part 5. Engineering Geocryology. Moscow, Izd. Mosk. Gos. Univ., 526 p. (in Russian).

Feldman G.M., 1988. The Movement of Water in Thawed and Freezing Soils. Novosibirsk, Nauka, 256 p. (in Russian).

Getz I.G., Meirmanov A.M., 2000. Generalized solution of the Stefan problem with kinetic supercooling. *Sib. Zh. Industial. Matemat.* **3** (1), 66–86 (in Russian).

Gilpin R., 1980. A model for the prediction of ice lensing and frost heave in soils. *Water Resour. Res.*, **16** (5), 918–930.

Gorelik Ya.B., 2010. On the calculation methods of the engineering construction displacements caused by freezing layer frost heave process. *Kriosfera Zemli,* **XIV** (1), 50–62 (in Russian).

Gorelik Ya.B., Kolunin V.S., 2002. Physics and Modeling of Cryogenic Processes in the Lithosphere. Novosibirsk, Publ. House SB RAS, Geo Branch, 317 p. (in Russian).

Grechishchev S.E., 1983. On the basics of thermorheology of cryogenic rocks. In: Problems of Geocryology. Moscow, Nauka, p. 90–100 (in Russian).

Konrad J.M., Morgenstern N.R., 1980. Mechanistic theory of ice lens formation in fine-grained soils. *Can. Geotech. J.*, **17**, 473–486.

Kudryavtsev V.A. (Ed.), 1978. General Geocryology. Moscow, Izd. Mosk. Gos. Univ., 464 p. (in Russian).

Kudryavtsev V.A., Ershov E.D., Cheverev V.G., 1973. Moisture transfer in frozen soils. *Byull. Mosk. Gos. Univ., Ser. Geol.*, 5, 26–34 (in Russian).

Lavrov S.A., 2000. Processes of heat and moisture transfer in the soil and snow cover. Author's abstract of Doctoral (Technical Sci.) theses. St. Petersburg, 40 p. (in Russian).

Li Z., Liu S., Feng Y. et al., 2013. Numerical study on the effect of frost heave prevention with different canal lining structures in seasonally frozen ground regions. *Cold Reg. Sci. Technol.,* **85**, 242–249.

Li S., Zhang M., Pei W. et al., 2018. Experimental and numerical simulations on heat-water-mechanics interaction mechanism in a freezing soil. *Appl. Thermal Engin.*, **132**, 209–220.

Loranger B., 2020. Laboratory investigation of frost susceptibility of crushed rock aggregates and field assessment of frost heave and frost depth. Thesis for the Degree of Ph. D. Norway, Trondheim, 189 p.

Lykov A.B., Mikhailov Yu.A., 1963. Theory of Heat and Mass Transfer. Moscow; Leningrad, Gosenergoizdat, 536 p. (in Russian).

Ma W., Zhang L., Yang C.-S., 2015. Discussion of the applicability of the generalized Clausius–Clapeyron equation and the frozen fringe process. *Earth-Sci. Rev.*, 142, 47–59.

Melamed V.G., 1969. Solution of the problem of freezing of fine-grained soils taking into account the migration of water to the freezing front. In: Merzlotn. Issled. (Mosk. Gos. Univ.), iss. 9, 90–100 (in Russian).

Michalowski R.L., Zhu M., 2006. Modelling of freezing in frost-susceptible soils. *Comp. Assisted Mechanics Engineer. Sci.*, 13, 613–625.

Miller R.D., 1978. Frost heaving in non-colloidal soils. In: 3rd Int. Conf. Permafrost (Edmonton, Alberta, Canada, July 10–13, 1978) Proc. Ottawa, Natl. Res. Council of Canada, vol. 1, p. 708–713.

Ming F., Zhang Y., Dongging Li., 2016. Experimental and theoretical investigations into the formation of ice lenses in deformable porous media. *Geosciences J.*, **20**, 667–679.

O'Neill K., Miller R., 1985. Exploration of a rigid ice model of frost heave. *Water Resour. Res.*, **21** (3), 281–296, DOI: 10.1029/WR021i003p00281.

Pavlov A.R., Permyakov P.P., 1983. Mathematical model and algorithms for calculating heat and mass transfer on a computer during soil freezing. *Inzhenern.-Fizich. Zh.,* **44** (2), 311–316 (in Russian).

Permyakov P.P., Romanov P.G., 2000. Heat and Salt Transfer in Frozen Unsaturated Soils, Yakutsk, Publ. House SO RAN, 128 p. (in Russian).

Popov V.I., 2006. Mathematical modeling of heat and mass transfer in rocks using a phase equilibrium diagram. Cand. Sci. (Technical Sci.) Diss., Yakutsk, 120 p. (in Russian).

Razbegin V.N., 1983. Thermodynamic Aspects of Mechanics of Frozen Soils. Moscow, Nauka, 104 p. (in Russian).

Tikhonov A.N., Samarsky A.A., 1999. Equations of Mathematical Physics. Moscow, Nauka, 196 p. (in Russian).

Received July 3, 2021
Revised January 17, 2022
Accepted April 19, 2022

Translated by S.B. Sokolov

EARTH'S CRYOSPHERE
SCIENTIFIC JOURNAL

Earth's Cryosphere, 2022, vol. XXVI, No. 3, pp. 37–42

CRYOGENIC PHENOMENA IN SEAS AND OCEANS

ON THE DIFFERENCES BETWEEN DRIFTING ICE RIDGES AND ICE RIDGES IN THE LANDFAST ICE

V.V. Kharitonov[1,*], O.M. Andreev[1]

[1] *Arctic and Antarctic Research Institute, ul. Beringa 38, St. Petersburg, 199397 Russia*

**Corresponding author; e-mail: kharitonov@aari.ru*

The analysis of differences in the structure of drifting ice ridges and ice ridges in the landfast ice was carried out on the basis of information obtained during research work done by the Arctic and Antarctic Research Institute in 2007–2019 in the Kara and Laptev seas. The studies were carried out using thermal water drilling with logger recording of the penetration rate. The main attention was focused on the distribution of ice ridge porosity and the thickness of the consolidated layer. The unconsolidated part of the ice ridge keel and its compaction in the process of ice ridge formation under the action of the Archimedes force were considered. It was revealed that the ice ridges in the landfast ice differed from drifting ice ridges in their somewhat smaller geometric dimensions, but in steeper sail and keel slopes, as well as in a different keel/sail ratio (3.1 versus 3.6). In the landfast ice ridges, the porosity of the unconsolidated part of the keel was lower than in drifting ice ridges (by 6% on average). It was confirmed that the gradual decrease in the porosity of the unconsolidated part of the keel of the ice ridges in the landfast ice was caused by the under-ice currents.

Keywords: *ice ridge, drifting ice, landfast ice, thermal drilling, sail, keel, consolidated layer, porosity.*

Recommended citation: Kharitonov V.V., Andreev O.M., 2022. On the differences between drifting ice ridges and ice ridges in the landfast ice. *Earth's Cryosphere,* XXVI (3), 37–42.

INTRODUCTION

According to the nomenclature of the World Meteorological Organization [*WMO..., 1970–2017*], landfast ice is a type of sea ice that forms and remains motionless along a coast, where it is attached to a coastline, to an ice wall or an ice barrier between shallows and icebergs grounded on the shallow sea floor.

It may form naturally from salt water or by adfreezing to the coast or to the already existing floating landfast ice of any age range. It can extend to a distance of only a few meters or to several hundred kilometers from the coast. The term drifting ice is used in a broad sense and includes any kind of ice, except for the motionless landfast ice.

An ice ridge is a chaotic pile-up of ice blocks, which occur in a sail under the force of gravity, and in a keel under the force of gravity and Archimedes' force. The ice ridges are the intrinsic part of the ice cover of the Earth's polar regions and are subdivided into drifting and motionless (landfast) types. In terms of the formation, the drifting ice ridges and the landfast ice ridges are almost the same, because in both cases they are the result of the ice piling up during compression of ice floes. At the initial stage of the ice ridge development, the pile-up of ice blocks is formed, and most of them become submerged in the water. This leads to strong local thermal gradients between the cold ice blocks and the surrounding water. Therefore, at the initial point of time, the vertical distribution of the temperature in the ice ridge keel will look like a sawtooth line with "teeth" unequal in height and shape. As the consolidated layer (CL)* grows, the sawtooth line will transform into the piecewise linear line, which, later, will be smoothed and deviated towards low temperatures in the upper part of the keel.

The end of the initial phase of the ice ridge formation can be defined as the moment, when the unconsolidated keel becomes isothermal and comes to the state of thermodynamic equilibrium. The initial phase of the ice ridge life is rather short (16–96 h [*Høyland, Liferov, 2005*]) and proceeds equally for both drifting ice ridges and ice ridges in landfast ice. Then the main phase begins, and the breakpoint on the temperature profile, located between the sloping section in the CL and the isothermal section (in the unconsolidated keel), determines position of the CL lower boundary [*Høyland, 2002*].

The consolidated layer isolates the underlying keel from cold air. This results in continuous degrada-

* A consolidated layer of the ice ridge is a layer of dense (solid) ice with an upper boundary near a waterline. This layer is formed by the action of cold and water freezing in the space between blocks of ridged ice. It includes these blocks and is characterized by the strength close to that of level ice.

tion of the unconsolidated keel and leads to the transformation of the ice ridge into the second-year ice ridge or to the melting/decay of the ice ridge. At this stage, the living conditions of the ice ridges are already different, because under-ice currents strongly affect the keel of the ice ridges in landfast ice. Drifting ice ridges move (in the absence of wind load) directly under the action of currents. Therefore, the relative movement of water masses and keels of the drifting ice ridges is insignificant or absent at all.

The purpose of this work is to discuss the results of the comparative analysis of the main morphometric characteristics and the internal structure of the drifting ice ridges and the ice ridges in landfast ice. Our study is based on data obtained during the works of the Arctic and Antarctic Research Institute in 2007–2019 in the Kara and Laptev seas.

The work [*Guzenko et al., 2021*] is one of the recent works on this topic in the studied region. Morphometry of the ice ridges in the Spitsbergen fjords, in the central part of the Barents Sea, and in the Fram Strait was considered in the works [*Strub-Klein, Høyland, 2011; Sand et al., 2013*]. Much attention was paid to the impact of ocean currents on keel erosion. It was noted that small ice ridges in landfast ice are more affected by keel erosion than large ice ridges. The currently accepted theory considering the flow through consolidated layers states that up to 20% of the boundary flow falling on the keel can seep through it [*Amundrud et al., 2006*]. The extremely interesting results, which are not yet confirmed by other researchers, are given in [*Shestov, Marchenko, 2014*]. These data indicate that inside the unconsolidated part of the keel, a velocity of sea water flows in voids can be up to three times higher than the flow velocity under the level ice surrounding the ice ridge. Subsequent studies [S*hestov, Marchenko, 2016a,b*] give reasons for the ice growing and decreasing macroporosity of the unconsolidated keel over time owing to the keel permeability for seawater and changes in water salinity.

METHODS

The ice ridge structure was studied with the use of thermal water drilling with logger recording of the penetration rate. The description, scheme, and technical characteristics of the system are given in [*Mironov et al., 2003*]. The drilling was generally carried out along the profiles routed across the ice ridge crest. The distance from the top of the snow cover (ice) to the sea level was additionally measured at each drilling point. The morphometric characteristics of the ice ridges and their internal structure were determined on the basis of the subsequent processing of the rates of a thermal drill [*Morev et al., 2000*]. The penetration rate depends on the thermal power supplied to the thermal drill as well as on ice porosity and (to a small extent) on ice temperature. Therefore, the location of voids, consolidated and unconsolidated ice in the borehole sections was determined directly from the drilling rate. The movement of the thermal drill is dramatically accelerated in the areas of porous ice (especially in voids filled with snow, slush, water, or air). The necessary condition for validity of the determination of voids is the drilling at the constant thermal power (if thermal power is not constant, accurate registration of the changes in the power during drilling is required). The values of the above-water and underwater parts of the ice cover, CL boundaries of the ice ridges, boundaries of voids, and zones of ice with different porosity were determined during the subsequent processing of the obtained thermal drilling data.

An important characteristic of the internal structure of ice ridges is their porosity. K. Høyland [*2002*] distinguishes two levels of this parameter: macroporosity and total porosity. The macroporosity is defined as the ratio of the volume of voids in the selected area of the ice ridge to the total volume of this area. The total porosity also includes the porosity of the level ice, from which the ice ridge is composed. In other words, the total porosity also includes micropores located directly in ice blocks. The boundaries and sizes of the voids are recorded on the basis of the thermal drilling rate. In this work, the porosity θ is defined as the following value:

$\theta(x, y, z) = 0$, with ice in the point with coordinates (x, y, z),

$\theta(x, y, z) = 1$, without ice.

The linear porosity is obtained by averaging this function vertically, over the given depth interval, while the volumetric porosity is obtained by averaging over the given volume. The distribution of porosity by depth at each drilling point is determined by the step function, where zero corresponds to ice and unity corresponds to void. Air bubbles and cells with brine in the ice blocks are not taken into consideration. It is impossible to determine the volumetric porosity in detail by the point drilling due to the complicated internal structure of the ice ridge.

However, it can be estimated using the obtained distributions of the linear porosity at different points. It is believed that the volumetric porosity is equal to the average value of the infinite number of linear (in this case, vertical) porosities. Currently, it is considered that the volumetric porosity of the ice ridge corresponds to the averaged values of its linear porosity [*Høyland, 2002*].

When calculating ice loads on hydraulic structures, an ice ridge is often considered as a special case of loose medium with the wide range of fractions [*Alekseev et al., 2001; Bolgov et al., 2007*]. Consolidation of the loose medium under gravity was considered in [*Oleinikov, Skachkov, 2011*]; the proposed models were compared with experimental data on

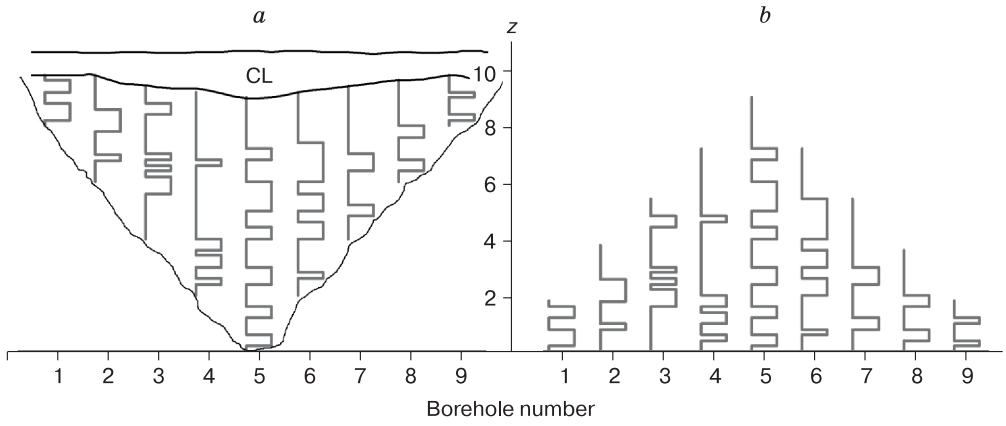

Fig. 1. The distribution of porosity of the unconsolidated part of the keel of the ice ridge in individual boreholes (*a*) and in the case of the shift to the depth of the maximum keel draft (*b*).

CL – consolidated layer; *z* – distance from the lower edge of the keel.

rocks and snow. According to the model [*Oleinikov, Skachkov, 2011*], the decrease in porosity of the loose medium with depth occurs due to an increase in pressure. The authors believe that the similar process may be quite important at the initial stage of the ice ridge formation. Thus, the possible manifestations of the process were given in more detail.

According to these authors, the keel of the ice ridge can also be considered as the turned over pile of ice blocks, which, during the process of the ice ridge formation, may be affected by consolidation not only under the action of gravity but also under the action of the Archimedean force. In this case, the zone directly bordering the lower surface of the keel will be the zone, where compression stress is absent. With distance upward from the lower edge of the keel, the porosity will decrease under pressure of ice block piles. Due to the fact that the CL porosity, in most cases, is equal to zero, let us consider only the unconsolidated part of the ice ridge keels. To establish the nature of the porosity distribution of this part, we will average individual distributions of the unconsolidated keel porosity at all points of ice ridge drilling, grouping them according to regions. The averaging procedure will be as follows. In M.N. Skachkov's model, the loose medium is condensed in depth. The zero depth corresponds to the medium surface, and then it grows downward. In our case, the ice ridge keel is the turned over loose medium; therefore, the depth will grow upwards, and the zero depth now corresponds to the lower surface of the keel. Due to the fact that the bottom surface of the keel is not a plane, and all individual distributions of porosity are in different depth intervals, it is necessary to level them by depth before averaging. This can be done, for example, by shifting the distributions down to the depth of the maximum keel draft.

Figure 1 schematically demonstrates this process. The lines indicate the distributions of the unconsolidated keel porosities in individual boreholes. The height of the curves corresponds to the borehole length in the unconsolidated keel. After the levelling, all individual distributions at the depth of the maximum keel draft, it is necessary to consider all depths (from the maximum keel depth to the lower CL boundary) consistently and to average the step curves on the basis of those boreholes that exceed the considered horizon. Let us use this technique to assess possible differences in the distribution of porosity of the unconsolidated keel for the ice ridges formed on drifting ice and in landfast ice.

DISCUSSION

This work was based on the data obtained from the Sea of Okhotsk, the Kara Sea, and the Laptev Sea in 1998–2019. The drifting ice ridges studied in these seas were combined into one group. The second group included the ice ridges of Baidaratskaya Bay of the Kara Sea, Khatanga Bay of the Laptev Sea, and the ice ridges of Shokalsky Strait, which were in the landfast ice at the time of the study. We considered 134 drifting ice ridges and 56 ice ridges in the landfast ice. Table 1 demonstrates the main features of the ice ridges from the first and second groups.

In terms of morphometric parameters (size), the landfast ice ridges are slightly smaller than the drifting ice ridges. They have steeper slopes of the sail and keel; CL is significantly thicker, the ratio of the CL thickness to the average thickness of ice blocks in the sail is twice as large. The latter parameter is an indirect indicator of a more significant age of the ice ridges in the landfast ice, which was confirmed in [*Guzenko et al., 2021*]. A somewhat lower value of the keel/sail ratio for the ice ridges in the landfast ice (3.1 vs. 3.6 for drifting ice ridges) is probably due to more intensive thawing and subsequent decay of ice blocks at the lower edge of the keel.

Table 1. **Averaged characteristics of drifting ice ridges and ice ridges in the landfast ice**

Characteristics	Ice ridges	
	drifting	in landfast ice
Number of ice ridges	134	56
Average sail height, m	3.1	2.5
Average keel draft, m	11.0	7.6
Ratio keel/sail	3.6	3.1
Average CL thickness, m	1.9	2.5
Average porosity of the unconsolidated part of a sail	0.20	0.22
Average porosity of the unconsolidated part of a keel	0.27	0.21
Average vertical size of voids in a sail, m	0.24	0.14
Average vertical size of voids in a keel, m	0.39	0.20
Average ratio of CL thickness to the total ice thickness	0.32	0.54
Average thickness of ice blocks in the ice ridge sail, m	0.50	0.35
Average thickness of level ice nearby the ice ridge, m	1.2	1.7
Average ratio of CL thickness to the block thickness in the ice ridge sail	4.4	8.4
Average sail slope angle, degrees	26	33
Average keel slope angle, degrees	25	29

In [*Naumov et al., 2019*], the morphometric parameters of the Baidaratskaya Bay ice ridges, which were in the landfast ice at the time of the study, were considered and the results of the studies for the period 2005–2017 were summarized. According to these data, the average height of a sail in different years was 0.9–2.7 m, and keel draft was 4.4–8.0 m. These values agree well with the data from Table 1: 2.5-m-high sail and 7.6-m keel draft for ice ridges in the landfast ice. In reference to the CL thickness, the data from the paper do not clearly demonstrate the increased CL thickness in the landfast ice. The studies have been carried out for 10 years, and the range of the average CL thicknesses (1.5–2.4) is quite evenly distributed over the years of the study. The porosity of the unconsolidated part of the keel also varies in the wide range, from 0.13 to 0.44; however, the most frequent porosities range from 0.32 to 0.36, which is also much higher than the values in Table 1. The porosity value of 0.74 for 2013 reported in [*Naumov et al., 2019*] is probably a random value or a typing mistake. This value slightly reduces representativeness and confidence for the represented data.

Høyland's formula [*Høyland, 2002*] gives a straight correlation between the porosity of the unconsolidated part of the keel, the thickness of the ice surrounding the ice ridge, and the CL thickness. Assuming that the CL is absent at the moment of the ice ridge formation and its thickness is zero, the formula looks like

$$H_{CL} = \sqrt{\frac{H_{LI}^2 - H_{LI0}^2}{\theta_{av}}},$$

where H_{CL} is the CL thickness, m; H_{LI0}, H_{LI} are the ice thickness in the ridging moment and the thickness of the ice surrounding the ice ridge, respectively, m; θ_{av} is the average porosity of the unconsolidated part of the keel.

Taking the average thickness of ice blocks in the ice ridge sail as the ice thickness at the moment of ridging and using the data from Table 1, we can calculate the expected CL thickness of the drifting ice ridge. It turns out to be 2.01 m, which is close enough to the CL average thickness of 1.90 m from Table 1. At the same time, for the ice ridges in the landfast ice, the same calculation gives a significantly overestimated CL thickness equal to 3.65 m. The value of 2.4 m (Table 1) is obtained only if the value of 0.45 is taken as the porosity of the unconsolidated keel. Such porosity for fresh ice ridges in the landfast ice is unlikely, especially if we consider that the resulting porosity of the ice ridge sails in both groups is almost the same, 0.20 and 0.22 (Table 1). Therefore, it follows that the keel porosity of the fresh ice ridges should also be in the range of 0.24–0.30. In this case, theoretically, there should be a factor limiting the CL growth. According to [*Naumov et al., 2019*], the most important factor affecting the CL thickness is the presence of the significant snow cover. The thickness of the snow cover for the considered ice ridges in the landfast ice ranged from 0.2 to 0.8 m. The average thickness of the snow cover in the Khatanga Bay was about 0.3 m; in the Shokalsky Strait, it ranged within 0.2–0.8 m (although at some points it was up to 2.3 m). Therefore, the role of the snow cover in the CL growth for different types of ice ridges does not seem to be unambiguous. Alternatively, we can suggest that the slowing down of the consolidation of the landfast ice ridges is affected by the increased geothermal flux.

Figure 2 demonstrates the smoothed distributions of porosity of the unconsolidated keel for drifting ice ridges and for the ice ridges in the landfast ice. These data were obtained using the averaging procedure described above. Figure 2 also represents the relative amount of data averaged in this process. The

smoothing was performed by moving average with 2-m width. The zero of the ordinate axis corresponds to the zero distance from the bottom edge of the keel. Line *5* shows the boundary distance, beyond which the number of averaged data does not exceed 5% of the total number. It can be seen that curve *1* of the porosity of ice ridges in the landfast ice at a distance of about 9 m is shifted towards the lower values in relation to the drifting ice ridges (curve *2*). Figure 2 also illustrates the difference in the values of the average porosity of the drifting ice ridges and the ice ridges in the landfast ice (curve *3*) in the most informative range. It follows that the porosity of the unconsolidated keel of the ice ridges in the landfast ice is, on average, 8.5% lower than that of the drifting ice ridges (at the maximum difference of 12.7%). The average porosity of the unconsolidated keel of the landfast ice ridges is 6% lower than that of the drifting ice ridges (Table 1). It should be taken into account that the average values of porosity are given for the entire thickness of the unconsolidated part of the keel, and the above value of 8.5% was obtained only for distances (from the lower edge of the keel) in the range of 2–8 m.

The obtained difference can be related to the size of the ice ridges. The rate of water filtration through a porous medium depends on the size of the pores, in our case, on the unconsolidated keel voids. The size of the voids depends on the size of ice blocks composing the keel. This was shown in [*Amundrud et al., 2006*]. Voids in the landfast ice ridges are smaller (Table 1); therefore, when the current affects the unconsolidated keel of such ice ridge, it turns out that under-ice water hardly penetrates inside the keel, but leads to melting of the keel from its external edge (generally, from the bottom of the ice ridge, where the current is stronger [*Schramm et al., 2000*]). Thus, macroporosity θ_{av} of the unconsolidated part of the keel of the landfast ice ridge decreases, because the most porous lower part thaws or is decayed due to erosion.

To verify this assumption, the computer simulation of decay of the lower parts of the keel under the action of the currents was additionally carried out.

The porosity distribution according to [*Oleinikov, Skachkov, 2011*] was simulated for 16 unconsolidated keels with 15-m draft each. Then, the lower parts of the keels, ranging in size from 0.3 to 4.5 m, were randomly removed. The remaining fragments of the porosity distributions were shifted and averaged using the procedure described above. As a result, the averaged porosity curve was shifted toward the lower values by about 10% at the maximum value, which agrees well with the difference in Fig. 2.

According to field observations, in the Shokalsky Strait (directly in the area of the studies of landfast ice ridges), there are daily tidal currents with the average velocity of 0.04 m/s at a depth of 10 m and the maximum velocity of 0.23 m/s [*Kharitonov, Borodkin, 2020*]. These data indirectly indicate that the main

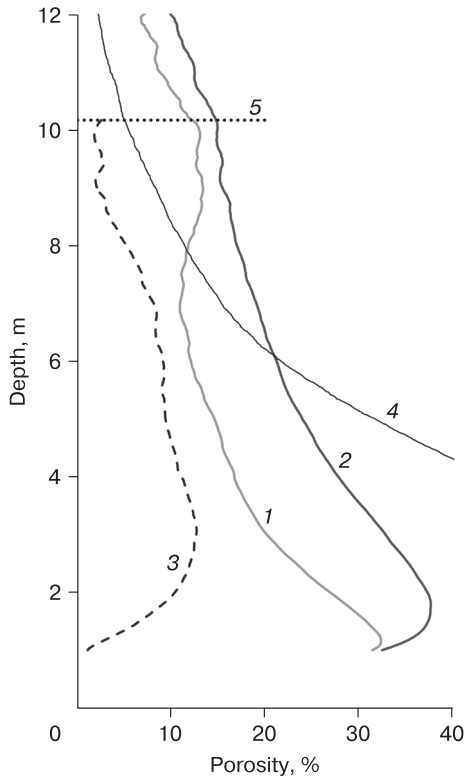

Fig. 2. The smoothed averaged porosity of the unconsolidated part of the keel of the drifting ice ridges and the ice ridges in landfast ice and the relative number of the averaged data.

1 – landfast ice; *2* – drifting ice; *3* – difference in values; *4* – relative number of the averaged values; *5* – the depth, above which the amount of the averaged data does not exceed 5% of the total.

reason for the decreased porosity of the keels of the landfast ice ridges is the action of under-ice currents.

In [*Shestov, Marchenko, 2016a,b*], the mathematic and laboratory simulations, as well as the results of in situ experiments were considered. These data confirm the impact of seawater penetrating into the ice ridge keels on the decrease in porosity of the unconsolidated part of the keel. The generalized porosity plots in Fig. 2 and the comparison of the average vertical sizes of voids in the sail and keel for the ice ridges of both groups (Table 1) support this effect.

The authors of [*Ervik et al., 2018*] note that macroporosity of the keel decreased during the period of staying under the conditions of heat transfer from the ocean to the atmosphere. This may be due to the double effect on the unconsolidated part of the keel from the above-described under-ice current and from the growth of the CL thickness due to its thermodynamic evolution. This is confirmed by the data of field measurements (Table 1), according to which the ice ridges in the landfast ice generally were formed earlier

than the ice ridges on the drifting ice. This is indicated by the CL thickness and the size of ice blocks (i.e., a lower thickness of the level ice, from which the ice ridges were formed).

Therefore, the ice ridges in the landfast ice at the time of measurements (April–May) on average should be somewhat smaller in size (due to thawing the lower part of the keel) and should have lower porosity of the unconsolidated keel than the ice ridges on drifting ice.

CONCLUSIONS

After the analysis of the data, it is possible to draw the following conclusions:

– The ice ridges in the landfast ice differed from the drifting ice ridges in their smaller geometric size and the keel/sail ratio (3.1 vs. 3.6), but in steeper slopes of the sail and keel;

– The CL thickness of the studied drifting ice ridges on average was 1.9 m; for the ice ridges in the landfast ice, it was 2.5 m;

– The average degree of consolidation of the studied ice ridges, i.e., the ratio of CL thickness to the total ice thickness in ice ridges was 32% for the drifting ice ridges and 54% for ice ridges in the landfast ice;

– Porosity of the nonconsolidated part of the keel of the ice ridges in the landfast ice was on average 6% lower than that of the drifting ice ridges; in the keel zone, at distances less than 8 m from the keel edge, this difference averaged 8.5%;

– Our data confirm the conclusion by other researchers that macroporosity of the unconsolidated part of the ice ridge keel gradually decreases under the impact of under-ice currents.

Funding. *This work was performed as a part of the planned research of the Arctic and Antarctic Research Institute on theme 5.1.5 NITR (2020–2024) of the Russian Committee on Hydrology and Meteorology (Rosgidromet).*

References

Alekseev Yu.N., Afanas'ev V.P., Litonov O.E. et al., 2001. Ice Engineering Aspects of Offshore Oil and Gas Fields Development. St. Petersburg, Gidrometeoizdat, 360 p. (in Russian).

Amundrud T.L., Melling H., Ingram R.G., Allen S.E., 2006. The effect of structural porosity on the ablation of sea ice ridges. *J. Geophys. Res.*, **111**, C06004.

Bolgov M.V., Krasnozhon G.F., Liubushin A.A., 2007. The Caspian Sea: Extreme Hydrological Events. Moscow, Nauka, 381 p. (in Russian).

Ervic Å., Høyland K.V., Shestov A., Nord T.S., 2018. On the decay of first-year ice ridges: Measurements and evolution of rubble microporosity, ridge drilling resistance and consolidated layer strength. *Cold Reg. Sci. Technol.*, **151**, 196–207.

Guzenko R.B., Mironov Ye.U., May R.I. et al., 2021. Relation between the consolidated layer thickness and other morphometric characteristics of one-year ice ridges. In: Proc. 26th Int. Conf. Port and Ocean Engineering under Arctic Conditions (Moscow, Russia, June 15–18, 2021), Moscow, 2021.

Høyland K.V., 2002. Consolidation of first-year ice ridges. *J. Geophys. Res.*, **107**, 15,1–15,15.

Høyland K.V., Liferov P., 2005. On the initial phase of consolidation. *Cold Reg. Sci. Technol.*, **41** (1), 49–59.

Kharitonov V.V., Borodkin V.A., 2020. On the results if studying ice ridges in the Shokal'skogo Strait. Part I: Morphology and physical parameters in situ. *Cold Reg. Sci. Technol.*, **174**, 103041.

Mironov Ye.U., Morev V.A., Porubaev V.S., Kharitonov V.V., 2003. Study of geometry and internal structure of ice ridges and stamukhas using thermal water drilling. In: Proc. 17th Int. Conf. Port and Ocean Engineering under Arctic Conditions (Trondheim, Norway, June 16–19, 2003), Trondheim, 623–634.

Morev V.A., Morev A.V., Kharitonov V.V., 2000. Patent RU 2153070 C1. Method of determination of ice ridge and stamukha structure, ice features and boundaries of ice and ground. Russian Federation: MPK E21C 39/00 (2000.01), G01N 9/00 (2000.01). Patent Holders: authors. – No. 2153070. Claimed 19.11.1998. Published 20.07.2000, Bull. no. 20 (in Russian).

Naumov A.K., Skutina E.A., Golovin N.V. et al., 2019. Peculiarities of morphometric features and inner structures of the ridged formation in Ob' Bay. In: Proc. 29th Int. Ocean and Polar Engineering Conf. ISOPE'19 (Honolulu, June 16–21, 2019), Hawaii, USA, 684–690.

Oleinikov A.I., Skachkov M.N., 2011. Model of compacted bulk solids and some of its applications. *Informatika i Sistemy Upravleniia*, **4** (30), 48–57 (in Russian).

Sand B., Petrich C., Sudom D., 2013. Morphologies of ridges surveyed off Svalbard and in Fram Strait, 2011 and 2012 field expeditions. In: Proc. 22nd Int. Conf. Port and Ocean Engineering under Arctic Conditions (POAC) (Espoo, Finland, June 9–13, 2013), Espoo.

Schramm J., Flato G., Curry J., 2000. Toward the modeling of enhanced basal melting in ridge keels. *J. Geophys. Res.*, **105** (C6), 14081–14092.

Shestov A.S., Marchenko A.V., 2014. Properties of ice ridge keels and sea currents in their vicinity in the Barents Sea. In: Proc. 22nd IAHR Int. Symp. on Ice (Singapore, August 11–15, 2014), Singapore.

Shestov A.S., Marchenko A.V., 2016a. The consolidation of saline ice blocks in water of varying freezing points: Laboratory experiments and computer simulations. *Cold Reg. Sci. Technol.*, **122**, 71–79.

Shestov A.S., Marchenko A.V., 2016b. Thermodynamic consolidation of ice ridge keels in water at varying freezing points. *Cold Reg. Sci. Technol.*, **121**, 1–10.

Strub-Klein L., Høyland K., 2011. One season of a 1st year sea ice ridge investigation – Winter 2009. In: Proc. 21st Int. Conf. on Port and Ocean Engineering under Arctic Conditions (Montréal, Canada, July 10–14, 2011), Montreal.

Word Meteorological Organization, 2014. WMO Sea Ice Nomenclature: Terminology, Codes and Illustrated Glossary. *WMO No. 259*, 1970–2017.

Received May 4, 2021
Revised March 13, 2022
Accepted April 14, 2022

Translated by V.A. Krutikova

EARTH'S CRYOSPHERE
SCIENTIFIC JOURNAL

Earth's Cryosphere, 2022, vol. XXVI, No. 3, pp. 43–53

SNOW COVER AND GLACIERS

MODELING OF DEBRIS FLOW TRIGGERED BY SNOW MELTING: CASE STUDY OF THE BARSEMDARA RIVER, TAJIKISTAN

V.A. Iudina (Kurovskaia)[1,*], S.S. Chernomorets[1], T.A. Vinogradova[2], I.N. Krylenko[1,3]

[1] *Lomonosov Moscow State University, Faculty of Geography, Leninskie gory 1, Moscow, 119991 Russia*
[2] *Research and Production Association Gidrotekhproekt LLC, ul. Oktyabrskaya 55A, Valdai, Novgorod oblast, 175400 Russia*
[3] *Water Problems Institute, Russian Academy of Sciences, ul. Gubkina 3, Moscow, 119333 Russia*

**Corresponding author; e-mail: viktoriiakurovskaia@gmail.com*

One of the latest catastrophic debris flow disasters took place in the Barsemdara River valley (Tajikistan) in 2015. The aim of this study was to apply chain modeling to consider the characteristics of this debris flow. This approach was also applied to assess potential flood-prone zones for future debris flows. To consider the characteristics of debris flow in the source, the transport-shift model developed by Yu.B. Vinogradov was applied. Based on this model, debris flow hydrographs were obtained and used as input data for valley zoning based on the FLO-2D model. So, for scenario I, the debris flow discharge of the forward wave (maximum 1630 m^3/s) was used as the input hydrograph; for scenario II, the debris flow discharge at the source outlet (maximum 650 m^3/s) was used. The digital elevation model ALOS PALSAR (12.5 m) was used as the relief data. As there were no rheological data, the modeling was carried out using several sets of parameters. The simulated debris flow discharges based on the most realistic option for scenario I varied from 1494 to 2860 m^3/s for individual waves. Additionally, the authors carried out modeling using digital elevation model from an unmanned aerial vehicle obtained during the survey in 2019. The results showed that the considered approach makes it possible to estimate the boundaries of both actual and potential flood-prone zones.

Keywords: *debris flow, Barsemdara River, transport-shift debris flow formation model, FLO-2D model, Pamir Mountains.*

***Recommended citation*:** Iudina (Kurovskaia) V.A., Chernomorets S.S., Vinogradova T.A., Krylenko I.N., 2022. Modeling of debris flow triggered by snow melting: case study of the Barsemdara River, Tajikistan. *Earth's Cryosphere*, XXVI (3), 43–53.

INTRODUCTION

In 1969–2015, eight catastrophic debris flow disasters were documented in the Gorno-Badakhshan Autonomous Oblast (GBAO) of Tajikistan. Information about individual rainstorm-induced debris flow events from 2007 to 2010 was presented by I. Mal'neva and N. Kononova [*2012*]. In 2002, glacial debris flow caused by lake outburst took place in the Dasht River valley. Assessment of catastrophic debris flow characteristics by modeling with FLO-2D and RAMMS was given in [*Mergili et al., 2011*]. The latest mass debris flow events in the Barsemdara River valley were observed in July 2015. Glacial origin of largest debris flows is normally considered, while the role of snowmelt as the main control is often underestimated. In the GBAO, there are 6650 glaciers in the GBAO, and their total area reaches 6785.6 km^2 [*Osipova, 1978; Shchetinnikov, Podkopaeva, 1978; Varnakova, Rototaeva, 1978, 1979; Shchetinnikov, 1979; Musoev, Atlas, 1980; Tukeev, 2002*], or 5.4% of the total glaciated area in Eurasia [*Kotlyakov, 1984*]. Despite the presence of a glacier in the Barsemdara River catchment, snowmelt was the main trigger of catastrophic debris flow events [*Dokukin et al., 2019*].

During the debris flow disaster in 2015, a debris fan dammed the Gunt River, which resulted in the appearance of a dammed lake that was later named Barsemkul' Lake. This led to the flooding of about 70 households, more than two kilometers of the highway connecting Tajikistan with China and Kyrgyzstan, five bridges (three road and two pedestrian), medical center, school, retail outlets, orchards, and fertile land, including tens of kilometers of irrigation networks. The main high-voltage power supply line from the Pamir-1 hydropower plant was also destroyed [*Chernomorets et al., 2015*].

Debris flow characteristics were determined based on visual observation and satellite data analysis [*Chernomorets et al., 2015; Keiler et al., 2018; Dokukin et al., 2019*]. Earlier, authors of this paper assessed discharges of debris flow using transport-shift model and video footage [*Kurovskaia et al., 2020*]. The aim of this work is the application of chain modelling to consider the increment of material in the source and valley zoning for the debris flow of 2015, as well as the flood zone assessment. The particular tasks included (i) preparation of digital elevation model,

(ii) improvement of the transport-shift model [*Vinogradov, 1980a,b*], (iii) selection of necessary parameters for modelling in FLO-2D software, and (iv) calculations and quality assessment.

STUDY OBJECT

The Barsemdara River is the right tributary of the Gunt River and belongs to the Panj (Pyandzh) River catchment. The river length is 8.6 km, and its catchment area is 28 km^2. Mean and maximum elevations within the catchment are 3912 and 4919 m asl, respectively. There were at least 14 series of debris flow events documented for the period of 16 to 20 of July 2015. The total amount of debris flow waves varied from 30 to 40 according to M. Keiler [*Keiler et al., 2018*]. Debris flow sites were at the elevation of ca. 4100 m in the upper part of the Barsemdara's headwaters from the edge of Chirmintarman glacier (Fig. 1).

The area of the debris flow cut on the moraine pedestal is 72 000 m^2. Morphometric properties of the debris flow site were estimated from Kanopus-V1 images acquired on October 6, 2015 and July 26, 2016. According to these data, the cut length at elevations 3800–4150 is 800 m, average width is 90 m, maximum width is 400 m [*Chernomorets et al., 2015; Dokukin et al., 2019*], and estimated depth reaches 50 m (Fig. 2).

The period of long-lasting positive temperatures resulting in the intense snow melting on the glacier and in the periglacial area is the main cause of catastrophic debris flow. Fluctuations of the temperatures within the debris flow site according to hourly ERA5 reanalysis at 30-km resolution performed by the European Centre for Medium-Range Weather Forecasts (ECMWF) are shown in Fig. 3.

The rise in temperature had been observed for two weeks before the catastrophe and reached the maximum (20°C) on July 16, 2015. In July 2014, the mean monthly temperature in this area was 9°C.

The length of the debris flow path from the source to the discharge point at the confluence of the Barsemdara and Gunt rivers was 7250 m with the average slope of 13.5°. According to M. Keiler's assessment [*Keiler et al., 2018*], the total volume of debris flow mass reached 4.2 M m^3. The debris flow mass dammed the Gunt River, so that Barsemkul' dammed lake with the area of 378 000 m^2 and max volume of about 4 M m^3 was formed [*Chernomorets et al., 2015*].

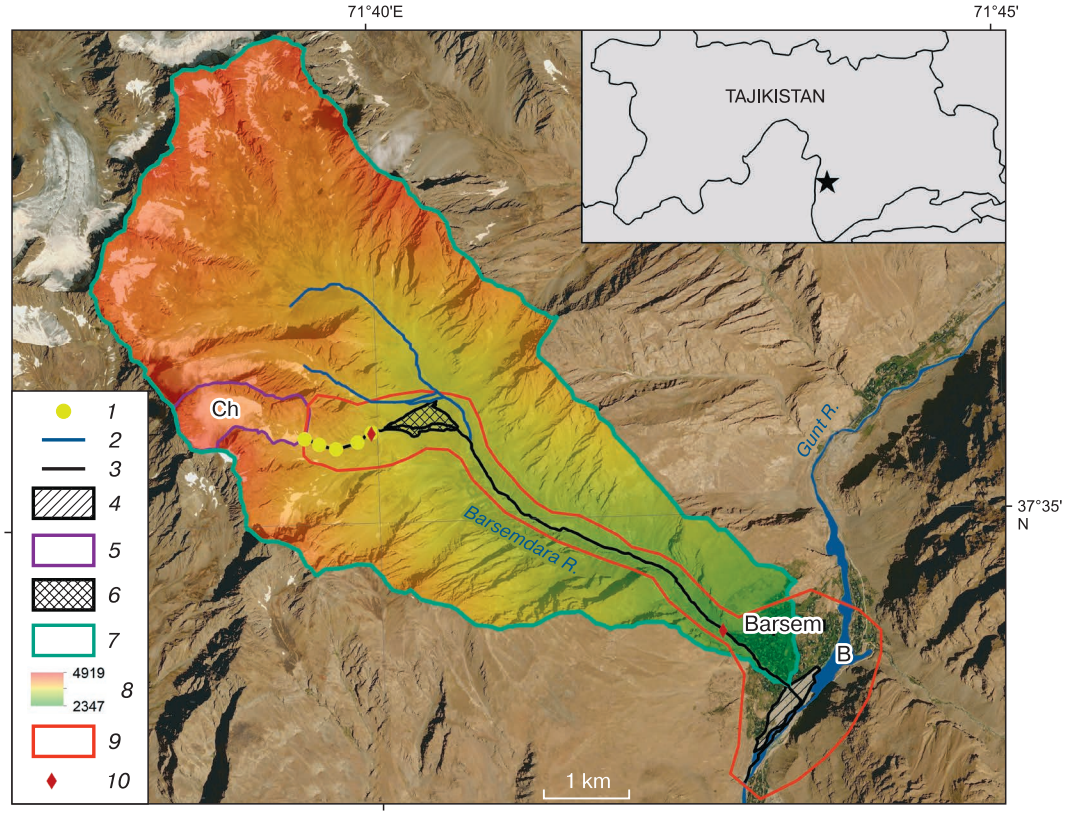

Fig. 1. The Barsemdara River catchment.

1 – areas within the debris flow site for the transport-shift model; *2* – streams, *3* – area of debris flow movement in 2015; *4* – section of intermediate debris flow accumulation in 2015; *5* – debris flow site boundaries; *6* – debris cone in 2015; *7* – Barsemdara River catchment; *8* – elevation, m; *9* – FLO-2D modelling extent; *10* – FLO-2D modelling sites; Ch – Chirmintarman Glacier; B – Barsemkul' Lake.

Fig. 2. Debris flow site in the Barsemdara River valley.

Photo by S.S. Chernomorets, 2019.

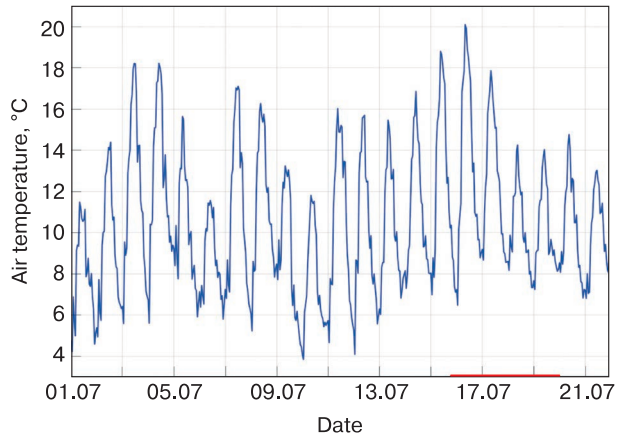

Fig. 3. Hourly air temperatures for the period from 1 to 21 of July, 2015 over the debris flow site according to ERA5 reanalysis data.

Red line is the debris flow activity.

Later, the area of this lake was reduced to 300 000 m^2 due to the construction of a discharge channel [*Dokukin et al., 2019*].

However, the danger of Lake Barsemkul' potential outburst flood is still preserved. Khorugh – the administrative center of the GBAO – is found just 15 km downstream the Gunt River. Earlier, a bathymetric survey of the lake was carried out [*Chernomorets et al., 2015*]. Moreover, possible scenarios of the lake outburst potentially resulting from (i) some lowering of the dam-break point, (ii) repeated debris flow from the Barsemdara valley, or (iii) outbursts in the cascade of glacial lakes triggering the catastrophic debris flow from the neighboring Sharipdara River valley were also discussed [*Kidyaeva et al., 2018*].

METHODS AND INPUT DATA

In this study, we applied a chain of numerical models, including the transport-shift model of debris flow formation, for calculating flow characteristics at the source site [*Vinogradov, 1980a,b*] and a hydrodynamic model FLO-2D for the valley zoning [*O'Brient et al., 1993*].

Transport-shift model of debris flow formation. The choice of the transport-shift model of debris flow formation was conditioned by the possibility to consider the increment of material in the forming debris flow. This is a one-dimensional model, and it is applied for calculating high-density debris flows. Model equations were developed by Yu.B. Vinogradov on the basis of debris flows experiments in the catchment of the Chemolgan River [*Vinogradova, Vinogradov, 2017*]. Earlier, modelling results were compared with observation data and were found to be satisfactory [*Vinogradova, Vinogradov, 2017*]. The model equations for calculating the discharge of solid material and the discharge and density of debris flow are now implemented into Python environment. The discharge of solid material is calculated first. Herewith, areas with approximately similar slopes and morphometric properties are delineated within the debris flow site. The main equation is solved not for the target variable G, but for the argument l [*Vinogradova, Vinogradov, 2017*]:

$$l = \left[\frac{Q\rho_0}{\varsigma\rho_0 + \rho} \ln \frac{Q\rho_0 + (\varsigma\rho_0 + \rho)G}{Q\rho_0 + (\varsigma\rho_0 + \rho)G_0} - \right.$$

$$\left. - \frac{Q}{\varsigma - \theta_{pp}} \ln \frac{Q + (\varsigma - \theta_{pp})G}{Q + (\varsigma - \theta_{pp})G_0} \right] \times$$

$$\times \left[A \frac{\mathrm{tg}\alpha}{\mathrm{tg}\varphi} g \sin\alpha \left[Q\rho_0 (\varsigma - \theta_{pp}) + Q(\varsigma\rho_0 + \rho) \right] \right]^{-1} + l_0, \quad (1)$$

where l is the distance along the thalweg of debris flow site, m; l_0 is the distance to the current sector, m; G is the solid material discharge, m^3/s; G_0 is the initial value of G for the certain sector and the previous upper sector (for the first upper sector $G_0 = 0$), m^3/s; α is the thalweg slope at the debris flow site, degrees; Q is the water discharge, m^3/s; φ is the static angle of internal friction of sediments, degrees; θ_{pp} is the ratio of the volume of water to the volume of solid material in the debris flow sediments at the liquid limit (in a stable immobile state); ζ is the ratio of the volume of water to the volume of solid material of debris flow sediments (dimensionless), g is the acceleration of gravity, m^2/s; ρ_0 is water density, kg/m^3; ρ is the density of debris flow sediments at the potential flow state, kg/m^3; and A is the coefficient of proportionality, m/(s^2·kg) [*Vinogradov, Vinogradova, 2010*]. According to scarce data of debris flow simulation under natural conditions, coefficient A was estimated to be in the range

of (3–5)·10^{-6} m/(s^2·kg), closer to 5·10^{-6} m/(s^2·kg) [*Vinogradova, Vinogradov, 2017*]. The debris flow discharge at the site of its origin (Q_{df}) can be calculated using Eq. (2):

$$Q_{df} = Q + (1 + \zeta)G, \quad (2)$$

where Q is the discharge of water entering the source of debris flow, m^3/s. The maximum debris flow discharge with the forward wave was estimated via multiplying its discharge at the outlet site by coefficient 2.5 (first approximation) [*Vinogradov, Vinogradova, 2010*].

The density of debris flow (y) moving along the site, is calculated by Eq. (3) [*Vinogradov, Vinogradova, 2010*]:

$$y = \frac{Qp_0 + (\varsigma p_0 + p)G}{Q + (1+\varsigma)G}. \quad (3)$$

Increment in the debris flow mass and changes in its density and discharge for each section along the site length are determined. As the input data in hydrodynamic models are hydrographs rather than a single discharge value, we have improved the transport-shift model via adding equations to calculate the wave velocity and lag time.

Most of the equations for calculating velocity of debris flows include such characteristics as the debris flow density, flow velocity, and empirical coefficients only. Herewith, empirical coefficients are obtained from observation data on particular debris flow catchments [*Golubtsov, 1969; RD 52.30.238-90, 1990*], or from laboratory experiments. Significant discrepancies have been found while comparing the observed velocities of debris flows at Chemolgan experiments and their calculated model values [*Sokolova et al., 2018*].

In this study, we have applied the equation for calculating debris flow velocity proposed by Yu.B. Vinogradov [*Vinogradov, Vinogradova, 2010*]. This equation includes not only the flow slope and depth but also internal angle of sediment friction, flow density, and various coefficients. To simplify the main equation, Vinogradov introduced three additional parameters:

$$M = \mu/(2\gamma\beta^2),$$

$$N = g\,(\sin\alpha - \mathrm{tg}\varphi^*\cdot\cos\alpha)/\beta^2,$$

$$S = gh\,\sin\alpha/\beta^2,$$

where μ is the coefficient of dynamic viscosity, Pa·s; γ is the debris flow density, kg/m^3; β is the mixing resistance coefficient, dimensionless; α is the slope of the debris flow thalweg, degrees; φ^* is the dynamic angle of internal friction of the sediments, degrees; g is the acceleration of gravity, m^2/s; and h is the flow depth, m. The final equation for calculating the maximum debris flow velocity (Vm) takes the form [*Vinogradov, Vinogradova, 2010*]:

$$Vm = \left(\frac{1}{1.5Nh}\right)\left[\left(\frac{M^2}{h^2} + S + Nh\right)^{1.5} - \left(\frac{M^2}{h^2} + S\right)^{1.5}\right] - \frac{M}{h}. \quad (4)$$

Herewith, the internal friction of debris flow sediments is expressed through μ, β, and φ^*. Viscosity factor (μ) characterizes the friction that occurs when individual layers and various elements slide over each other. With an increase in the size of the inclusions, their interaction also increases, i.e., more energy is dissipated, the viscosity factor varies between 100 and 1000 Pa·s. Mixing resistance coefficient (β) is the relative average distance perpendicular to the longitudinal axis of the debris flow, which the elements of the debris flow should pass before being involved in the general longitudinal motion. Its values vary between 0.1 and 0.5 [*Vinogradov, Vinogradova, 2010*].

Initial flow depth value for calculating the debris flow velocity was considered equal to 1 m at each section. Knowing the debris flow discharge and velocity, one can obtain its approximate cross-sectional area. The flow width was estimated using various satellite data at 15 to 30 m spatial resolution. Then, the flow depth was recalculated, and the resulting values were substituted into Eq. (4). To estimate the wave propagation time, the distance between the boundaries of the sections was divided by the velocity value.

Topographic data were extracted from digital elevation model ALOS PALSAR acquired on August 8, 2007 (12.5 m spatial resolution) [*https://search.asf.alaska.edu/#/*]. In total, four sectors with approximately similar morphometric characteristics were delineated within the debris flow channel (Fig. 1).

The input hydrograph for calculations was created for the first three debris flow waves based on the information obtained from local residents. The first wave was registered on July 16 at 14:30. According to eyewitnesses, the most powerful third wave took place on the same day less than an hour after the first and second waves. According to field survey in August 2019 carried out jointly by specialists from the Faculty of Geography of Moscow State University and the Aga Khan Agency for Habitat (AKAH), the discharge in front of the debris flow site during the third wave was estimated at 25 m^3/s. The base discharge in the upper reaches was estimated at 5 m^3/s. In the following days, floods and small debris flows were observed along the valley that were formed due to the natural snow melting and had no destructive power [*Chernomorets et al., 2015*]. Figure 4 shows the input hydrograph; the starting point corresponds to 14:30 (July 16, 2015).

Density of debris flow-forming deposits ρ was taken equal to 2600 kg/m^3; water density ρ_0, 1000 kg/m^3. The mean thalweg slope was 13.5°. The angles of internal friction of the sediments – static φ and dynamic φ^* – were estimated at 40° and 22°, respectively, according to construction design rules [*SP 425.1325800, 2019*], survey reports of the North Caucasian Institute for Water Management and Land Reclamation (Sevkavgiprovodkhoz) [*Nikulin, 2009*], and works of Yu.B. Vinogradov [*Vinogradov, Vinogra-*

dova, 2010]. Earlier, we presented the calculations of this debris flow for three scenarios of the initial water content of the deposits: completely dry, moistened to the liquid limit, and inundated [*Kurovskaia et al., 2020*]. We also compared model characteristics with the values of the debris flow velocity and discharge at the outlet as estimated from video records. It was found that the best fit of the model to the factual observations was in the case of rock moistening to the liquid limit. In this paper, we consider only this option for further calculations.

Hydrodynamic model FLO-2D. A two-dimensional hydrodynamic model FLO-2D [*O'Brien et al., 1993*] was used to estimate the distribution of flow velocities and depths within the channel. This model is widely applied in scientific research related to the dynamics of water and debris flows [*Cesca, D'Agostino, 2008; Mikhailov, Chernomorets, 2011; Petrakov et al., 2012; Wu et al., 2013*]. It is based on the solution of Saint-Venant equations, in which the flow characteristics are averaged over depths (the so-called shallow-water equations) [*Cunge et al., 1980*]. When modeling debris flow in the FLO-2D model, it is assumed that it moves as a Bingham fluid (viscous-plastic fluid) [*O'Brien et al., 1993*]. The model operates with the following input data: topographic maps and topographic survey data synthesized in digital elevation models (DEM), background discharges and levels of the water in the main channel and tributaries, and input hydrograph and its shape. As an output, the model gives depths, velocities, and levels of water or debris flow surfaces, as well as other flow parameters in plane.

As the input hydrological information, we used hydrographs obtained from the transport-shift model. For scenario I, we used discharges of the forward wave as an input hydrograph; for scenario II, debris flow discharges at the site outlet. Background discharge of the Gunt River was taken at 100 m^3/s. This value corresponds to the average discharge over the observation period and the discharge of 50% probability.

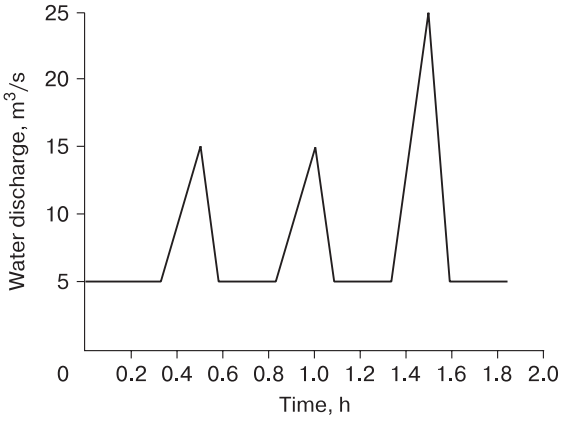

Fig. 4. Input hydrograph for debris flow modeling.

We used digital elevation model from ALOS PALSAR (12.5 m resolution) acquired on August 8, 2007 as input topographic data [*https://search.asf.alaska.edu/#/*]. After correction, the DEM was re-interpolated with the cell size of 12.5 m to be used in the FLO-2D model. Further, we used unmanned aerial vehicle (UAV) data for the area of the debris cone obtained during the field survey by the authors in August 2019. UAV-based DEM was resampled to 5 × 5 m grid. We also used bathymetric data for Lake Barsemkul' surveyed in 2017.

The input parameters for the FLO-2D model were also volumetric concentration of sediments in the debris flow, plastic friction stress, and flow viscosities. Concentration of sediments was set to be 45%, which corresponds to incoherent debris flow with intensive mixing [*O'Brien et al., 1993*]. If it is impossible to conduct a detailed rheological analysis of debris flows, the following empirical formulas are used to calculate the plastic friction stress and flow viscosity in the model:

$$\eta = \alpha_1 \exp(\beta_1 C_v); \quad (5)$$

$$\tau_y = \alpha_2 \exp(\beta_2 C_v), \quad (6)$$

where τ_y is plastic friction stress, η is flow viscosity, and C_v is sediment volumetric concentration; $\alpha_{1,2}$, and $\beta_{1,2}$ are empirical coefficients determined in laboratory [*O'Brien, Julien, 1988*]. As seen from Eqs. (5) and (6), η and τ_y are functions of the volumetric concentration of sediments considering only the volume of silt, clay, and, in some cases, sand fractions. However, these equations do not consider coarse-grained sediments. The viscosity of a fluid is also a function of the volumetric concentration of sediments. The authors of the model estimated the parameters of these equations using debris flow samples collected in the Rocky Mountains, Colorado, near the cities of Aspen and Glenwood Springs. The values of the empirical coefficients α_i and β_i were obtained using regression analysis for each sample and are presented in Table 1 [*O'Brien, Julien, 1988*]. By default, parameter e is recommended for simulating the movement of a more viscous flow, and parameter a is recommended for less coherent flows, including sediment-water floods [*O'Brien, Julien,*

Table 1. **Parameters for calculating plastic flow stress and viscosity as a function of sediment concentration [*O'Brien, Julien, 1988*]**

Parameter set	Debris flow deposit sample	Parameters for calculating plastic friction stress		Parameters for calculating flow viscosity	
		α_2	β_2	α_1	β_1
a	Aspen natural soil	0.1520	18.7	0.001 36	28.4
b	Glenwood 1	0.0345	20.1	0.002 83	23.0
c	Glenwood 2	0.0765	16.9	0.064 80	6.2
d	Glenwood 3	0.000 707	29.8	0.006 32	19.9
e	Glenwood 4	0.001 72	29.5	0.000 602	33.1

1988]. Since there were no field data for the studied catchment, simulation was performed using several sets of parameters presented in Table 1.

MODELING RESULTS

We have obtained flow discharge values for each of the four sectors within the debris flow site by applying Eqs. (1) and (2). Flow velocities are required for debris flow hydrographs. The results of velocity calculations according to Eq. (4) for each sector and for the forefront wave are presented in Table 2.

Calculations for the first two waves and for the third wave were separately performed, because water discharge values for first two waves entering the channel were the same and equal to 15 m^3/s. Flow density values calculated using Eq. (3) were then used in calculations of the velocity. As seen from Table 2, flow velocities differed among sectors. Average velocity for the first two waves (excluding the forefront wave) was 13.4 m/s; the third wave had the flow velocity of 13.2 m/s.

Figure 5 shows hydrographs of debris flow waves for all four sectors within the site and the maximum discharge values for the forefront wave. A gradual increase in the flow discharge from the first to the fourth sector is clearly seen.

For the first two waves, debris flow discharge along the entire site increased from 145 to 391 m^3/s. According to approximate estimates, the discharge of the forefront wave reached 978 m^3/s. For the third wave, the discharge increased from 255 to 625 m^3/s from the first to the fourth sector; the discharge of the forefront wave reached 1630 m^3/s. Minimum debris flow discharge time (13 s) was found for the first and fourth sectors. and maximum discharge time (22 s) was found for the third sector. Time lag of the front wave in the fourth sector varied from 18 to 20 s.

Further, we performed a zoning of the valley using FLO-2D model. As noted earlier, two simulation scenarios were considered. In scenario I (for the forefront wave), the discharge changed significantly depending on the input values of plastic friction stress and flow viscosity (Table 3).

The most realistic results, close to the estimates based on field data, were obtained using option Ib. Calculations with other options are given for comparison to show how the use of different debris flow parameters in the FLO-2D model affects the results. Thus, the flow rates for option Ib were from 1494 to 2860 m^3/s for individual waves, while the flow rate estimated from video records was 1536 m^3/s, and the velocity was 16.6 m/s [*Kurovskaia et al., 2020*]. Note that we used records for one of 40 debris flow waves,

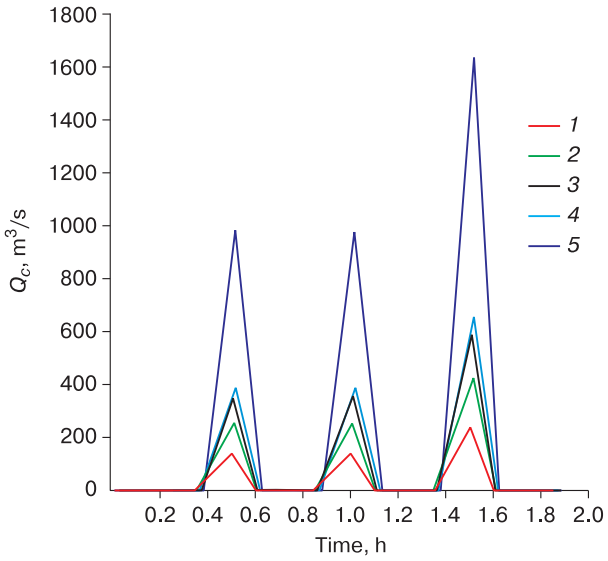

Fig. 5. Debris flow hydrographs for the four sectors of the debris flow site (lines *1–4*) and for the forefront wave (line *5*) obtained as transport-shift model output.

Table 2. **Debris flow velocity**

Sector number	Slope, degrees	Flow depth for the first and second waves, m	Velocity of the first and second waves, m/s	Flow depth for the third wave, m	Velocity of the third wave, m/s
1	28.2	2.2	14.6	2.0	15.0
2	26.6	2.0	13.9	2.1	14.3
3	24.6	2.1	13.1	2.3	13.1
4	20.4	2.8	11.2	2.3	11.2
5 (forefront wave)	20.4	4.0	8.3	6.2	7.2
Entire site	25.2	2.7	12.4	3.0	11.9

Table 3. **Results of hydrodynamic modelling for scenarios I and II**

Calculation option	Max discharge, m^3/s (first wave)	Passing time, min	Max discharge, m^3/s (second wave)	Passing time, min	Max discharge, m^3/s (third wave)	Passing time, min
Ia	855	15.6	1477	5.4	2513	12.0
Ib	1494	12.6	1639	12.0	2860	9.6
Ic	1433	9.0	1378	7.8	3297	3.0
Id	977	11.4	1744	12.0	2993	9.0
Ie	430	21.0	1134	4.8	1939	3.0
IIa	164	18.2	674	9.1	1322	6.7
IIb	295	21.1	554	9.1	648	15.1
IIc	777	9.7	1153	11.5	1045	8.5
IId	412	18.7	404	13.9	683	15.1
IIe	30	21.1	394	10.9	580	8.5

presumably the third, the most destructive, so we obtained approximate estimates.

The highest discharge of the forefront wave at the top of debris cone was 3297 m^3/s during the third wave according to Ic option. Debris flow discharges for the first and second waves were lower than the values assessed using video records. Minimum values for the top of debris cone were obtained for option Ie (most viscous flow). The discharge for the first and second waves was 430 and 1134 m^3/s, respectively. The discharge for the third wave was by 403 m^3/s higher than the value estimated using video records. Herewith, parameters of option e are recommended for cement-like debris flow, which was not the case for the observed debris flow. Slightly higher discharges were obtained for the parameters of option Ia typical for a low-density debris flow. The discharge of the first wavy reached 855 m^3/s; the discharge of the second wave was 60 m^3/s lower than the video-based estimate. For the third wave, the simulated discharge was 1.6 times higher than the video-based estimate. In option Id, the discharge of the first wave reached 977 m^3/s; the discharges of the second and third waves exceeded the video-based estimates by 1.1–1.9 times.

Then, the same parameters were used to simulate debris flow discharges at the site outlet according to scenario II.

The highest discharge of the third wave at the top of debris cone was 1321 m^3/s according to option IIa. For the first and second waves, discharge values were 164 and 674 m^3/s, respectively. The highest discharges for these two waves were obtained using option IIc: 777 and 1153 m^3/s, respectively. The minimum debris flow discharge of the first wave (30 m^3/s) was obtained using option IIe. For the second and third waves, the discharge varied from 394 to 560 m^3/s. In general, options IIb and IId were close to one another; discharge values changed from 295 to 683 m^3/s.

For calculating the debris flow characteristics at the debris cone, we used the set of parameters b as the most realistic one. The discharge in this case was close to the value obtained from video records [*Kurovskaia et al., 2020*]. To estimate the maximum possible discharge at the debris cone, we made a calculation using a set of parameters c.

Discharges at the debris cone calculated using option Ib (scenario I) varied between 556 and 2181 m^3/s. The flow passed this section of debris cone in 1.8–4.8 min. The flow velocity in the Barsemdara River channel exceeded 5 m/s; in the adjacent area, is was up to 3.2 m/s (Fig. 6*b*). A considerable number of buildings on the left bank of the river were within the flood zone. The distribution of depths in the flow is shown in Fig. 6*a*.

According to scenario II, discharges within the debris cone changed from 101 to 543 m^3/s. The spreading of the first wave was wherein observed. The flow travel time was from 6 to 7.8 min. The flow depth within the debris cone averaged 4.8 m reaching 9.5 m in some areas. The debris flow velocity in the Barsemdara and Gunt rivers, as well as within the debris cone, was 5 m/s.

When modeling the passage of the forefront wave, the debris flow discharge at the debris cone turned out to be much higher and ranged from 1580 to 3351 m^3/s for the third wave according to option c. Lag time varied from 0.6 to 1.2 min. Maximum debris flow velocities within the Barsemdara River channel and in the adjacent area were 19.4 and 10.8 m/s, respectively. Flow depth within the debris cone varied

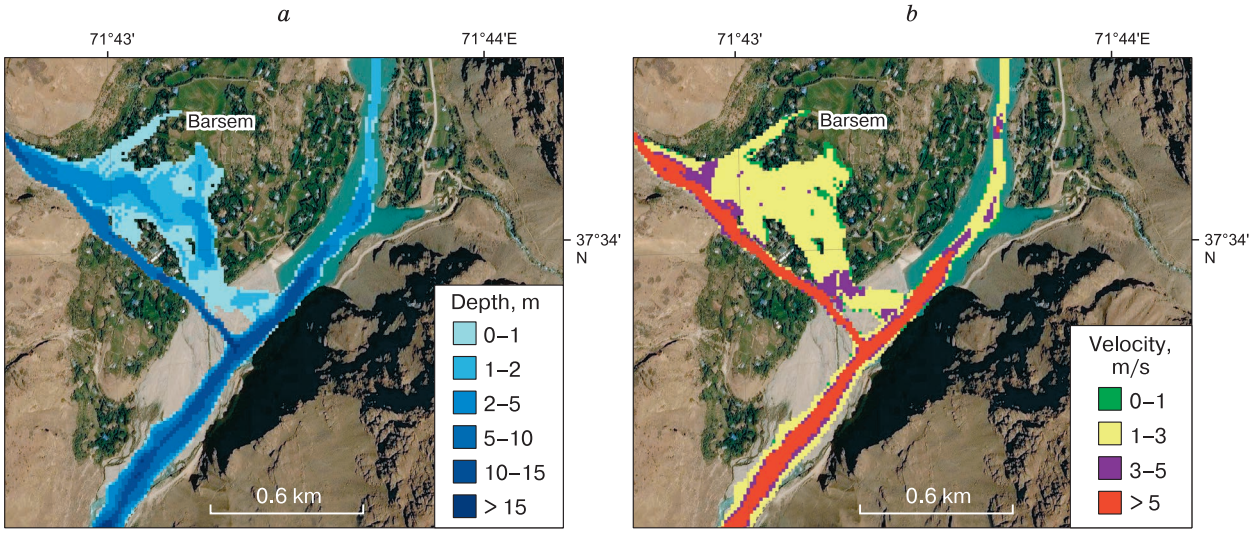

Fig. 6. Plane distribution of flow parameters for the 2015 debris flow simulated using FLO-2D model according to scenario I, parameter set b.

a – flow depth, *b* – flow velocity.

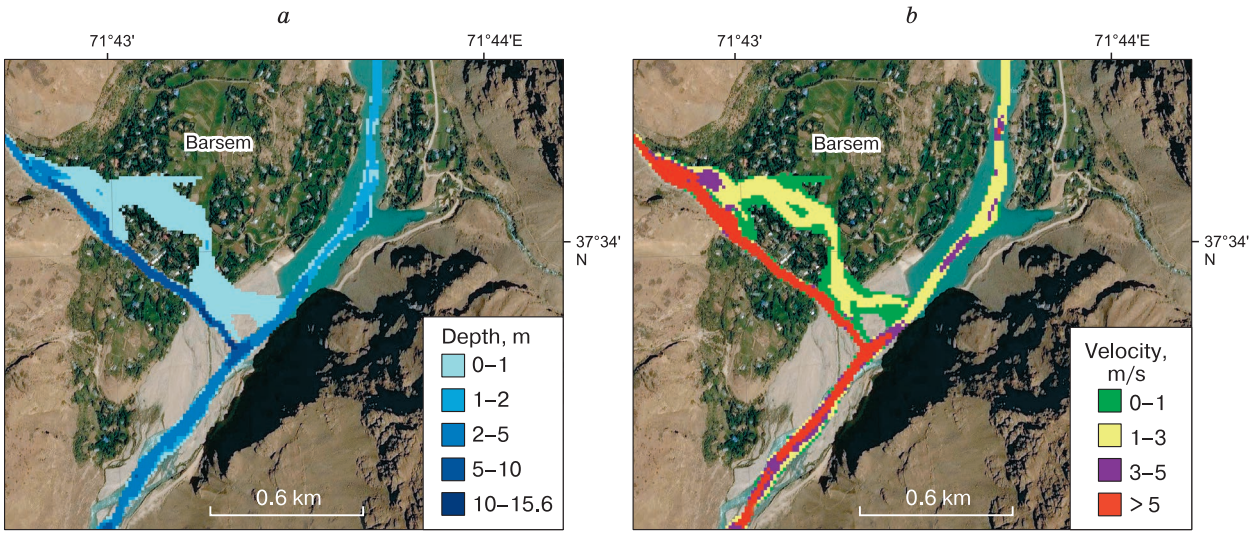

Fig. 7. Plane distribution of flow parameters for the 2015 debris flow simulated using FLO-2D model according to II scenario, parameter set c.

a – flow depth, *b* – flow velocity.

from 1 to 5 m and was up to 15 m in the Barsemdara River channel.

The debris flow discharges for option c (scenario II) were 534–840 m^3/s. The lag time of the waves varied from 0.6 to 1.8 min. At the debris cone section, the maximum debris flow velocity within the Barsemdara River channel was 15.1 m/s; on the adjacent area, it reached 6.7 m/s; in the Gunt River channel, 11.8 m/s (Fig. 7).

A comparison of modeling and observation data indicates that, in reality, there was no flow spreading along the debris cone to its left side. Waves passed exclusively within the Barsemdara River channel, despite its lowered left bank (Fig. 8). Thus, the flow incised into the surface of the debris cone.

Fig. 8. Barsemdara River channel.

Photo by S.S. Chernomorets, 2019.

One of the reasons for the inconsistency of factual and simulated flood zones within the cone could be due to erosional processes that are not considered in the FLO-2D model calculation, except for the initial input morphometric data. In our study, we used satellite images of 12.5-m resolution, which smoothed meso- and microtopographic features. However, this was the only option available for this valley before the debris flow of 2015.

Calculations of potential modern debris flow in the Barsemdara valley were made using 2019 UAV-based DEM covering the debris cone, hydrographs (scenario I) in the FLO-2D model with parameter sets b (as the most realistic one) and c (giving maximum values). These calculations reflect the flood-prone zones in case of the repeated debris flow and the modern topographic conditions.

Modelling using the set of parameters b indicates that the flow is almost entirely concentrated within the Barsemdara channel above the debris cone, while the cone is flooded (Fig. 9). During the debris flow in 2015, the debris cone was not flooded. According to 2019 UAV-based DEM data, the debris cone is characterized by a sharp change in the heights (from 2541 to 2519 m asl). This can cause the flooding of the territory in case of another intense debris flow.

The results obtained with parameter set c indicate that in the event of a similarly strong debris flow, not only the debris cone but also houses near the Barsemdara River channel upstream the cone will be in the flood-prone zone. Flow depth for both sets of parameters will vary from 8 m on the debris cone to 15 m in the Barsemdara River channel.

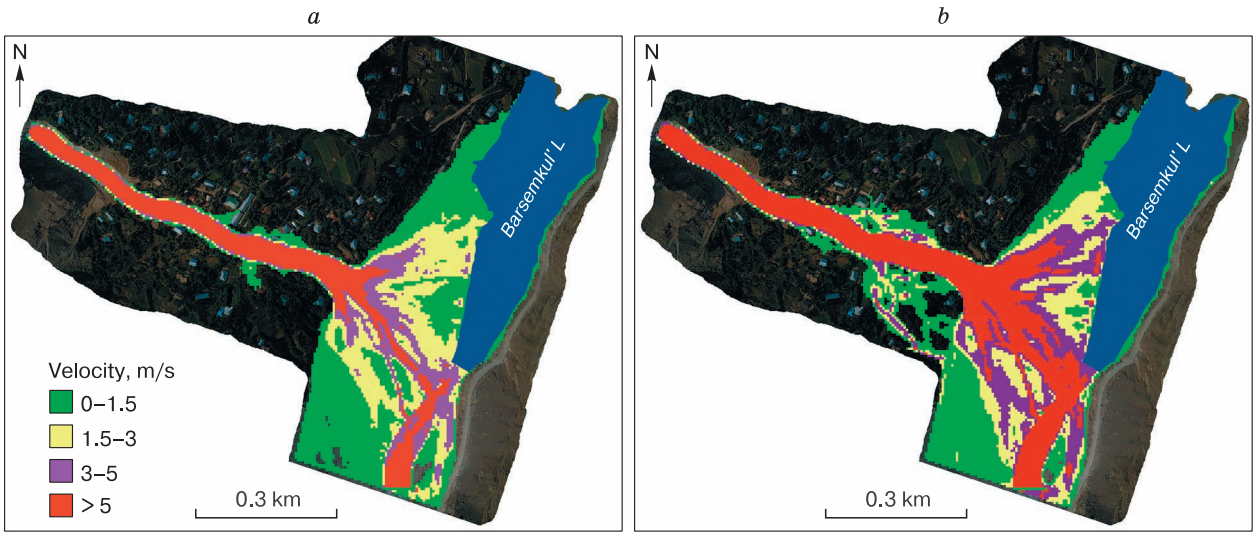

Fig. 9. Plane distribution of the flow velocity of the first wave simulated using FLO-2D model and UAV data according to scenario I.

a – scenario Ib, *b* – scenario Ic.

The Barsemdara channel topography was relatively stable before 2015. After the catastrophe, the topography has stabilized and there are no changes now. In case of using high-resolution DEM data, we should bear in mind that debris cones are unstable landforms, and their topography is subjected to changes after each high-water event. Intense water flood or debris flows can form a new channel in the area of the village beyond the current channel. The FLO-2D model does not consider erosional processes. Therefore, in case of catastrophic high-water event, the flood zone picture may change significantly. At the same time, initially such a territory may not be identified as potentially dangerous when modeling with the use of available UAV-based DEM data. In fact, such high-resolution DEMs rapidly become outdated. More accurate results for the moment will be obtained using detailed modeling on the basis of state-of-the-art DEM. Therefore, it is better to assess flood-prone zones regularly. The application of a publicly available 12.5-m resolution DEM is suitable for obtaining a quick generalized assessment of potentially hazardous areas, as well as for calculating past debris flows.

CONCLUSIONS

In this work, we have assessed the possibility to apply chain modeling for calculating the debris flow in the Barsemdara River valley in 2015, including models for calculating the debris flow characteristics at the site and while moving along the valley. We have used transport-shift model to calculate the debris flow characteristics at the site. A distinctive feature of this model is the ability to estimate the increment of solid material during the formation of a debris flow and the relative simplicity of the input information, which is especially important in conditions of insufficient data.

We improved the model via adding the calculation of the flow velocity according to the equation suggested by Yu.B. Vinogradov and of the time of the wave passing. These improvements made it possible to obtain physically substantiated discharge hydrographs for the first three most destructive flow waves. We further conducted the valley zoning using the hydrodynamic model FLO-2D. Transport-shift model outputs – discharges of forefront wave (scenario I) and at the site outlet (scenario) – were used as input hydrographs. As it was impossible to conduct laboratory experiments to refine the parameters in the formulas for calculating the plastic friction stress and flow viscosity, we carried out experimental calculations with five options of parameter sets. Thus, the discharge values with set b (Table 3) at top of the debris cone varied from 1494 to 2860 m^3/s for the first and third waves (scenario I). The highest forefront wave discharge (3297 m^3/s) was obtained with parameter set c for the third wave. Discharges for the first and second waves were slightly lower (1433 and 1378 m^3/s). Discharges obtained using parameter set b (scenario I) varied between 556 and 2181 m^3/s in the section of debris cone. Though the discharge values calculated with this set of parameters are overestimated as compared with video-based estimates, the authors believe that parameter set b is more probable for a particular debris flow.

Given the resolution of the satellite-based DEM (12.5 m) used in the calculations, the flood zone turned out to be much larger than the actual data observed in 2015. This discrepancy of field and modeling data is explained by the generalization of local topographic features on satellite data of such a resolution. We have therefore performed an additional modeling with the use of UAV data collected in 2019 as input data. The results of calculations illustrate the flood zone during the passage of a debris flow of similar intensity over the modern topography. For the parameter set b, the debris flow is completely concentrated in the channel down to the top of the debris cone with subsequent spreading. Modeling with the parameter set c indicates that not only the debris cone but also houses near the Barsemdara River channel will be in the flood zone. In general, our results attest to the applicability of the considered chain of mathematical models for the assessments of flood zones.

Acknowledgements. *The authors express their gratitude to F.O. Marodaseynov and A. Akdodov from the Aga Khan Agency for Habitat and I.V. Krylenko and K.S. Viskhadzhieva from Moscow State University for their help in field data collection.*

Funding. *This study has been carried out within the framework of state assignments of the Lomonosov Moscow State University, sections I.7 (CITIS 121051300175-4) and I.10 (CITIS 121051400038-1) and the Water Problems Institute of the Russian Academy of Science, theme 0147-2019-0001 (CITIS AAAA-A18-118022090056-0) and supported by the Russian Foundation for Basic Research (project no. 20-35-90006).*

References

Cesca M., D'Agostino V., 2008. Comparison between FLO-2D and RAMMS in debris-flow modelling: a case study in the Dolomites. *WIT Transactions on Eng. Sciences*, vol. LX, 197–206.

Chernomorets S.S., Savernyuk E.A., Bobov R. et al., 2015. Mudflows in the valley of the Barsemdara River in July 2015 and the dammed lake Barsemkul on the Gunt River (Gorno-Badakhshan Autonomous Region, Tajikistan). In: Proc. Int. Conf. Second Vinogradov's Readings. The Art of Hydrology (St. Petersburg, Nov. 18–22, 2015). St. Petersburg, Saint-Petersburg State University, p. 261–264 (in Russian).

Cunge J.A., Holly F.M., Verwey A., 1980. Practical Aspects of Computational River Hydraulics. London, Pitman. Translated under the title Chislennye Metody v zdachakh Rechnoi Gidravliki (Moscow, Energoatomizdat, 1985), 255 p. (in Russian).

Dokukin M.D., Chernomorets S.S., Savernyuk E.A. et al., 2019. Barsem debris flow disaster in the Pamirs in 2015 and its analogues in the Central Caucasus. *Georisk,* **XIII** (1), 26–36 (in Russian).

Golubtsov V.V., 1969. On hydraulic resistance and the formula for calculating the average flow rate of mountain rivers. *Proc. KazNIGMI,* 33, 30–41 (in Russian).

Keiler M., Zimmermann M., Bigler S., Fuchs S., 2018. Assessing a large-scale debris flow in Barsem, Tajikistan: exceptional size, duration and process chain. In: Proc. European Geosciences Union General Assembly Conf. (Vienna, April 8–13, 2018), Vienna, Austria, p. 5405.

Kidyaeva V.M., Chernomorets S.S., Savernyuk E.A. et al., 2018. Modeling of breakthroughs of mountain lakes and mudflows in the Gorno-Badakhshan Autonomous region, Tajikistan. In: Proc. III Int. Conf. Facets of Hydrology (St. Petersburg, March 28–30, 2018). St. Petersburg, St. Petersburg State Univ., p. 897–902 (in Russian).

Kotlyakov V.M. (Ed.), 1984. Glaciological Dictionary. Leningrad, Gidrometeoizdat, 528 p. (in Russian).

Kurovskaia V.A., Chernomorets S.S., Vinogradova T.A. et al., 2020. Assessment of the quantitative characteristics of the mudflow in the Barsemdara River valley (Tajikistan) in 2015 based on video materials and modeling results. *Georisk*, **XIV** (3), 12–22 (in Russian).

Mal'neva I.V., Kononova N.K., 2012. Mudflow activity in Russia and neighboring countries in the XXI century. *Georisk,* **IV** (4), 48–54 (in Russian).

Mergili M., Schneider D., Worni R., Schneider J., 2011. Glacial lake outburst floods in the Pamir of Tajikistan: Challenges in prediction and modelling. In: Proc. Fifth Int. Conf. Debris-Flow Hazards Mitigation: Mechanics, Prediction, and Assessment (Padua, June 14–17, 2011). Padua, Italy, p. 973–982.

Mikhailov V.O., Chernomorets S.S., 2011. Mathematical Modeling of Mudflows, Collapses and Landslides. Moscow, Lambert, 131 p. (in Russian).

Musoev Z., Atlas L.I. (Eds.), 1980. Basins of the right tributaries of the Panj River from the mouth of the Vakhsh River to the mouth of the Vanj River (chapter 10), The Vostochnyi Kyzylsu River basin (chapter 19). In: Catalogue of Glaciers of the USSR. Vol. 14. Central Asia. Issue 3. Amu Darya. Leningrad, GIMIZ, 56 p. (in Russian).

Nikulin A.S., 2009. Experience in determining the angles of internal friction of mudflow undercoats. In: Collection of Scientific Works of JSC Sevkavgiprovodkhoz, iss. 18, 30–33 (in Russian).

O'Brien J.S., Julien P.Y., 1988. Laboratory analysis of mudflow properties. *J. Hydraul. Engin.,* CXIV (8), 877–887.

O'Brien J.S., Julien P.Y., Fullerton W.T., 1993. Two-dimensional water flood and mudflow simulation. *J. Hydraul. Engin.,* CXIX (2), 244–261.

Osipova G.B. (Ed.), 1978. The Vanj River basin (chapter 11), The Yazgulem River basin (chapter 12). In: Catalogue of Glaciers of the USSR. Vol. 14. Central Asia. Issue 3. Amu Darya. Leningrad, GIMIZ, 84 p. (in Russian).

Petrakov D.A., Tutubalina O.V., Aleinikov A.A. et al., 2012. Monitoring of Bashkara Glacier lakes (Central Caucasus, Russia) and modelling of their potential outburst. *Nat. Hazards,* LXI (3), 1293–1316.

RD 52.30.238-90, 1990. Management of Mudflow Stations and Hydrographic Parties. Vol. I. Moscow, Gidrometeoizdat, 199 p. (in Russian).

Shchetinnikov A.S. (Ed.), 1979. The Marghab River basin (chapter 14). In: Catalogue of Glaciers of the USSR. Vol. 14. Central Asia. Issue 3. Amu Darya. Leningrad, GIMIZ, 91 p. (in Russian).

Shchetinnikov A.S., Podkopaeva L.D. (Eds.), 1978. The Bartang River basin (chapter 13). In: Catalogue of Glaciers of the USSR. Vol. 14. Central Asia. Issue 3. Amu Darya. Leningrad, GIMIZ, 107 p. (in Russian).

Sokolova D.P., Vinogradova T.A., Ostashov A.A., 2018. Comparison of various methods for calculating the rate of mudflow. *Georisk,* **VIII** (4), 76–86 (in Russian).

SP 425.1325800, 2019. Engineering Protection of Territories from Erosion. Design Rules. Moscow, Standartinform, 36 p. (in Russian).

Tukeev O.V., 2002. Mudflows in the Pamirs: Disasters, Patterns, Forecast. Moscow, VNII GOChS, 176 p. (in Russian).

URL: https://search.asf.alaska.edu/#/ (last visited: 28.10.2020).

Varnakova G.M., Rototaeva O.V. (Eds.), 1978. The Obikhingou River Basin (chapter 9). In: Catalogue of Glaciers of the USSR. Vol. 14. Central Asia. Issue 3. Amu Darya. Leningrad, GIMIZ, 110 p. (in Russian).

Varnakova G.M., Rototaeva O.V. (Eds.), 1979. The Gunt River basin (chapter 15). In: Catalogue of Glaciers of the USSR. Vol. 14. Central Asia. Issue 3. Amu Darya. Leningrad, GIMIZ, 126 p. (in Russian).

Vinogradov Yu.B., 1980a. Transport and transport-shift mudflow processes. In: Debris Flows. Almaty, KazNIGMI, iss. 4, 3–18 (in Russian).

Vinogradov Yu.B., 1980b. Etudes on Debris Flows. Leningrad, Gidrometeoizdat, 160 p. (in Russian).

Vinogradov Yu.B., Vinogradova T.A., 2010. Mathematical Modeling in Hydrology. Moscow, Academy, 304 p. (in Russian).

Vinogradova T.A., Vinogradov A.Y., 2017. The experimental debris flows in the Chemolgan River basin. *Nat. Hazards,* LXXXVIII, 189–198.

Wu Y.H., Liu K.F., Chen Y.C., 2013. Comparison between FLO-2D and Debris-2D on the application of assessment of granular debris flow hazards with case study. *J. Mountain Sci.,* **X** (2), 293–304.

Received July 15, 2021
Revised January 28, 2022
Accepted April 3, 2022

Translated by Yu.A. Dvornikov

EARTH'S CRYOSPHERE
SCIENTIFIC JOURNAL

Earth's Cryosphere, 2022, vol. XXVI, No. 3, pp. 54–62

CHRONICLE

CONTRIBUTION OF PERMAFROST SCIENTISTS TO SAFE OPERATION OF THE YAKUTSK COMBINED HEAT AND POWER PLANT (to the 85th anniversary of the Yakutsk CHPP)

P.S. Zabolotnik[1,], S.I. Zabolotnik[1,*]**

[1]*Melnikov Permafrost Institute, Siberian Branch of the Russian Academy of Sciences, ul. Merzlotnaya 36, Yakutsk, 677010 Russia*

[*]*Corresponding author; e-mail: sizabol@mpi.ysn.ru*

[**]*E-mail: poulza@mail.ru*

The role and contribution of P.I. Melnikov, Academician of the USSR Academy of Sciences; N.A. Tsytovich, Corresponding Member of the USSR Academy of Sciences; N.I. Saltykov, Professor, and V.F. Zhukov, Candidate of Technical Sciences, to construction of the Yakutsk Combined Heat and Power Plant are elucidated. These outstanding figures, known for their pioneering researches in different fields of the permafrost science and engineering, were actively and directly involved in the construction project, including the planning and design, foundation analysis, site investigation, foundation construction, and post-construction monitoring. The foundation condition at the plant site, the causes for talik development, and the dynamics of talik distribution since the beginning of the study are discussed. The reasons of the quite stable state of the plant facilities despite the widespread talik occurrence are explained.

Keywords: *Yakutsk Combined Heat and Power Plant, permafrost, talik, ground temperature.*

Recommended citation: Zabolotnik P.S., Zabolotnik S.I., 2022. Contribution of permafrost scientists to safe operation of the Yakutsk combined heat and power plant (to the 85th anniversary of the Yakutsk CHPP). *Earth's Cryosphere,* XXVI (3), 54–62.

INTRODUCTION

Since November 7, 1937, the Yakutsk Central Power Plant (YaCPP) has been providing the city of Yakutsk with electric power and, since 1961, also with heat [*Zavatskaya, Danilevskaya, 2007*]. The plant generates 52 million kW of electric power and 916 thousand Gcal of heat. In 1969, the Yakutsk CPP was renamed into the Yakutsk Combined Heat and Power Plant (YaCHPP) (Fig. 1).

The YaCHPP became the first industrial facility in the Soviet Union built on the principle of using permafrost as foundation, so permafrost researchers were actively involved in all stages of its design, construction, and operation.

The first power plant in Yakutsk appeared in 1914. Its power capacity soon became insufficient for the growing city. In 1931, the Energy Planning Commission (Energoplan) decided to build a heat power plant in Yakutsk. When choosing the site of construction, three options were considered: (1) on the bedrock outcrops in the area of the Kangalass coal deposit, (2) on the northeastern outskirt of Yakutsk, at the Golminka pier, and (3) on the territory of the Spassky Monastery. The first variant assumed the provision of the plant with local coal and the foundations footing in strong bedrock. The advantage of the second variant was the water supply and proximity to the main industrial enterprises, as well as the possibility of coal delivery by barges on the river. The third option was characterized by the absence of topsoil loams on the surface, a low ice content of sandy sediments in the area of the monastery, and good drainage conditions.

Preference was given to the second variant because of the impossibility to provide a large number of aluminum wires necessary for power lines in the first and third variants.

Participation of permafrost scientists in pre-construction survey, design, construction, and monitoring during the first years of the plant operation

The YaCPP project was developed in the construction sector of Teploelektroproekt Institute under the supervision of senior engineer N.V. Arkhipov in 1932. N.A. Tsytovich*, a Soviet scientist

* All information about the activities of N.A. Tsytovich and other prominent scientists was obtained from handwritten reports and archival documents.

Fig. 1. A general view of the Yakutsk CHPP.

Photo by P.S. Zabolotnik, September 5, 2013.

and educator in the field of soil mechanics, geomechanics, and engineering geology, participated in the design of the Yakutsk CPP as a consultant (Fig. 2).

From 1936 to 1956, he worked in the Obruchev Permafrost Institute (Moscow). The Presidium of the Academy of Sciences of the USSR concurrently entrusted him to organize the base of the Academy of

Fig. 2. Nikolai Alexandrovich Tsytovich (1900–1984).

Doctor of Technical Sciences, Professor, Corresponding Member of the USSR Academy of Sciences (1943), Hero of Socialist Labor (1980), winner of the Stalin Prize (1950), three times Commander of the Order of Lenin and the Order of Red Banner of Labor, Honored Worker of Science and Technology of the RSFSR (1969).

Fig. 3. Nikolai Ivanovich Saltykov (1888–1964).

Doctor of Technical Sciences, Professor, Honored Scientist of the Yakut ASSR, Commander of the Order of the Red Star, "Badge of Honor". From 1936 to 1960, he worked at the Obruchev Institute of Permafrost (Moscow). From 1960 to 1964 he worked at the Permafrost Institute of the Siberian Branch of the Academy of Sciences of the USSR (Yakutsk), and headed the Laboratory of Foundations and Ground Constructions.

Sciences in Yakutsk. In 1947–1953, he was the first Chairman of the Presidium of the Yakutsk Branch of the Academy of Sciences of the USSR. The calculations of permafrost stability under the YaCPP and the calculations of foundations were based on his work *Lectures on Foundation Calculations under the Permafrost Conditions*.

The thermometric observation and the permafrost-soil survey of the power plant site was carried out by N.I. Saltykov, Candidate of Technical Science (later, Doctor of Technical Science, professor) (Fig. 3). Temperatures were measured with the use of lazy thermometers; the permafrost-soil survey was carried out by means of the description of core samples from boreholes and pit walls.

Central Yakutia is the area with continuous permafrost, the thickness of which varies from 100 to 300 m, and the mean annual temperature at a depth of 20 m ranges from –2 to –4°C [*Balobaev, 1991*].

The first stage of the YaCPP was built on the alluvial terrace, 9–10 m above the low-water level, at a distance of 70 m from the bank ledge of the Lena River's branch.

According to data of N.I. Saltykov, the permafrost thickness was up to 180–200 m, and the mean annual permafrost temperatures at a depth of 15 m ranged from –3 to –5°C at the construction site before the construction [*Tsytovich et al., 1947*].

The site around the main building of the plant and a number of other facilities was composed of the filled layer of uneven-grained sand, 1–4 m thickness; less often, the filled layer consisted of loam with an admixture of gravels, rock debris, and slag. Fine-grained alluvial sands, often with interlayers of medium- and coarse-grained sands were found below. In the upper part of the section, to a depth of 11–15 m, there were also interlayers and lenses of sandy loam, loam, and fine-grained sand, as well as inclusions of

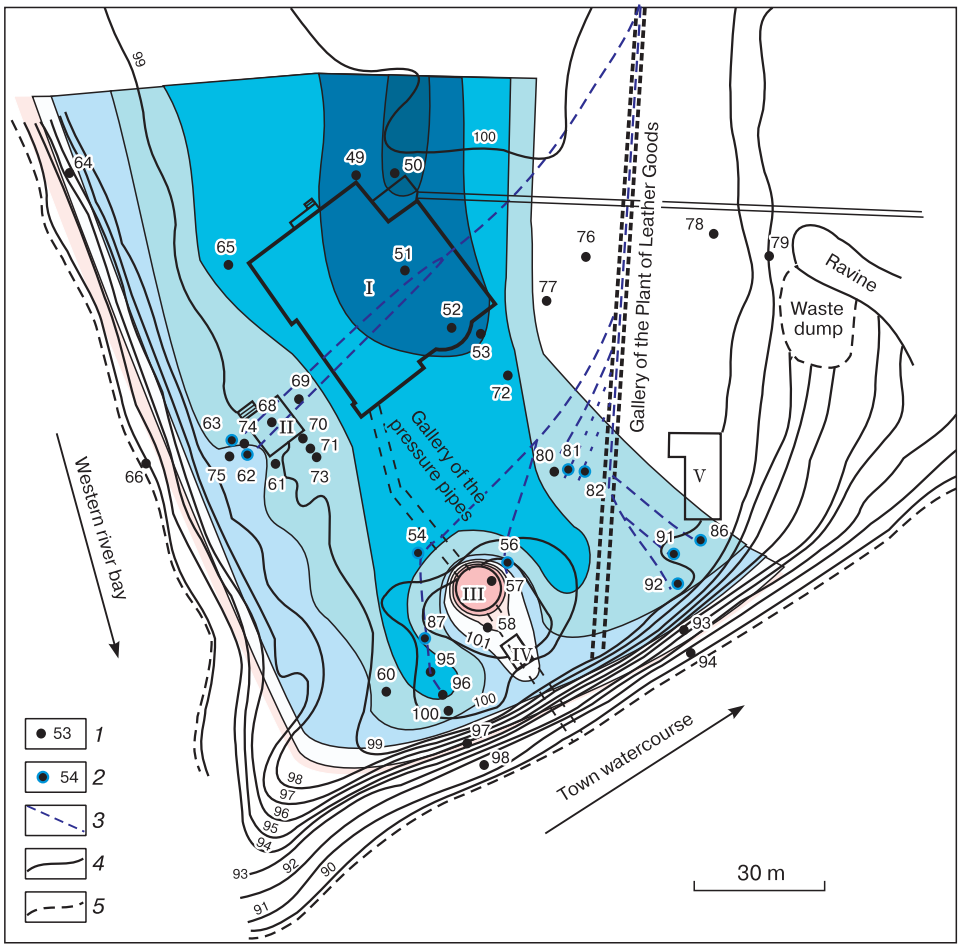

Fig. 4. The temperature field of the Yakutsk CHPP site at a depth of 5 m in 1939.

The color designates the mean annual temperature of the soils. I – main building, II – diesel station, III – pumping station, IV – well, V – garage; *1* – boreholes, *2* – boreholes with mineralized water, *3* – paths of mineralized water, *4* – contour lines and height levels, *5* – water surface level.

plant detritus. On the basis of the survey conducted in 1938–1939, N.I. Saltykov prepared a map of the soil temperature distribution at a depth of 5 m for the territory of the YaCPP (Fig. 4).

The construction of the YaCPP began in 1932. The project involved the installation of foundations on the permafrost with special measures to prevent its thawing. During the first three years, the construction was managed by V.F. Zhukov, a graduate of the Moscow Institute of Transport Engineers, one of the founders of the method of pre-construction thawing and compaction of soils, Candidate of Technical Sciences (Fig. 5). He was assigned as a chief engineer and supervised the preparation of the foundation pit, the footing of concrete slabs and larch timbers, as well as the footing and installation of foundation supports.

The frozen state of soils was retained by installing the building on columns with shoes. A cross-ventilated 1.2–1.8-m-high basement was left between the ground surface and the building to protect the foundation soil from deep thawing under the internal heat of the building, as well as to accumulate cold in them in winter time (Fig. 6).

The foundations of the first stage of the YaCHPP were freestanding reinforced concrete columns with shoes. Depending on the load, the columns had a cross-section from 30 × 30 cm to 80 × 80 cm, and the

Fig. 5. Vladimir Fedorovich Zhukov (1906–1996).

Candidate of Technical Sciences. From 1940 to 1964, he worked at the Obruchev Institute of Permafrost (Moscow). In 1956–1958, he was Deputy Director of the Institute. From 1965 he worked at the Gersevanov Research Institute of Bases and Underground Structures, Gosstroi of the USSR.

Fig. 6. The cross ventilated basement under the main building of the Yakutsk CHPP.

Photo of S.I. Zabolotnik, November 5, 2009.

shoes had a cross-section from 130 × 130 cm to 317 × 317 cm. The foundations were installed at a depth of 4.5 m from the site surface on a deck consisting of two rows of 20 × 20 cm larch timbers laid crosswise. The foundations for the turbine generators were made of 1-m-thick concrete slabs.

The pits were prepared and the foundation columns and slabs were installed and backfilled with soil in winter time. Uncovered deposits were frozen through simultaneously. The pits were backfilled with frozen soil in 20–25 cm layers; the soil was taken from dumps. Hollows between lumps of the frozen soil were filled with dry sand, and the mass, formed afterwards, was rammed. The space directly around the columns was filled with gravelly sand soil.

In the absence of practical experience at that time, the principle of the construction with retaining permafrost at the base of the large structure with significant heat generation, such as the YaCHPP, required continuous monitoring of the state of permafrost in the foundation and of the building itself. P.I. Melnikov, the head of the permafrost research station, Candidate of Geological-Mineralogical Sciences (later an academician) undertook this work (Fig. 7).

Fig. 7. Pavel Ivanovich Melnikov (1908–1994).

Doctor of Geological and Mineralogical Sciences, Professor, Academician of the USSR Academy of Sciences, Hero of Socialist Labor (1984), Honored Worker of Science and Technology of the RSFSR, twice Commander of the Order of Lenin and the Order of the Red Banner of Labor. From 1941, he was head of the Yakutsk Permafrost Research Station, which in 1956 became the Northeastern Branch of the Obruchev Institute of Permafrost, Academy of Sciences of the USSR. From 1960 to 1988, he headed the Permafrost Institute of the Siberian Branch of the Academy of Sciences of the USSR. He was President (1983–1988) and Vice-President (1988–1994) of the International Permafrost Association. In 1995, his name was given to the Permafrost Institute, Siberian Branch of the Russian Academy of Sciences.

In the first decades, P.I. Melnikov constantly monitored the temperature condition of permafrost at the YaCPP foundations and the structure itself and measured the temperatures in boreholes with lazy thermometers. He found that 10 years after the foundations were footed, the soil temperature at a depth of 5 m varied from –3.2 to –3.6°C despite the beginning of water leakages, and the thickness of the seasonally thawing layer decreased by 0.8 m and did not exceed 1 m [*Tsytovich et al., 1947*].

In the following decades, no special problems were revealed in the operation of the YaCHPP constructions, so permafrost scientists did not study its territory repeatedly. At the same time, the city of Yakutsk was growing, and it needed more and more heat and electricity. To provide this, the buildings of the power plant were repeatedly expanded and reconstructed; the entire complex was maintained according to the modern requirements. In 1978, the building of hot water boilers was constructed; in 1989, the extension for KVGM-100 boilers was added to it. All new buildings were constructed according to the first principle of construction – retaining base soils in the perennially frozen state.

Problems in the operation of the YaCHPP and the current state of base soils

Due to the construction of the complex of new structures, it was necessary to control the state of base soils of the foundations and bearing structures of the buildings themselves. Therefore, the Permafrost Institute restarted the studies on the territory of the YaCHPP. Since 1982, the studies have been conducted by S.I. Zabolotnik; since 2005, also by P.S. Zabolotnik. From 1986 to 2015, these works were carried out intermittently. From 2016 to the present time, the research has been carried out continuously. Soil temperatures have been quarterly measured in more than 90 boreholes and vertical movements of the foundations and technological equipment have been monitored during the spring and autumn seasons.

During the long-term operation of the power plant, the problems concerning stability of the structures arose due to partial thawing of the permafrost underneath them. They were generally caused by leaking heated industrial waters from drainage pipes, sewage system, and other utilities directly into the base soils.

To freeze soils beneath the main building near the part of its wall, where the circulating pump station (CPS) is located, six multi-tube seasonally cooling devices (SCDs) of the S.I. Gapeev system were installed and put into operation in 1967. Each one had a capacity of 500 liters of kerosene. In 1973, 17 more devices of the same type were installed on three

sides of this building. The SCDs were installed at a distance of 1.7–3.5 meters from the walls of the building; the space between them varied from 2.9–3.1 m to 5–7 m (Fig. 8). According to the report of the Sibtech-Energo Company, the installed SDSs at the Yakutsk CHPP lowered the soil temperature at a depth of 6 m from positive values to –3°C during two winters. The author of the invention said: "Applying... of multi-tube automatically operating cooling devices allowed... to restore the frozen base and reinforce it under the deforming buildings of the Yakutsk CHPP" [*Gapeev, 1983, p. 54*].

The operation of SCDs did enhance the permafrost regime of soils in their immediate vicinity. However, it was not possible to obtain the full expected effect of freezing the foundation bases. One of the main reasons is that SCDs were installed at a rather large distance both from the building walls and from one another. On the basis of numerous experimental data, L.N. Khrustalev, O.M. Yanchenko, and L.A. Naumova [*1983*] have concluded that, "depending on climatic and permafrost conditions, it is possible to achieve the soil freezing in a radius from 1 m (Krasnoyarsk) to 2.5 m (Vorkuta)" (*p. 5*). Similar data on the soil freezing radius with the use of SCDs for one winter season were reported by other researchers [*Alexandrov, 1983; Mirenburg, Fedoseev, 1983*]. There was little chance of freezing the talik under the build-

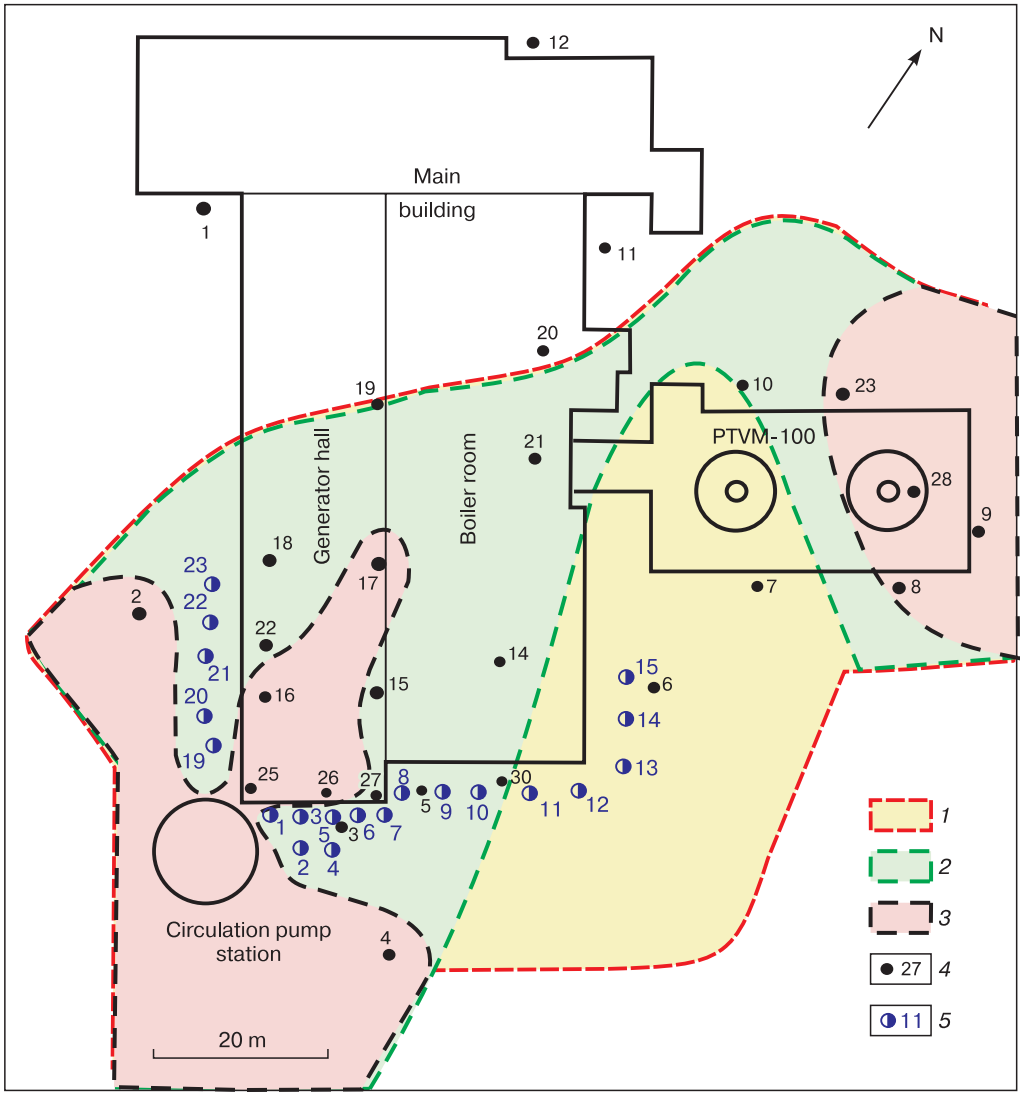

Fig. 8. Changes in the talik boundaries at the Yakutsk CHPP site from 1976 to 1986 [*Zabolotnik, Zabolotnik, 2016*].

Talik boundaries according to data of (*1*) Yakutsk Branch of the Krasnoyarsk Trust of Engineering Construction Surveys (KrasTECS), 1976; (*2*) Novosibirsk Sibtech-Energo Production Company, 1978; (*3*) Permafrost Institute, Siberian Branch of the Russian Academy of Sciences, 1986; (*4*) borehole and its number; (*5*) SCD and its number.

ing, because most of SCDs were away from its walls and beyond the radius of their action.

During further research on the territory of the YaCHPP, the authors found that the talik under the main building was not completely frozen. Measurements of the soil temperature with thermoresistors in boreholes nos. 3, 5, and 30 in the immediate vicinity of the main building (about 1 m), showed that, from October 1982 to February 1986, the soil temperature at depths of 5–14 m varied from –0.5 to –6.9°C. Nevertheless, the talik was retained directly under the southern corner of the main building, around which SCDs were installed on the outer side (Fig. 8), and the soil temperature varied from –0.4 to +1.8°C at a depth of 4 m from May 1985 to April 1986.

Constant heat emissions from CPS (buried more than 10 m) and semi-buried pipelines, as well as the repeated hot water leaks significantly prevented the freezing of the talik in this location. A heated room of the plant is a constant source of high-power heat. Prolonged heat radiation from it has caused thawing of soils around it to a considerable depth. In July 2005, during drilling of borehole 31 located in close proximity to CPS, it was revealed that the soils had thawed to a depth of 23 m, and the talik zone around it extended at least 25 m and captured the southern corner of the main building [*Zabolotnik, Zabolotnik, 2016*].

Over almost 85 years of operation of the entire complex of buildings and structures, the state of soils has changed significantly, which led to the development of talik zones of 19–25 m in thickness with positive temperatures up to +7°C or more, both at the foundation bases and in the adjoining areas. Owing to the additional measures, the talik zones were significantly reduced; nevertheless, they remained in the

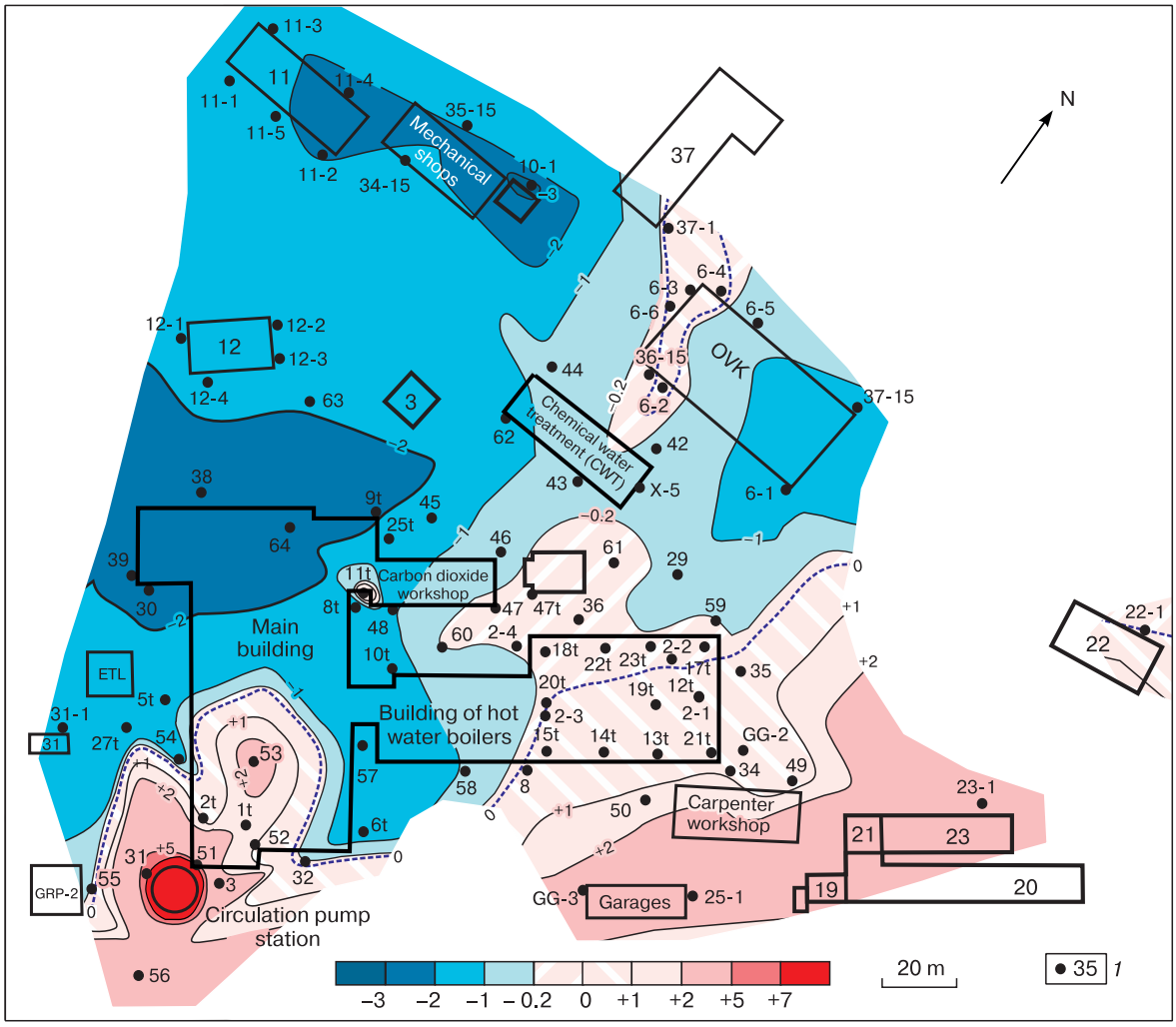

Fig. 9. Soil temperature at a depth of 10 m in November 2020.

CAC – combined auxiliary complex, ETL – electro-technical laboratory, 3 – GRP, 10 – gatehouse of the Yakutsk CHPP, 11 – office of the Yakutsk CHPP, 12 – PTO and medical station, 20 – greenhouse, 19 – control room, 21 – room for personnel, 22 – storehouse no. 1, 23 – storehouse no. 2, 31 – pumping equipment repair zone, 37 – operative dispatching service; *1* – borehole and its number.

same places and were formed under the newly built structures (Fig. 9).

Around CPS and under the southern corner of the main building, the talik remains to this day, but with lower temperatures. The foundations under the rest of the main building rested on frozen soils until 2014. However, due to subsequent water leaks, the soils thawed dramatically; in November 2021, their temperature rose to +8.5°C, and the talik occupied almost the entire southern part of the main building.

The second deep talik was formed under the eastern part of the first stage of the building of hot-water boilers (BHB-1). In 1986, its thickness was 24.5 m in the immediate vicinity of the eastern end of BHB-1 (Fig. 8). In 1989, the new building (BHB-2) with KVGM-100 boilers was added to BHB-1; it was a little larger in size than the previous one. Although the pit was frozen in winter before construction of the new building, the talik has been preserved up to this day. It is located in a larger part of BHB-2 and extends far beyond it. During the recent years, soils have been gradually freezing from the top to a depth of more than 4 m. By now, thawed soils have remained under the seasonal freezing layer only under the southeastern part of the building (Fig. 10). At the same time, at a depth of 10 m, the talik zone is retained under almost half of BHB and has spread far beyond its limits (Fig. 9).

CONCLUSIONS

The results of the studies at the YaCHPP site demonstrate that the main cause of the talik formation under the buildings and adjacent areas are leaks of hot and aggressive waters. They were almost annually recorded by the authors, when measuring the temperatures under various parts of the structures.

Considering the geocryological setting in the entire site of the YaCHPP, it should be noted that the base soils of some structures are thawed. According to P.I. Melnikov, ten years after the YaCPP was put in

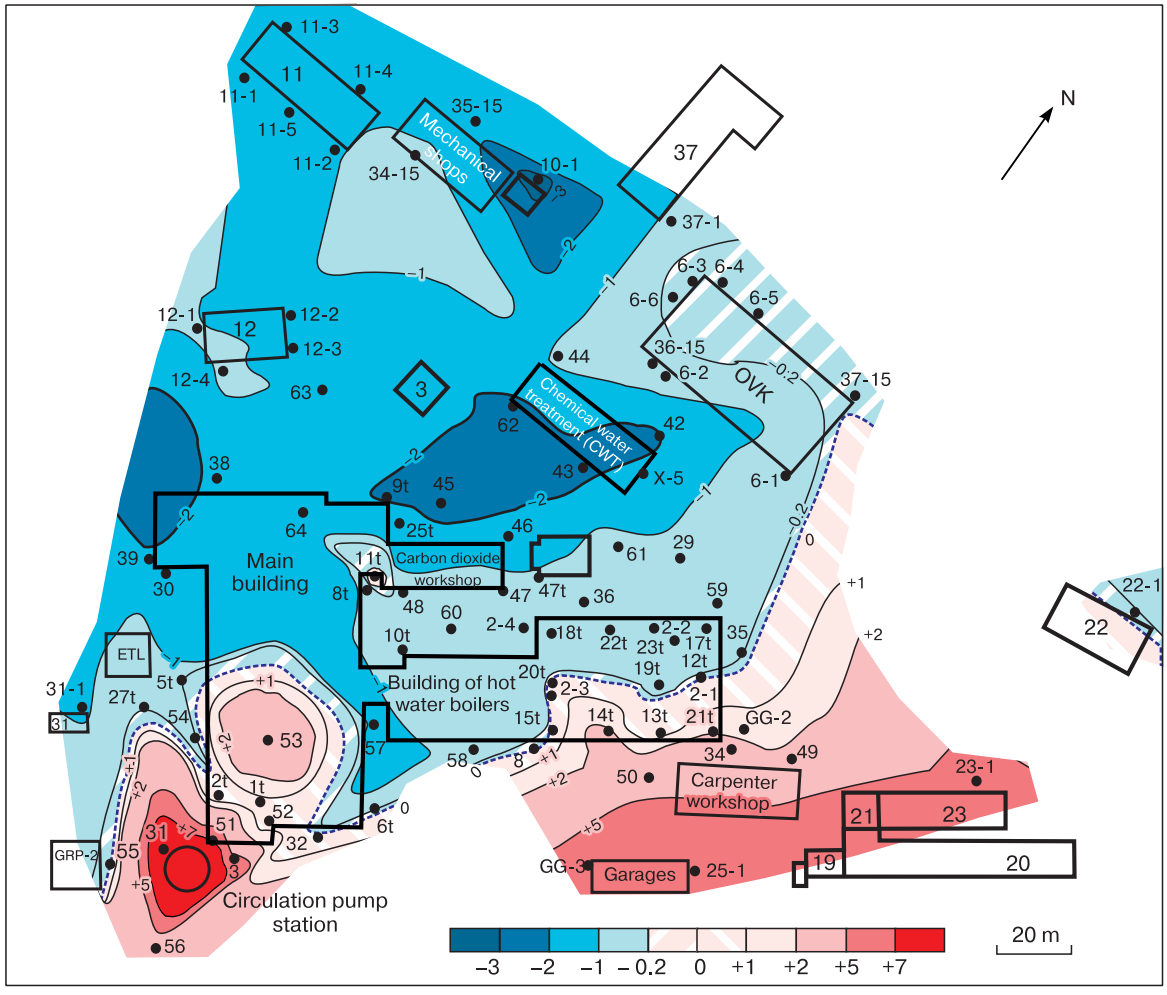

Fig. 10. The temperature field at a depth of 4 m in November 2020.

See legend to Fig. 9.

operation, the soil temperature varied from –3.2 to –3.6°C at a depth of 5 m [*Tsytovich et al., 1947*]. At present, at a depth of 4 m (close to the depth of the foundation footing) it varies from –0.2 to –2.0°C under most buildings and from –2.0 to –3.0°C only in small areas (Fig. 10). A similar picture is observed at a depth of 10 m, where the soil temperature below –2°C is established only under the western corner of the main building, on the part of the territory adjacent to it from the northwest, under the CPS mechanical workshops and some administrative buildings (Fig. 9).

Long-term studies on the territory of the YaCHPP showed that, for almost 85 years of the operation of buildings and structures, the temperature regime of soils has changed significantly. In some places, taliks were formed to a depth of 25 m; the mean annual soil temperature in them was up to 12–13°C. However, the state of the whole set of structures remains quite stable. This occurs because the sufficiently large factor of safety in the design of the buildings. Loamy and sandy-loamy soils in their bases were replaced with non-heaving and non-subsiding (upon thawing) sandy substrates; the foundations for boilers and turbine generators were made of solid concrete slabs of about 60 m^2 in area and 1 m thick.

Owing to the authors' regular studies of the permafrost state at the YaCHPP, the plant management is able to apply the proactive measures to prevent the development of negative consequences. Timely obtained data allow us to urgently eliminate water leaks from utilities, clear ice accumulations, create drainage ditches in order to remove water from ventilated basements, and to repair and reinforce the corroded and destructed bearing structures, etc.

All this makes it possible to provide the stability of the combined heat and power plant up to the present time. As a result, the condition of the entire complex of structures remains fully suitable for further operation, although some of them have been partially located on thawed soils for many years.

Recently, due to natural cold and in the absence of water leakage, gradual restoration of the temperature regime of the base soils of the buildings and in the adjacent areas has been observed. However, it is a very slow process, which will take many, many years to fully restore the frozen state of the soils.

References

Alexandrov Yu.A., 1983. Experience in using thermal piles during construction in the Vorkuta region. In: Regulation of the Temperature of Base Soils Using Seasonal Cooling Devices. Yakutsk, Permafrost Inst. SB USSR Acad. Sci., p. 88–94 (in Russian).

Balobaev V.T., 1991. Geothermics of the Frozen Zone of the Lithosphere in Northern Asia. Novosibirsk, Nauka, 194 p. (in Russian).

Gapeev S.I., 1983. Experience of using cooling units in permafrost areas. In: Regulation of the Temperature of Base Soils Using Seasonal Cooling Devices. Yakutsk, Permafrost Inst. SB USSR Acad. Sci., p. 41–58 (in Russian).

Khrustalev L.N., Yanchenko O.M., Naumova L.A., 1983. Experience and prospects of using autonomous vapor-liquid cooling devices in construction on permafrost soils. In: Regulation of the Temperature of Base Soils Using Seasonal Cooling Devices. Yakutsk, Permafrost Inst. SB USSR Acad. Sci., p. 3–12 (in Russian).

Mirenburg Yu.S., Fedoseev Yu.G., 1983. Interaction of thermal piles with a frozen base. In: Regulation of the Temperature of Base Soils Using Seasonal Cooling Devices. Yakutsk, Permafrost Inst. SB USSR Acad. Sci., p. 82–88 (in Russian).

Tsytovich N.A., Saltykov N.I., Zhukov V.F., Melnikov P.I., 1947. The foundations of a power plant on permafrost (experience in the design, construction and operation of the Yakutsk central power plant based on the principle of preserving permafrost). Moscow; Leningrad, Izd. Akad. Nauk SSSR, 104 p. (in Russian).

Zabolotnik S.I., Zabolotnik P.S., 2016. Ground temperature dynamics around and beneath the Yakutsk Combined Heat and Power Plant buildings. *Earth's Cryosphere*, XX (1), 64–74.

Zavatskaya L., Danilevskaya T. (Eds.), 2007. The CHPP above the Lena – Like a Brigantine. Krasnoyarsk, Platina, 136 p. (in Russian).

Received January 11, 2022
Revised April 7, 2022
Accepted April 27, 2022

Translated by V.A. Krutikova